A sedimentary perspective from Lake Junín on monsoon strength and glaciation in the tropical Andes over multiple glacial cycles

by

Arielle Woods

BA – Biological Aspects of Conservation, University of Wisconsin-Madison, 2010

Submitted to the Graduate Faculty of the

Dietrich School of Arts and Sciences in partial fulfillment

of the requirements for the degree of

Doctor of Philosophy

University of Pittsburgh

2021

UNIVERSITY OF PITTSBURGH

DIETRICH SCHOOL OF ARTS AND SCIENCES

This dissertation was presented

by

Arielle Woods

It was defended on

March 30, 2021

and approved by

Josef Werne, Professor and Chair, Department of Geology & Environmental Science, University of Pittsburgh

Eitan Shelef, Assistant Professor, Department of Geology & Environmental Science, University of Pittsburgh

William Harbert, Professor, Department of Geology & Environmental Science, University of Pittsburgh

Mathias Vuille, Professor, Department of Atmospheric & Environmental Sciences, University at Albany, State University of New York

Donald Rodbell, Professor, Geology Department, Union College

Dissertation Director: Mark Abbott, Professor, Department of Geology & Environmental Science, University of Pittsburgh

A sedimentary perspective from Lake Junín on monsoon strength and glaciation in the tropical Andes over multiple glacial cycles

Arielle Woods, PhD

University of Pittsburgh, 2021

The South American Summer Monsoon (SASM) sustains water resources from the Amazon lowlands to the high-elevation Andes. This system is influenced by low and high latitude climate forcing with impacts on precipitation across numerous spatiotemporal scales. Relatively little is known about long-term hydroclimate in the region, however, due to the limited number of well-dated, high-resolution paleoclimate records. This dissertation presents a multi-proxy reconstruction of changes in monsoon strength and glaciation in the tropical Peruvian Andes using sediment cores spanning ~700 ka from Lake Junín. Chapter 2 explores glacier history and precipitation-evaporation balance during the deglacial and Holocene period. Deglaciation occurred earlier in the tropical Andes compared to higher latitudes and was accompanied by lake level reductions. A delayed onset of wet conditions is observed during Heinrich Stadial 1, and the abrupt isotope excursion registered in many Andean records occurred earlier than previously thought. Unconformities indicate major drops in lake level during the early and mid-Holocene, consistent with a weaker SASM. The findings demonstrate that climatic changes at Junín were at times in and out of phase with high latitude regions. Chapter 3 examines the past 50 ka with sufficient chronologic precision to document Junín's response to Dansgaard-Oeschger (D-O) cycles, the millennial-scale climatic fluctuations that characterized the last glacial. The results demonstrate rapid glacial retreat and reductions in lake level during D-O events, suggesting intense periods of aridity. This study is the first to reveal the magnitude of the climatic disruptions in the Andes and highlights the sensitivity of the region to Northern Hemisphere forcing. Chapter 4 explores two complete glacial/interglacial cycles during Marine Isotope Stages (MIS) 12-15 (~420-620 ka). High amplitude $\delta^{18}O$ variability during MIS 15 follows precession, indicating greatly enhanced SASM intensity, whereas no precessional signal is apparent during the more arid MIS 13. MIS 14 shows moderate glacial advance and millennial-scale climatic instability, whereas major expansion of ice during MIS 12 contributed to more stable lake level. This study showcases the large

range of past climatic variability in the tropical Andes at unprecedented resolution and demonstrates considerably different responses to climatic forcing among individual glacial and interglacial periods.

Table of contents

Preface xiii

1.0 Introduction 1

1.1 Importance of tropical (paleo)climate variability 1

1.2 Paleoclimate insights into tropical monsoons systems 2

1.3 Outstanding questions about South American paleoclimate 5

1.4 Prior work on Lake Junín and rationale for deep drilling 7

1.5 Objectives and outline of dissertation 11

2.0 Hydroclimate and lake level in the central Peruvian Andes during the last deglaciation and Holocene 14

2.1 Introduction 14

2.2 Site description and regional climate 16

2.3 Methods 19

2.3.1 Sediment coring 19

2.3.2 Physical and geochemical analysis 20

2.3.3 Chronology 20

2.4 Results 21

2.4.1 Composite core and chronology 21

2.4.2 Stratigraphy 23

2.4.3 Unit 1 (7.65-6.67 mblf) 25

2.4.4 Unit 2 (6.67-6.37 mblf) 25

2.4.5 Unit 3 (6.37-6.13 mblf) 25

2.4.6 Unit 4 (6.13-5.91, 5.71-5.5 mblf) and unit 5 (5.91-5.71 mblf) 27

2.4.7 Unit 6 (5.5-4.82 mblf) 27

2.4.8 Unit 7 (4.82-4.37 mblf) 28

2.4.9 Unit 8 (4.37-2.12 mblf) 28

2.4.10 Unit 9 (2.12-1.58 mblf) 29

2.4.11 Unit 10 (1.58-0.15 mblf) 29

2.5 Discussion 31

2.5.1 Sedimentology of the Lake Junín transect cores 31

2.5.2 Interpretation of clastic sediment inputs to proglacial Andean lakes 31

2.5.3 Interpretation of organic matter and carbonate content in Lake Junín sediments 33

2.5.4 Lake level curve 34

2.5.5 The local LGM and deglaciation of the Junín watershed (25 – 18 ka) 36

2.5.6 Heinrich Stadial 1 (18-14.6 ka) 39

2.5.7 The Antarctic Cold Reversal (14.6 – 13.0 ka) 42

2.5.8 The Younger Dryas (12.9-11.7 ka) 43

2.5.9 Hydroclimate trends during the Holocene 46

3.0 Andean drought and glacial retreat tied to Greenland warming during the last glacial period 51

3.1 Introduction 51

3.2 Methods 54

3.2.1 Chronology 54

3.2.2 Physical analysis of sediment cores ... 55

3.3 Results ... 56

3.3.1 Lake setting and glacial connection ... 56

3.3.2 Sedimentary context ... 57

3.3.3 Synchronous changes in lake level and paleoglacier extent ... 60

3.4 Discussion ... 62

4.0 Monsoon strength and glaciation in the tropical Andes during MIS 15-12 ... 68

4.1 Introduction ... 68

4.1.1 Study location and modern climate ... 71

4.1.2 Sedimentology ... 72

4.1.3 Interpretation of bulk sediment properties and scanning XRF data ... 73

4.1.4 Controls on $\delta^{18}O$ values at Lake Junín ... 74

4.2 Materials and methods ... 75

4.2.1 Chronology ... 75

4.2.2 Bulk sediment and geochemical analysis ... 79

4.3 Results ... 80

4.3.1 MIS 15 (75-70.3 m) ... 80

4.3.2 MIS 14 (70.3-68.4 m) ... 82

4.3.3 MIS 13 (68.4-63.7 m) ... 84

4.3.4 MIS 12 (63.7-56.5 m) ... 84

4.4 Discussion – interglacial periods ... 85

4.4.1 Differences in monsoon strength and P-E balance among interglacials ... 85

4.4.2 The influence of evaporation on carbonate isotopes and lake hydrology ... 92

4.4.3 Negative offset of $\delta^{18}O$ values relative to insolation forcing during MIS 15...94

4.4.4 Atypical MIS 13 95

4.5 Discussion – glacial periods 98

4.5.1 Differences in tropical Andean glaciation......98

4.5.2 Millennial scale variability during glacial periods......101

4.5.3 Abrupt glacial terminations in the tropical Andes 102

4.6 Conclusions 103

5.0 Summary and future directions 104

Bibliography 106

List of tables

Table 1. Locations and depths of transect cores 19

Table 2. Radiocarbon ages for the Junín C/D composite core 48

Table 3. Radiocarbon ages for the Junín transect cores 49

Table 4. Radiocarbon ages for the Junín cores 66

Table 5. Tie points used in the modified age-depth model for MIS 12-15 79

Table 6. Interpretation of facies and bulk sediment properties 85

List of figures

Figure 1. Seasonal precipitation patterns for tropical South America. 2

Figure 2. Map of Lake Junín and the surrounding watershed. 8

Figure 3. Lake Junín watershed and locations of transect cores. 18

Figure 4. Age-depth model for the C/D composite core. 22

Figure 5. Stratigraphy of the transect cores. 24

Figure 6. Bulk sediment properties and isotopic data for the C/D composite core. 26

Figure 7. Lake Junín proxy data over the past 25 ka 30

Figure 8. Deglaciation of the Junín watershed 38

Figure 9. Different moisture patterns during Heinrich Stadial 1. 41

Figure 10. Timing of the early Holocene isotopic excursion. 45

Figure 11. Location of the Lake Junín drainage basin and Pacupahuain cave. 53

Figure 12. Physical and geochemical sediment properties from the Junín drill core. 58

Figure 13. Variable carbonate content of Junín sediments. 59

Figure 14. The timing of Dansgaard-Oeschger (DO) interstadials 61

Figure 15. Comparison of regional and global proxy paleoclimatic records. 63

Figure 16. Global glacial/interglacial cycles of the past 700 kyr. 70

Figure 17. The Lake Junín watershed in the central Peruvian Andes. 72

Figure 18. Modified age-depth model for the older portion of the Junín record 77

Figure 19. Age model for MIS 15-12 and glacial/interglacial stratigraphy. 78

Figure 20. Proxies from Lake Junín during MIS 12-15 81

Figure 21. Differences in stable isotope values and carbon content among interglacials. 82

Figure 22. High resolution line-scan images of sediment cores... 83

Figure 23. Side-by-side comparison of Junín proxies during the three interglacial periods . 87

Figure 24. Side-by-side comparison of Junín proxies during the three glacial periods......... 88

Figure 25. Junín compared to records from the northern tropics. 91

Figure 26. Comparison of Junín and records of high latitude glaciation. 100

Preface

This work was made possible by the support and guidance from so many mentors, colleagues, friends and family over the years. First and foremost, I would like to thank my advisors Mark Abbott and Joe Werne who introduced me to the world of paleoclimate research, encouraged exploration in the field, lab, and intellectual realms, and offered invaluable guidance. I'm incredibly grateful for the opportunities to work on a variety of exciting projects with them, and so happy to see that work coming together. I would also like to acknowledge my committee members Don Rodbell, Mathias Vuille, Eitan Shelef, Bill Harbert, and Emily Elliott for lending their expertise through constructive feedback and thought-provoking questions.

So many current and former lab members helped with field and lab work, pondered the Junín data with me, and made grad school a lot of fun: Matt Finkenbinder, Dave Pompeani, Aubrey Hillman, Byron Steinman, Sophie Lehmann, Nick Weidhaas, Sam Mark, Everett Lasher, Melissa Griffore, Jamie Vornlocher, MG Bustamante, Nick Wondolowski, Sandy O'Hara, Darren Larsen, Shannon Christiansen, Michelle Kim. Many thanks to our collaborators from other universities who were part of the adventures in Peru, the basement of LacCore, and various AGU conferences: Christine Chen, Rob Hatfield, Joe Stoner, Pedro Tapia, David McGee, Kristina Brady, Amy Myrbo, Grace Delgado.

I would like to thank the Pitt staff and especially Annemarie Vranesevic for so much logistical support over the years, as well as my friends in the machine shop for all the troubleshooting and project building. Cheers to John Southon, Chanda Bertrand, and others at UC Irvine for welcoming me to their lab and making it possible to analyze ridiculously large batches of radiocarbon samples year after year.

Special thanks to Sophie Lehmann for being such a wonderful colleague and close friend and for keeping me sane. I owe many debts of gratitude to Sam Doctor for his endless support and help with late night coding challenges. Finally, I am deeply grateful to my family, Adrianne, John, and Miranda, who cheered me on and offered unconditional support throughout my life. This dissertation is dedicated to my dad, who was endlessly curious about the world and read books on every scientific discipline I took an interest in over the years so that we could always talk science.

1.0 Introduction

1.1 Importance of tropical (paleo)climate variability

Tropical regions contribute to global water vapor production and large-scale transport of moisture and heat to the high latitudes, and they interface with global climate changes via a multitude of ocean-atmosphere teleconnections. Tropical monsoon systems such as the South American Summer Monsoon (SASM) (Figure 1) have received attention for their considerable interannual to decadal variability, with wide-reaching effects on human populations and ecosystems. For example, precipitation associated with the SASM is influenced by several modes of oceanic-atmospheric variability including the El Niño Southern Oscillation (ENSO) (Garreaud 2009; Garreaud and Aceituno 2001; Paegle and Mo 2002), the Atlantic Multidecadal Oscillation (AMO) (Zhou and Lau 2001; Marengo 2004), and the Pacific Decadal Oscillation (PDO) (Garreaud 2009). Such phenomena can lead to both drought and excessive rains with a regionally variable fingerprint. Rainfall anomalies are particularly problematic in the tropical Andes, where ongoing glacier retreat further threatens freshwater supplies. However, instrumental records show that the timing, duration, and magnitude of drought conditions can vary considerably throughout the Andes (Garreaud et al. 2009).

Longer-term precipitation trends are harder to assess due to the paucity of high-quality observational stations, but there is some evidence for an increase in precipitation in the Andes north of 11°S and a decrease further south in the second half of the 20th century (Vuille et al. 2003; Haylock et al. 2006). The drivers of these trends remain uncertain, however, because monsoon systems respond to a variety of climatic forcings and fundamental aspects of their dynamics remain uncertain. Indeed, climate models differ in their projections for future precipitation patterns in the tropics (Lee and Wang 2014; Broecker and Putnam 2013; Neelin et al. 2006; Lin 2007), in part due to outstanding questions about the long-term behavior of monsoons systems. Paleoclimate archives from tropical regions can help address these questions by providing important insights into the full range of natural variability and by revealing the response of monsoon systems to large climatic changes in the past. While about 40% of lakes lie within the low latitudes (Verpoorter et al. 2014), tropical paleolimnological investigations remain under-represented compared to those from higher latitude lakes (Escobar et al.

2020). A growing recognition of the need for additional tropical terrestrial archives is demonstrated by the many ongoing and completed lacustrine deep drilling projects in recent decades, including from Central and South America (Bogota Basin, Peten Itza, Chalco, Titicaca, Junín), Africa (Bosumtwi, Challa, Malawi, Tanganyika), and the Indo-Pacific region (Towuti). Such paleolimnology studies are powerful because they offer the potential for multiproxy reconstructions that integrate information about the lake itself as well as the surrounding terrestrial watershed and regional climate conditions.

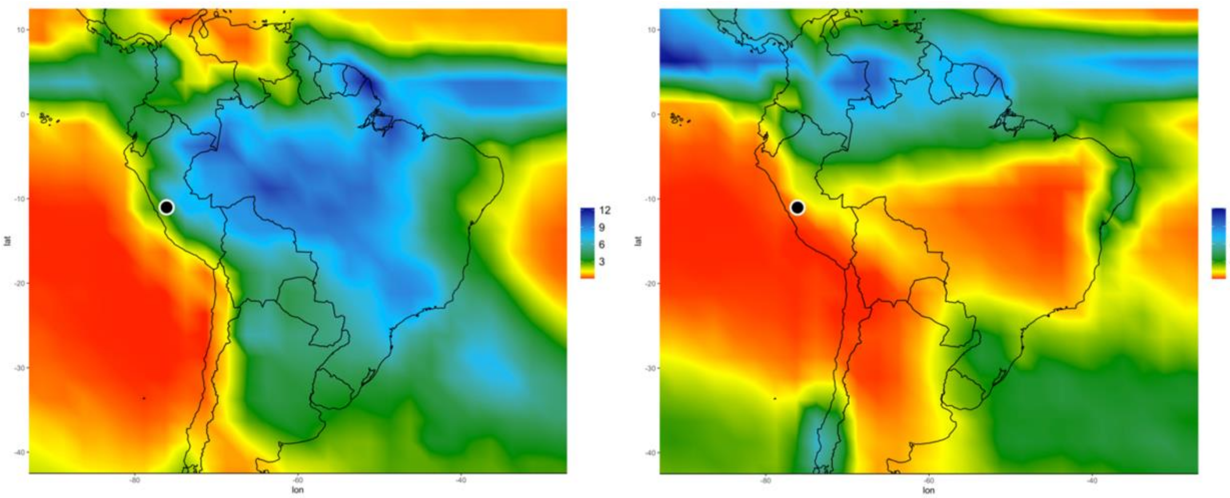

Figure 1. Seasonal precipitation patterns for tropical South America. Long-term monthly mean precipitation for the wet season (Dec.-Feb., left) and dry season (Jun.-Aug., right) from 1981-2010 based on satellite and gauge data. Units for the color scale bar are mm/day. Lake Junín is indicated by the black circle. CMAP precipitation data provided by the NOAA/OAR/ESRL PSL, Boulder, Colorado from their website at https://psl.noaa.gov/data/gridded/data.cmap.html.

1.2 Paleoclimate insights into tropical monsoons systems

In recent decades, paleoclimate reconstructions emerging from lacustrine, cave, and marine studies have revealed some common responses of tropical hydroclimate to long-term, global-scale climatic changes. A prominent example lies in how paleoclimate records from nearly all the major monsoon regions show precessionally-paced changes in precipitation that are antiphased when comparing the northern and southern tropics (deMenocal et al. 2000; Cruz et al. 2005; Wang et al. 2001). It was first proposed that on precessional timescales, higher summer insolation strengthens monsoons via increased heating of the land surface and overlying atmosphere relative to the surrounding ocean, resulting in landward low-level flow of moist air (Kutzbach 1981; Kutzbach and Guetter 1986). Many subsequent modeling studies and climate simulations also support land-sea heating contrasts as a fundamental driver of orbital-scale changes in monsoon strength (Clement et al. 2004; Battisti et al. 2014; Bosmans et al. 2015), including models that specifically focus on the SASM domain (Liu and Battisti 2015).

The other enduring mechanism to explain precipitation changes observed in monsoon regions involves shifts in the mean position of the Intertropical Convergence Zone (ITCZ), which is closely linked to large-scale meridional temperature gradients and overturning in the tropics. ITCZ rainfall arises from the convergence of trade winds near the surface and ascent of moist air masses, forming the rising branch of the Hadley circulation and resulting in deep convective precipitation. While the ITCZ over ocean regions is not synonymous with land-based monsoons, variations in tropical rainfall on centennial to orbital timescales are frequently attributed to shifts in the position of the ITCZ, and a framework has emerged in recent years (termed the ITCZ shifts or energy-budget framework) as a unifying theory for interpreting tropical rainfall variations in observations, simulations, and the geologic record (Schneider et al. 2014; Chiang and Friedman 2012; McGee et al. 2014; Donohoe et al. 2013). In short, it posits that shifting the ITCZ and the ascending branches of the Hadley cell to the warmer hemisphere facilitates cross-equatorial atmospheric energy transport towards the cooler hemisphere, thereby balancing energy fluxes into and out of the tropics.

A shift in the mean ITCZ position is a commonly invoked mechanism in paleoclimate literature because of its potential to explain the hemispherically-antiphased precipitation patterns revealed by many moisture-sensitive proxy records, and because it appears to be relevant on a variety of different timescales. For example, several records from South America interpret Holocene changes in precipitation in terms of precession-driven ITCZ shifts (Haug et al. 2001; Seltzer et al. 2000; Cruz et al. 2009; Peterson and Haug 2006). Speleothems from the Amazon Basin and the Andes also reliably show precessionally-paced changes in monsoon strength (inferred from $\delta^{18}O$) that are antiphased with speleothems from China and other northern tropical regions during many previous interglacial periods (Cruz et al. 2005; Cheng et al. 2013; Burns et al. 2019). A recent numerical precipitation model based on the ITCZ/energy budget framework relates the position and intensity of the ITCZ to orbital forcing, and successfully reproduces the precipitation changes indicated by terrestrial proxy records for the past 350 ka from the major monsoon regions including South America (Bischoff et al. 2017).

The ITCZ framework has also been employed to explain the millennial scale north-south shifts of the tropical rainbelt in response to abrupt climatic events during the last glacial period. Key to this interpretation is the role of the Atlantic Meridional Overturning Circulation (AMOC) because variations in heat transport associated with AMOC contribute to large-scale changes in the hemispheric thermal gradient and tropical circulation. Freshwater inputs to the North Atlantic during cold intervals, such as Heinrich Stadials, leads to reductions in the formation and sinking of deep water, causing a weakening or even collapse of AMOC (Broecker et al. 1985; Rahmstorf 2002; Clark et al. 2002). The attendant reduction in northward oceanic heat transport effectively causes excess heat to "pool" in the tropical Atlantic Ocean, drawing the ITCZ further south. A southward ITCZ shift during millennial scale cold events invigorated Southern Hemisphere monsoons, leading to increased rainfall throughout much of South America and other southern tropical regions (Kanner et al. 2012; Mosblech et al. 2012; Fritz et al. 2010), and decreased rainfall in the northern tropics (Peterson et al. 2000; Wang et al. 2001). During recent years, proxy records that track changes in Atlantic Ocean circulation have confirmed repeated fluctuations in AMOC strength during the last glacial period (McManus et al. 2004; Lynch-Stieglitz 2017), including during the shorter duration Dansgaard-Oeschger (D-O) warming events (Henry et al. 2016; Gottschalk et al. 2015), when an invigorated AMOC drew the ITCZ further northward.

While the similarities among many paleoclimate records point to a coherent response of regional monsoons to certain climatic forcings, many aspects of long-term tropical climate remain uncertain. For example, ITCZ shifts may be inadequate to explain the observed precipitation changes in certain cases because the ITCZ appears to be energetically limited in how far it can migrate from the equator – some numerical estimates and climate simulations suggest no more than a few degrees of latitude (McGee et al. 2014; Donohoe et al. 2013; Schneider et al. 2014), whereas proxy records indicate expansion of monsoon rainfall well beyond this range (Arbuszewski et al. 2013). Furthermore, some observations and climate models suggest that rainfall patterns are better described as expansions or contractions of the rainbelt, rather than north-south shifts of the ITCZ (Neelin et al. 2006; Byrne et al. 2018; Singarayer et al. 2017). Finally, the behavior of individual monsoon systems can depart from broader global or hemispheric scale patterns due to local feedbacks, topography, and unique teleconnections. Climate models focused on the tropics routinely indicate considerable regional variability in tropical precipitation that is not captured by the zonal mean monsoon response (Mohtadi et al. 2016; Biasutti et al. 2018; Boos and Korty 2016).

Many questions also remain regarding tropical climate changes on glacial-interglacial timescales. From a thermodynamic standpoint, colder glacial climates should be associated with less humidity (Clement et al. 2004), and a recent review finds that glacial periods were associated with drying across large regions of the tropics (McGee 2020). At the same time, preferential cooling of the Northern Hemisphere due to increased albedo during glacial periods is expected to result in a southward shift of the ITCZ (Chiang and Friedman 2012; Chiang et al. 2003; Donohoe et al. 2013), and several records point to wetter conditions in certain tropical regions during the last glacial period (Placzek et al. 2006; Hanselman et al. 2011; Cruz et al. 2007). More long and continuous paleoclimate records are needed to assess whether rainfall in the tropics shows synchronous shifts or hemispheric contrasts on glacial/interglacial scales, and to test expectations about tropical climate that are based on models and theory.

1.3 Outstanding questions about South American paleoclimate

While some paleoclimate records from tropical South America are broadly coherent in the direction and timing of major climatic changes, others deviate from these patterns and point to the need for further investigation into the long-term response of precipitation and tropical glaciers in the region. For example, the $\delta^{18}O$ records from many South American lakes and speleothems show a strong precessional signal during the Holocene (Wang et al. 2004; Seltzer et al. 2000; Bird et al. 2011; Cruz et al. 2009), as do a smaller number of non-isotopic rainfall records (Fritz et al. 2004; Haug et al. 2001). Yet on longer timescales, several records exhibit little to no apparent orbital pacing. One western Amazonian speleothem tracks summer insolation during the last three interglacial periods but not during glacial intervals (Cheng et al. 2013), while another displays orbital pacing during some, but not all, portions of the last glacial period (Mosblech et al. 2012). Similarly, speleothems from the central Peruvian Andes follow precession during glacial Marine Isotope Stage (MIS) 6 (Burns et al. 2019), but not during the last glacial period (e.g., MIS 2-3) (Kanner et al. 2012), contrary to model expectations (Liu and Battisti 2015). Together these records reveal an unpredictable response of $\delta^{18}O$ to insolation forcing that is most pronounced during certain glacial periods, but the limited duration and/or discontinuous nature of many speleothem records makes it difficult to assess if these are site-specific deviations or if certain locations respond to different forcings.

On glacial/interglacial timescales, a few records from South America show pronounced variations in pollen signatures (Torres et al. 2013; Hanselman et al. 2011; Groot et al. 2011), indicating a sensitivity to global temperature and ice volume. Surprisingly, relatively little is known about hydroclimate patterns in the region on glacial/interglacial scales, and the available records are in dispute and poorly dated. Limited proxy evidence from lakes in Bolivia and Colombia suggests the tropical Andes experience drier interglacials and wetter glacials (Torres et al. 2013; Hanselman et al. 2011), whereas records that reflect conditions in the Amazon Basin instead suggest that glacials may have been somewhat drier than interglacials (Harris and Mix 1999; Wang et al. 2017). Diverging moisture patterns between the Amazon lowlands and the Andean highlands are surprising considering the Amazon basin is the epicenter of convective activity that feeds the SASM, which is in turn the principal precipitation source to the tropical Andes. The discrepancies in records from South America may reflect true regional variability in moisture distribution or competing influences on tropical hydroclimate on glacial/interglacial scales. Alternatively, they may arise from ambiguous proxy interpretations, but our ability to resolve these issues is hampered by the small number of long records that are presently available.

On suborbital timescales, and particularly during the last glacial period, much of what we know about SASM dynamics is derived from speleothem $\delta^{18}O$ records, which have the advantages of high resolution and chronologic precision. The $\delta^{18}O$ signal recorded in South American proxy records largely reflects convective activity and the amount of rainfall in the Amazon Basin core monsoon region, i.e. regional monsoon intensity (Vuille and Werner 2005; Fiorella et al. 2015; Samuels-Crow et al. 2014). Following this interpretation, most studies conclude that the SASM weakened during warm interstadials and strengthened during cold stadial periods (Kanner et al. 2012; Mosblech et al. 2012; Cheng et al. 2013). However, recent findings increasingly point to the importance of additional controls on low-latitude water isotope values that may have a similar or greater relative influence than the amount effect. In the SASM domain, the $\delta^{18}O$ of precipitation likely integrates several secondary isotope effects that vary over time, such as the role of vegetation on evapotranspiration (Wang et al. 2017), changes in seasonality (Liu and Battisti 2015), and air mass transport pathways (Apaéstegui et al. 2018), among others (Konecky et al. 2019). Furthermore, because the $\delta^{18}O$ in Andean proxy records is an inherited signal that is largely reflective of upstream processes in the Amazon Basin, it does not necessarily represent local hydroclimate conditions (Fiorella et al. 2015; Samuels-Crow et al. 2014) so we cannot directly infer Andean precipitation levels from isotope records alone. For these reasons, there is a need for complementary lacustrine proxy records that reflect *in situ* conditions within the watershed and lake basin to corroborate isotopic records of monsoon strength.

While the balance of evidence points to a consistent response of the SASM to millennial scale climate fluctuations, less clear is the impact these events had on tropical Andean glaciers, which are known to be sensitive to both precipitation and temperature (Kaser 2001; Kaser et al. 2003; Sagredo et al. 2014). Most records of glaciation in the tropical Andes rely on moraine exposure ages to infer the timing and extent of glacial maximum advances and stages of retreat. This approach has been used extensively to document glacier activity during the last glacial maximum and the most recent deglacial interval (Shakun et al. 2015; Smith et al. 2005; Jomelli et al. 2014; Rodbell et al. 2009), and there is also evidence for advances during Heinrich Stadial 1 (Blard et al. 2011; Placzek et al. 2013; Martin et al. 2018; 2020). The discontinuous nature and relatively large chronological uncertainty of these datasets, however, precludes a comprehensive understanding of glacial responses on centennial to millennial timescales, and they lack information about smaller advances that occurred prior to glacial maxima. As such, little is known about glacier fluctuations that may have occurred in association with the earlier Heinrich Stadials and D-O cycles. Sediment records from glacier-fed lakes, however, provide excellent continuous terrestrial proxy archives (Carrivick and Tweed 2013), and the extent of ice cover has been demonstrated to be a primary control on the delivery of clastic sediment to Andean alpine lakes (Rodbell et al. 2008). As such, additional paleolimnology studies from the Andes are needed to complement moraine-based chronologies and improve our understanding of past tropical ice volume fluctuations.

1.4 Prior work on Lake Junín and rationale for deep drilling

Several decades of research on the Junín basin, its sediments, and geochemistry demonstrate why this lake was targeted for deep drilling in 2015 and highlight how the longer sediment record can help address outstanding questions about past monsoon strength and tropical glaciation. Located on a broad plain at 4080 m asl between the eastern and western cordilleras of the central Peruvian Andes, Lake Junín is the largest (280 km^2) extant lake entirely within Peru and is today a designated natural reserve for its unique biodiversity (Figure 2). The lake is relatively shallow (8-15 m of water in the deeper portions) and is ringed by dense marshlands that fluctuate in extent with seasonal water level changes of 1-2 m. H.E. Wright (1983) first recognized two distinct phases of glaciation in the region based on the preservation of moraines in the surrounding foothills. The older, more extensive phase is marked by smoother moraine topography, development of stream valleys, and loess covering, whereas the younger phase shows sharper terrain dotted with small lakes and depressions and less evidence of subsequent erosion. The formation of the basin was attributed to glacial outwash fans blocking the northern and southern ends of the plain (Wright 1983). Cosmogenic exposure dating of moraine sequences in many of the valleys later revealed that glaciers had advanced to within several km of the lake repeatedly over the past ~ 1 Ma (Smith et al. 2005a; Smith et al. 2005b). However, there is no indication that ice has ever overridden the lake throughout this period, suggesting the potential for a long and continuous sediment record.

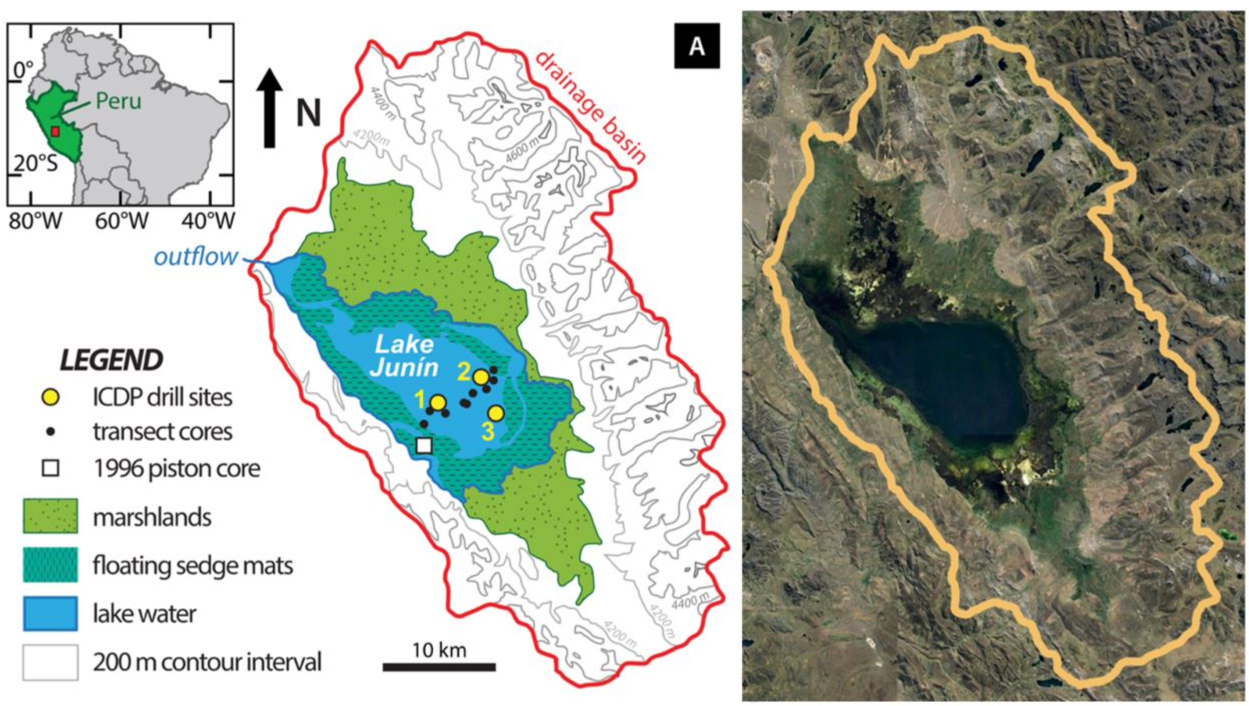

Figure 2. Map of Lake Junín and the surrounding watershed. Locations of the sediment cores discussed in the text are shown in (a); figure is from Chen et al. (2020). Right: Google Earth image of the Junín watershed.

The first effort to core Lake Junín yielded 30 m of sediment collected from a floating sedge mat in 4 m of water near the western shore of the lake (Hansen et al. 1984). Pollen analysis revealed a predominance of subpuna shrubland types during the early to mid-Holocene, with as much as 30% of pollen sourced from more distant east Andean forests. Contributions from this distant source diminished in the late Holocene, possibly due to human disturbance of the forest landscape or climatic change. Glacial-aged silty sediments contained very sparse pollen concentrations dominated by puna grassland types which, along with a major unconformity from ~24-39 ka, were taken as evidence of drier conditions during the last glacial period (Hansen et al. 1984).

G.O. Seltzer and colleagues in 1996, using a Livingstone piston corer, obtained another sediment core from the western side of the lake that showed no apparent unconformities, and established a more reliable chronology. The Holocene is dominated by light-colored, carbonate-rich sediments with variable organic content (e.g., marls), and sediments dating to the late glacial period are characterized by fine-grained, grey glacial silts with high magnetic susceptibility that were likely eroded by piedmont glaciers in the adjacent valleys (Seltzer et al. 2000). Paleozoic-Mesozoic marine limestones and dolostones comprise the majority of bedrock in the Junín watershed (Cobbing et al. 1981), and all major input streams to the lake are supersaturated with respect to carbonate (Flusche et al. 2005). This results in high authigenic carbonate content during interglacial intervals when the influx of glacial silt is cut off. Oxygen isotope analysis of the carbonate fraction revealed a ~6‰ enrichment in the late glacial followed by a gradual depletion from the early to late Holocene, interpreted as a decrease followed by a long-term increase in effective moisture (Seltzer et al. 2000). The close agreement between the $\delta^{18}O$ record and local summer insolation established that Lake Junín responds to orbital forcing and thus SASM strength. Finally, a Holocene record from the nearby, open-basin Lake Pumacocha (Bird et al. 2011) helped to demonstrate the sensitivity of Lake Junín to local precipitation-evaporation (P-E) balance. Both records show a similar trend of decreasing $\delta^{18}O$ values throughout the Holocene, yet the $\delta^{18}O$ values from Lake Junín are ~4-6‰ more positive because of evaporative enrichment of its lake waters. Moreover, the enrichment is most pronounced during the early Holocene insolation minimum, indicating a greater sensitivity of Lake Junín to periods of aridity.

The findings described above established Lake Junín's potential to yield a continuous sediment record of late Quaternary climate change, glaciation, P-E balance, vegetation, and paleomagnetic secular variation in the tropical Andes. A seismic survey was conducted in 2011, and while the shallow lake water posed technical difficulties, a sedimentary sequence was successfully imaged that revealed ~200 m of layered sediments with minimal deformation and evidence of multiple glacial cycles. To assess the potential for establishing an independent chronology from Lake Junín, a pilot study was undertaken in which authigenic carbonates from the deglacial and Holocene sections of the 1996 core were U-Th dated. The results indicated high uranium concentrations, low detrital content, and 20 of 23 U-Th ages were consistent with the radiocarbon chronology, suggesting that the U-Th method could be successfully employed to date previous interglacial intervals. This groundwork contributed to the acquisition of funding from the International Continental Scientific Drilling Program (ICDP) and the National Science Foundation to proceed with deep drilling of Lake Junín.

Drilling operations commenced in June of 2015 with international collaboration of scientists from 5 ICDP member countries and Peru. Three sites were selected for drilling (Figure 2) with cores collected from multiple adjacent holes at each site to minimize gaps between sequential cores and thereby ensure complete recovery of the stratigraphic section. The deepest sediments were recovered from Site 1 to a depth of ~104 m, below which lies a gravel layer that could not be further penetrated by the drilling equipment. Two overlapping cores were collected off the side of the drilling platform using a Livingstone piston corer to account for disturbance of the upper, unconsolidated sediments by the drilling equipment. Correlation of overlapping core sections was achieved by alignment of stratigraphically-equivalent horizons visible at mm-scale in high-resolution line-scan images as well as physical property data such as magnetic susceptibility, gamma ray attenuation, and natural gamma radiation (Hatfield et al. 2020). A composite splice depth scale was established for Site 1 by selecting the most continuous and representative core sections to a total depth of ~95 m, which provided the template for subsequent sampling efforts (Hatfield et al. 2020). Finally, a series of 8 additional Livingstone cores were collected along a NE-SW transect spanning from the shallow lake margins to the depocenter to investigate patterns of sedimentation across the basin during the late glacial and Holocene.

The drill cores revealed the expected sequence of alternating carbonates and glacial silts, suggestive of multiple glacial/interglacial cycles. U-Th dating of the carbonate-rich intervals confirmed a basal age estimate of ~700 ka (Chen et al. 2020), indicating that seven complete glacial/interglacial cycles were captured that extend to at least MIS 16. The initial age-depth model incorporates 72 U-Th analyses from 18 bulk carbonate samples, along with 79 radiocarbon ages in the upper ~18 m of sediment, making Lake Junín the oldest continuous record in the tropical Andes that is constrained entirely by independent radiometric dates (Chen et al. 2020). Because the glacial silt intervals cannot be dated with the U-Th method, additional chronologic control was established using measurements of normalized remanence, a proxy for relative geomagnetic paleointensity, that were aligned to a well-dated relative paleointensity stack (Hatfield et al. 2020). The resulting paleomagnetic tie points were incorporated with the existing radiometric dates to refine the age model during the glacial stages, with both age models generally in good agreement within their respective error margins (Hatfield et al. 2020).

Lake Junín offers major advantages compared to other long records from the region. To the south, sediments from Lake Titicaca (16°S) span the past ~370 ka (Fritz et al. 2007), and records from the Bogotá Basin in the northern (5°N) tropical Andes are older than 1 Ma (Hooghiemstra et al. 1993; Andriessen et al. 1993). Both records face significant chronologic challenges, however, namely the lack of sufficient independent, absolute age control for sections older than ~50 ka. Attempts at U-Th dating Lake Titicaca sediments yielded high scatter, and the interval beyond ~122 ka relies on tuning down-core peaks of calcium carbonate to the Antarctic CO_2 record (Fritz et al. 2007). In the Bogotá Basin, zircon fission-track ages of volcanic ash beds showed heavy contamination with lacustrine deposits (Andriessen et al. 1993), and the most recent age models rely on tuning pollen peaks to orbital forcing, although it remains unclear whether the record is paced by precessional or obliquity cycles (Torres et al. 2013). By comparison, the chronology for Lake Junín is significantly more reliable, and it also fills an important spatial gap in coverage between the northern and southern tropical Andes.

Finally, many of the proxies that can be analyzed from Lake Junín sediments have well-established relationships to regional climatic phenomena. The connection between clastic inputs and glaciation in the Junín watershed is more direct than it is for Lake Titicaca, as no moraines have been identified in the Titicaca drainage basin that date to 30-60 ka and its depocenter is > 50 km from the lake shore (Fritz et al. 2010). The oxygen isotope composition of carbonates during interglacial intervals at Lake Junín also has a clear link to SASM strength and local P-E balance, and there are no other isotope records from tropical South America that are older than ~250 ka. As such, the long drill core record from Lake Junín offers ample opportunities to improve our understanding of tropical glaciation and monsoon strength on a variety of timescales.

1.5 Objectives and outline of dissertation

This dissertation aims to improve our understanding of late Quaternary climate change in tropical South America via multi-proxy investigation of the Lake Junín sediment record during three key time periods: the deglacial interval and Holocene, the last glacial period, and Marine Isotope Stages 12-15. Chapter 2 focuses on the past 25 ka, a period characterized by a complex sequence of climatic changes associated with the most recent deglaciation and transition into the Holocene. Using the series of eight transect cores spanning from the shallow eastern lake margin to the depocenter, stratigraphic transitions and unconformities were targeted for radiocarbon dating to assess changes in depositional environment and to construct a lake level curve. Results indicate that the Junín watershed was mostly deglaciated by 18 ka, before the rise in global temperatures and greenhouse gases, which was likely due to a series of dry periods that contributed to glacial retreat. During Heinrich Stadial 1, an interval that should be associated with greater precipitation in tropical South America, Lake Junín indicates a delayed onset of wetter conditions that appears to be consistent with records from the Altiplano and Cariaco Basin. Improved dating of the late deglacial and early Holocene section indicates that the abrupt positive isotopic excursion that is observed in many records from the region likely occurred earlier than previously thought, possibly during the Younger Dryas. Finally, lake level dropped by as much as 8 m in the early Holocene, indicating that reduced monsoon strength during this time had profound effects on P-E balance at Junín.

Chapter 3 examines glacial-era climate variability during the last 50 ka, an interval that underwent major millennial scale temperature fluctuations that affected high latitude regions and the tropics alike. Proxies for clastic mineral inputs to Lake Junín are used in conjunction with organic matter content and stratigraphy to reconstruct changes in glacial erosion of bedrock in the surrounding valleys that coincide with lake level variations. A well-dated chronology based on 79 radiocarbon ages allows for precise correlation of the Junín record with other prominent records including Greenland ice cores and speleothems. The results demonstrate repeated episodes of glacial retreat during D-O interstadials as well as reductions in the level of Lake Junín, evidenced by the formation of peat layers. Taken together, these findings indicate rapid shifts to drier conditions in the Peruvian Andes coincident with abrupt warming events in the North Atlantic region. This scenario is consistent with studies showing intervals of reduced SASM strength linked to a northward shift of the ITCZ and enhanced overturning circulation in the Atlantic. Furthermore, the results provide compelling evidence for reduced precipitation in the Peruvian Andes, which had previously been inferred from speleothem isotope records that reflect upstream convective activity in the Amazon Basin.

Chapter 4 explores two complete glacial/interglacial cycles (MIS 12-15) that occurred from 420-620 ka. This time period is of interest because it is characterized by smaller amplitude variations in ice volume and greenhouse gases compared to more recent glacial cycles. However, this interval has not been investigated in detail in South America because very few records are long enough to cover it, so Lake Junín provides a rare case study into how the tropical Andes respond to long-term global climate forcings. Proxies for glacially eroded clastic inputs and organic content are used to infer changes in ice volume and lake level during glacial periods, and variations in oxygen and carbon isotopes further help to characterize monsoon strength during interglacials. Results indicate that MIS 12 was a period of major glacial expansion and stable lake levels, whereas MIS 14 experienced smaller ice advances and repeated episodes of lower lake level suggesting greater climatic instability. Interglacial MIS 15 displays very large amplitude changes in SASM strength that follow precession, and the stratigraphy confirms major fluctuations in lake level. In contrast, MIS 13 appears drier and displays no apparent precessional forcing, a surprising result that suggests alternative controls on SASM strength. Together, the findings reveal considerable diversity among glacial and interglacial periods at Lake Junín. Finally, chapter 5 briefly summarizes key findings and reflects on directions for future work.

2.0 Hydroclimate and lake level in the central Peruvian Andes during the last deglaciation and Holocene

2.1 Introduction

The period of time since the last glacial maximum (LGM) is of widespread interest to the paleoclimate community because the global climate system underwent major reorganizations that altered oceanic and atmospheric systems (Toggweiler 2009; McManus et al. 2004) and hemispheric temperature patterns (Broecker 1998; Barker et al. 2009). The relative impacts of Northern Hemisphere (NH) and Southern Hemisphere (SH) climate changes on tropical regions during the last deglaciation are the subject of ongoing investigation (Pedro et al. 2016; Martin et al. 2020; Jomelli et al. 2014) given the role of the tropics in bridging the two hemispheres, and because of the implications for monsoon systems and associated precipitation patterns. Monsoon records from the SH are relatively rare but critically important for understanding how tropical climate and hemispheric energy balance have varied over time.

Hydroclimate archives from South America have provided significant insight into the spatial and temporal expression of climatic changes since the LGM. The deglacial history of the tropical Andes, based primarily on lake sediment reconstructions and cosmogenic exposure dating of moraines, reveals a complex sequence of changes in ice margins during this period with episodes of glacial advance and retreat at times in and out of phase with temperature trends in the higher latitudes (Martin et al. 2018; Smith et al. 2005; Shakun et al. 2015; Bromley et al. 2016; Zech et al. 2009). The deglacial period is also characterized by a series of abrupt, millennial scale changes in the strength of the South American Summer Monsoon (SASM) that are well resolved in some high resolution speleothem (Novello et al. 2017; Cheng et al. 2013; Mosblech et al. 2012) and lake sediment records (Baker et al. 2001). These hydroclimatic variations have been linked to changes in the Atlantic Meridional Overturning Circulation (AMOC) (McManus et al. 2004; Lynch-Stieglitz 2017) and resultant shifts in the mean position of the Intertropical Convergence Zone (ITCZ).

The changing influences of both temperature and precipitation throughout this interval complicates our understanding of deglacial climate variability in the tropics. For example, the timing of glacial readvances on the Altiplano during the Heinrich 1 cold interval (18-14.6 ka) (Martin et al. 2018; 2020) corresponds with the paleolake Tauca highstand (Placzek et al. 2006; 2013), suggesting both occurrences may be related to an increase in SASM precipitation (Martin et al. 2018), but speleothems from the western Amazon and central Peruvian Andes do not support a stronger SASM during this time (Cheng et al. 2013; Kanner et al. 2012). Likewise, the climate signature of the Younger Dryas (YD, 12.9-11.7 ka) in tropical South America remains uncertain. Some speleothems suggest increased SASM strength during the YD (Deininger et al. 2019), but the timing and spatial pattern of Andean ice margin fluctuations remain the subject of considerable debate (Rodbell and Seltzer 2000; Kelly et al. 2012; Rodbell et al. 2009; Mark et al. 2017).

Well-dated lake sediment records can overcome some of the limitations of existing studies, namely the discontinuous nature of moraine chronologies, and they integrate changes throughout the broader watershed to provide insights into local precipitation-evaporation (P-E) balance. Here we present a sedimentary perspective from Lake Junín in the central Peruvian Andes from 25 ka to the present. Junín is downstream from the formerly glaciated valleys of the Eastern Cordillera and has been shown to document changes in paleoglacier extent during the last glacial cycle (Seltzer et al. 2000; Smith et al. 2005; Woods et al. 2020). Furthermore, the lake water in this semi-closed basin is sensitive to the strength of the SASM as well as evaporation (Seltzer et al. 2000), such that it experiences variations in lake level on a seasonal basis (Flusche et al. 2005) as well as during the millennial scale climate events of the last glacial period (Woods et al. 2020).

A series of eight transect cores spanning from the depocenter to the shallow eastern lake margin were collected from Lake Junín to characterize spatial and temporal patterns of sedimentation across the basin. An age model was developed for a continuous composite core from the depocenter, and unconformities and stratigraphic transitions in all cores were targeted for radiocarbon dating to assess the timing of lake level fluctuations. Stable oxygen and carbon isotopes of authigenic carbonate were measured along with bulk sediment properties, magnetic susceptibility (MS), and elemental data from scanning X-ray fluorescence (XRF). By coupling the record of variations in glacially-eroded clastic material to Lake Junín with visible changes in the composition and stratigraphy of the sediment, as well as dated unconformities in shore-proximal transect cores, we assess the relationship between glacier history, lake level, and local P-E balance during the last deglaciation and the Holocene.

2.2 Site description and regional climate

Lake Junín is a large semi-closed lake located at 4100 m asl in the central Peruvian Andes (Figure 3). The basin occupies a depression between the Eastern and Western Cordilleras, with the bathymetry characterized by a gently dipping slope from NE to SW. The shallow eastern side of Lake Junín is confronted by a dozen fluvio-glacial outwash fans emanating from southwest-facing valleys of the Eastern Cordillera, indicating that alpine glaciers repeatedly advanced towards the lake margin. However, ^{10}Be exposure ages from lateral and terminal moraines indicate that the lake has not been overridden by ice for at least the past million years (Smith et al. 2005).

The shallow depth (maximum 12 m) and large surface area (280 km^2) of Lake Junín makes the isotopic composition of its water (and authigenic calcite precipitated from the lake water) sensitive to evaporation and changes in lake level, which today can drop by 1-2 meters during years of drought (Flusche et al. 2005; Seltzer et al. 2000). The δ^{18}O value of the modern lake water ranges from -7 to -10‰, compared to -13 to -15‰ for stream waters in the catchment, reflecting a pronounced evaporative influence (Flusche et al. 2005). Likewise, carbonate δ^{18}O values throughout the Holocene are 4-6‰ more positive relative to nearby open basin lakes and speleothems (Bird et al. 2011; Kanner et al. 2013). Lake Junín occupies the Puna grasslands ecoregion where groundwater-fed cushion peatlands are located in depressions and along the margins of rivers and streams and are characterized by high organic matter content (Salvador et al. 2014; Squeo et al. 2006). The lake morphometry is influenced by a dense perimeter of interconnected wetlands and floating sedge mats that fluctuate in response to changes in lake surface area.

Precipitation in tropical South America is sourced primarily from the tropical Atlantic Ocean and transported to the Andes via the easterlies (Garreaud et al. 2009; Vera et al. 2006). A majority of rainfall reaching the Junín region occurs during the austral summer wet season in association with the SASM (Zhou and Lau 1998; Vuille et al. 2012; Maslin and Burns 2000), with less than 7% falling during the dry season according to unpublished rainfall data (1916-1998 *CE*) for La Oroya, Peru (Servicio Nacional de Meteorologia e Hidrologia del Peru, Ministeria del Ambiente). While the ITCZ is a distinct entity from the SASM, the southward shift of the ITCZ following the region of warmest sea surface temperatures during the austral summer contributes to the moisture advected to the South American continent (Vuille et al. 2012; Marengo et al. 2012). The δ^{18}O of precipitation in tropical South America is primarily interpreted to reflect the intensity of convection in the core monsoon region of the Amazon Basin and the degree of rainout during vapor transport (Vuille and Werner 2005; Lee et al. 2009; Samuels-Crow et al. 2014). Other factors can also play a role, including changes in the $\delta^{18}O$ of source waters, moisture recycling, seasonality, and cloud type (Vuille and Werner 2005; Konecky et al. 2019; Sturm et al. 2007), but they are generally of secondary importance especially on paleo-timescales.

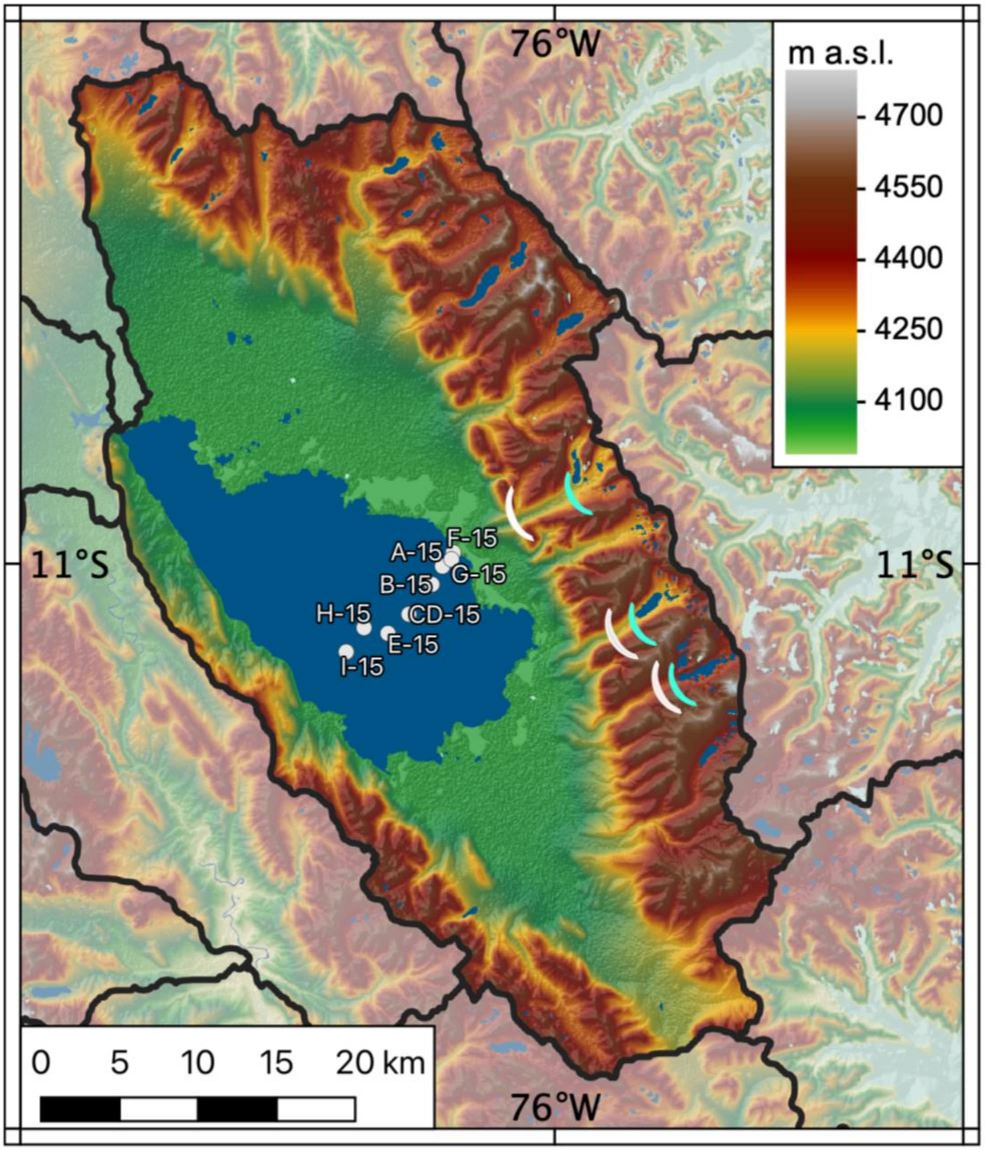

Figure 3. Lake Junín watershed and locations of transect cores. White ellipses denote the positions of moraines that date to the last glacial maximum (34-22 ka), and light blue ellipses denote the positions of moraines that date to 20-16 ka, based on Smith et al. (2005).

2.3 Methods

2.3.1 Sediment coring

The Lake Junín Drilling Project recovered a ~100 m sediment sequence from the depocenter of the lake in 2015, with the upper ~6 m from this location collected using a Livingstone corer to minimize disturbance in the upper unconsolidated sediments. A series of eight additional cores (A-15 through I-15) were collected across a NE-SW transect spanning the shallow lake margins to the depocenter to examine late glacial and Holocene changes in sediment composition and water level (Figure 3, Table 1). The upper cores were overlapped by 15 cm until the holes were cased and advanced by recovery. Composite core C-15/D-15 (referred to as C/D henceforth) is the exception, wherein two adjacent cores were collected so that overlapping sections could be spliced together for a continuous composite core sequence.

Table 1. Locations and depths of transect cores

Core	Water depth (m)	Latitude	Longitude	Sediment depths recovered (mblf)
A-15	2.84	-11.00145	-76.06550	0.00-9.05
B-15	5.95	-11.01181	-76.07165	0.00-8.95
C-15	8.56	-11.02893	-76.08503	0.00-7.74
D-15	8.50	-11.02895	-76.08500	0.65-7.35
E-15	8.82	-11.03984	-76.09728	0.00-8.38
F-15	1.81	-10.99362	-76.05917	0.19-0.98
G-15	2.42	-10.99751	-76.06025	0.18-2.07
H-15	8.14	-11.03664	-76.11124	0.16-8.26

2.3.2 Physical and geochemical analysis

All cores were sampled volumetrically (1 cm^3) at 2.5 cm intervals, dried at 60°C and weighed for bulk density, and subsequently burned for loss on ignition (LOI) (Heiri et al. 2001) for 4 hours at 550°C to estimate total organic matter content and for 2 hours at 1000°C to estimate total inorganic carbon content. Weight percentage total organic carbon (TOC) was estimated as LOI 550°C *0.40002 to reflect the molar ratio between TOC and organic matter. Weight percentage $CaCO_3$ was estimated as LOI 1000°C *2.273 to reflect the molar ratio between $CaCO_3$ and CO_2. Weight percentage residual mineral matter was estimated as 100 – (LOI 550°C + (LOI 1000°C *2.273)). Biogenic silica content was measured for 65 samples obtained randomly from all facies in the drill cores and the average weight percentage is 0.92 ± 1.12% and thus negligible so we did not include it in the residual mineral matter calculation.

Magnetic susceptibility was measured at 2 mm intervals with a custom Bartington-Tamiscan system. LOI and MS analysis was performed at the University of Pittsburgh. XRF scanning of the C/D composite core was performed at the LacCore XRF Lab, University of Minnesota-Duluth Large Lake Observatory using a Cox Analytical ITRAX with a Cr tube, 5 mm resolution, and 15 second dwell time.

Stable carbon and oxygen isotopes were measured on bulk carbonate samples every 1 cm. Samples were measured via a Thermo Gas Bench II connected to a Thermo Delta Advantage mass spectrometer in continuous flow mode at Union College. Reference standards (LSVEC, NBS-18, and NBS-19) were used for isotopic corrections, and to assign the data to the appropriate isotopic scale using linear regression. The following values were used for $\delta^{13}C$ and $\delta^{18}O$ respectively: LSVEC: -46.6‰, -26.7‰; NBS-18: -5.014‰, -23.2‰; and NBS-19: +1.95‰, -2.2‰. The combined uncertainty (analytical uncertainty) for $\delta^{13}C$ is ± 0.03‰ (VPDB) and $\delta^{18}O$ is ± 0.05‰ (VPDB), based on 11 NBS-19 standards over 3 analytical sessions.

2.3.3 Chronology

Plant macrofossils were isolated from all cores for radiocarbon age determination. Samples and standards were chemically pretreated according to standard protocols (https://sites.uci.edu/keckams/files/2016/12/aba_protocol.pdf), vacuum sealed, and combusted at the University of Pittsburgh, and graphitized and dated by accelerator mass spectrometry at the W.M. Keck Carbon Cycle AMS facility at the University of California, Irvine. Bayesian age-depth modeling for the C/D core was performed using the IntCal20 calibration curve (Reimer et al. 2020) and the R software package Bacon v2.5.1 (Blaauw and Christen 2011) with the following settings: acc.mean = 20 yr cm^{-1}, acc.shape = 1.5, mem.strength = 4, mem.mean = 0.7, and thick = 5 cm. Estimated mean ages are extrapolated from 6.675 mblf to the base of core C-15 D10 at 7.645 mblf.

2.4 Results

2.4.1 Composite core and chronology

A composite core was developed using adjacent overlapping sections from cores C-15 and D-15 in 8.53 m water depth (Weidhaas 2017). The C/D composite core is integrated with the long record from Drill Site 1 (Hatfield et al. 2020) and was used for the age-depth model (Figure 4, Table 2), and therefore serves as the backbone for the interpretations in this study. Radiocarbon ages from the other transect cores are used to constrain the ages of facies transitions and unconformities and were not incorporated into individual age models for those cores (Table 3).

The chronology for the C/D composite core is based on a combination of previously published (Weidhaas 2017; Woods et al. 2020) and new radiocarbon ages (Table 2), with a total of 38 ages spanning the upper 6.675 m of sediment. Six ages with errors >200 yrs indicating excessive sample contamination introduced during the pretreatment and/or graphitization processes were excluded from the age model, as was a single age representing a major reversal; these samples are marked with asterisks in Table 2. Calibrated median ages and their 95% probability ranges are rounded to the nearest 5 yr for ages <1,000, the nearest 10 yr for 1,000-10,000, the nearest 50 yr for 10,000-20,000, and the nearest 100 yr for >20,000 (Stuiver and Polach 1977).

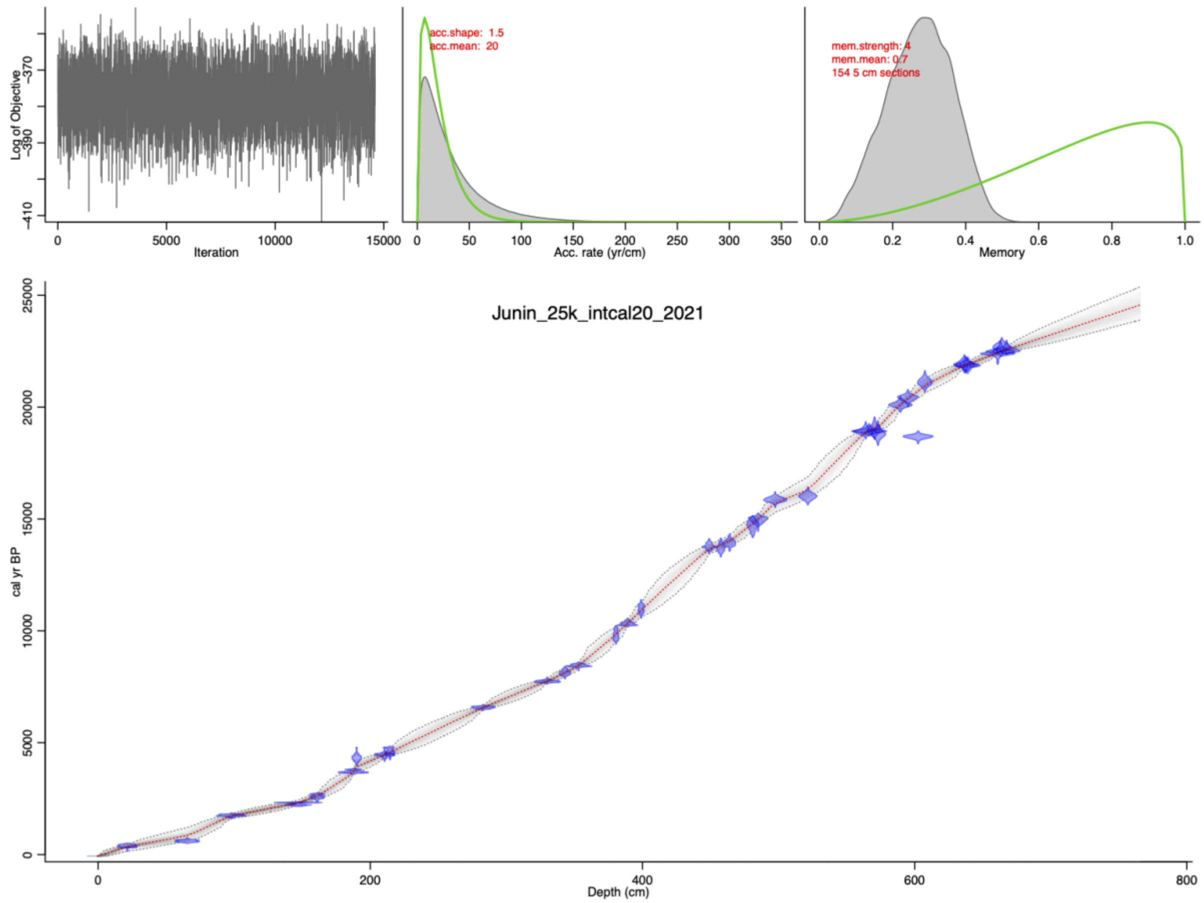

Figure 4. Age-depth model for the C/D composite core. The age model is based on 38 radiocarbon ages in the upper 6.68 m of sediment, and was generated using the R software package Bacon.

2.4.2 Stratigraphy

Changes in the stratigraphy of the Lake Junín sediment cores over the past 25 ka are characterized using core descriptions and physical and geochemical data that allow identification of ten lithologic units, described in order of appearance in the C/D composite core from the base to the sediment-water interface (Figure 5). The locations and water depths of the transect cores are listed in Table 1. To simplify discussion, the term "deep water cores" refers to I-15, H-15, E-15 and C/D-15, which were collected in 6.6-8.8 m of water in July-August of 2015 and are stratigraphically similar to each other. "Intermediate water cores" refers to B-15 and A-15, which were collected several km further east in 2.8-5.9 m of water and show distinct sedimentology as well as unconformities. "Shallow water cores" G-15 and F-15 were collected within 2 km of the eastern shore in 1.8-2.4 m of water, are significantly shorter and contain several substantial unconformities. The stratigraphic units discussed in the following sections refer primarily to those identified in the C/D core and their depths are expressed in meters below lake floor (mblf).

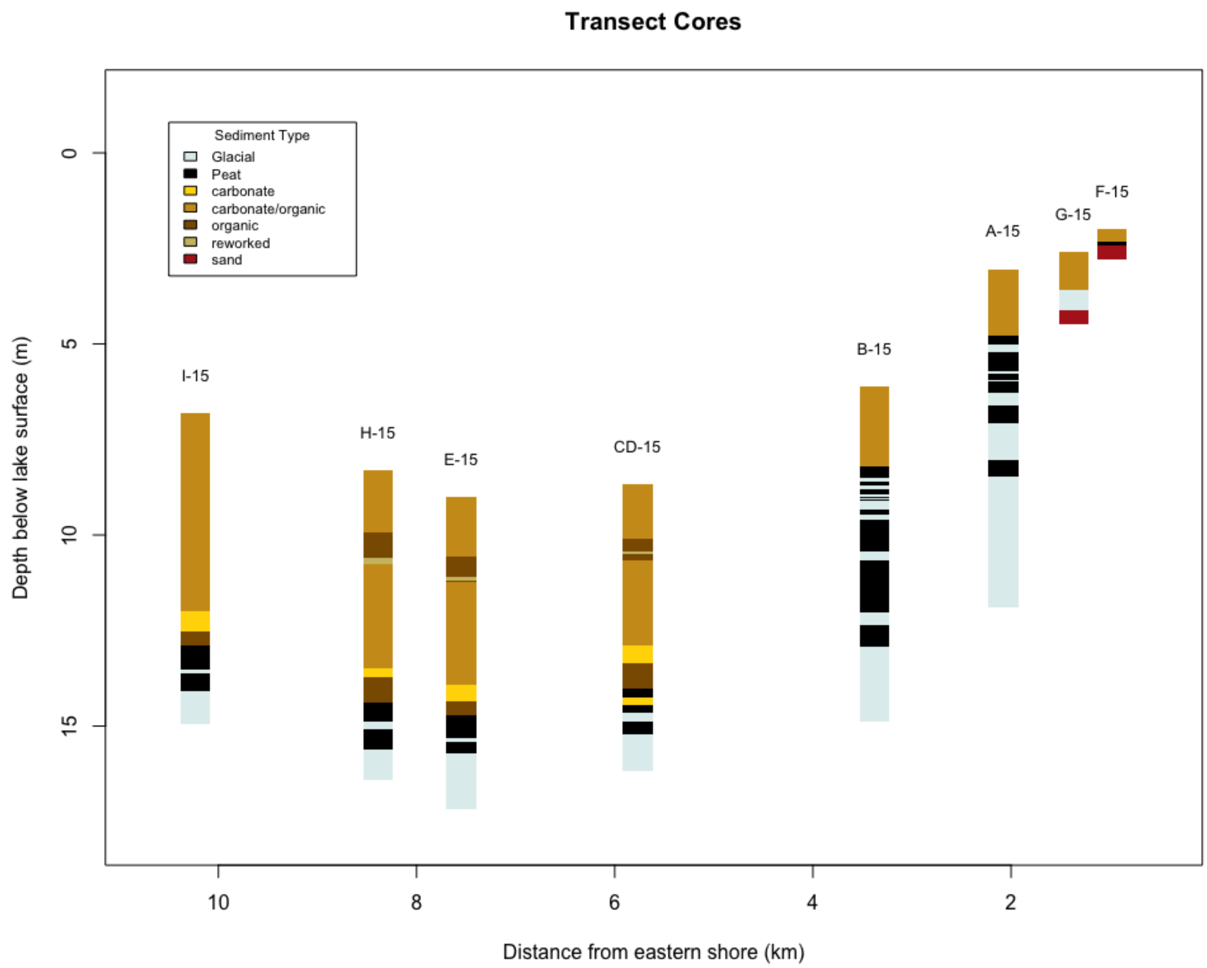

Figure 5. Stratigraphy of the transect cores. The deep water cores (I-15, H-15, E-15, CD-15) are similar to each other and capture the end of the LGM, alternating glacial silt and peat units during the deglacial phase, and Holocene carbonates, with no identifiable unconformities. The intermediate water cores (B-15, A-15) show a much thicker sequence of peat and glacial silt accumulation, and unconformities indicate that only part of the Holocene carbonate interval is present. The shallow water cores (G-15, F-15) capture only limited portions of the late glacial and Holocene.

2.4.3 Unit 1 (7.65-6.67 mblf)

Unit 1 extends from the base of C/D to 6.67 mblf and corresponds to the interval > 22.6 ka. The sediment consists of homogenous, gray glacial silt with high levels of MS, residual mineral content, and Ti and Si counts (Figure 6, Figure 7). Carbonate content is low and organic matter content is very low. This unit is present in transect cores from both intermediate and deep water sites, but absent in shallow water cores G-15 and F-15 indicating either that lake level was too low for deposition at those locations or that subsequent lowering of lake level resulted in removal of this unit by erosion.

2.4.4 Unit 2 (6.67-6.37 mblf)

Unit 2 extends from 6.67-6.37 mblf in core C/D, corresponding to 22.6-21.9 ka. The sediments are black to very dark brown with moderate organic content and very low carbonate. Abundant macrofossils such as charcoal and grass indicate encroachment of the surrounding peatlands toward the depocenter. Two samples that correspond to unit 2 yield C/N values of 15.3 (6.55 m) and 16.8 (6.63 m). Abrupt decreases in Ti, Si, and MS mark the first instance of declining glacial erosion after the Local Last Glacial Maximum (LLGM). The residual mineral content remains high in unit 2, suggesting either that glaciers had not retreated past the up-valley lakes that serve as local sediment traps, or that erosion of alluvial fans at the edge of the lake continued. No apparent unconformities are observed in the intermediate or shallow water cores.

2.4.5 Unit 3 (6.37-6.13 mblf)

Unit 3 spans 21.9-21.15 ka. It initially consists of grey glacial silt which develops more distinct laminations upwards that range in color from yellow to brown. High levels of MS, Ti, Si, and residual mineral material are diluted somewhat in the second half of unit 3 when carbonate content increases moderately. Organic content remains very low in the C/D core. The appearance of unit 3 in the intermediate-water core A-15 differs from the deeper cores, with fluctuating darker and lighter banding and considerably thicker sediment accumulation, likely reflecting closer proximity to the glacial source and the shifting boundary between peatlands and open water. Radiocarbon ages from cores B-15 and A-15 corroborate the timing of the end of unit 3 around 21 ka.

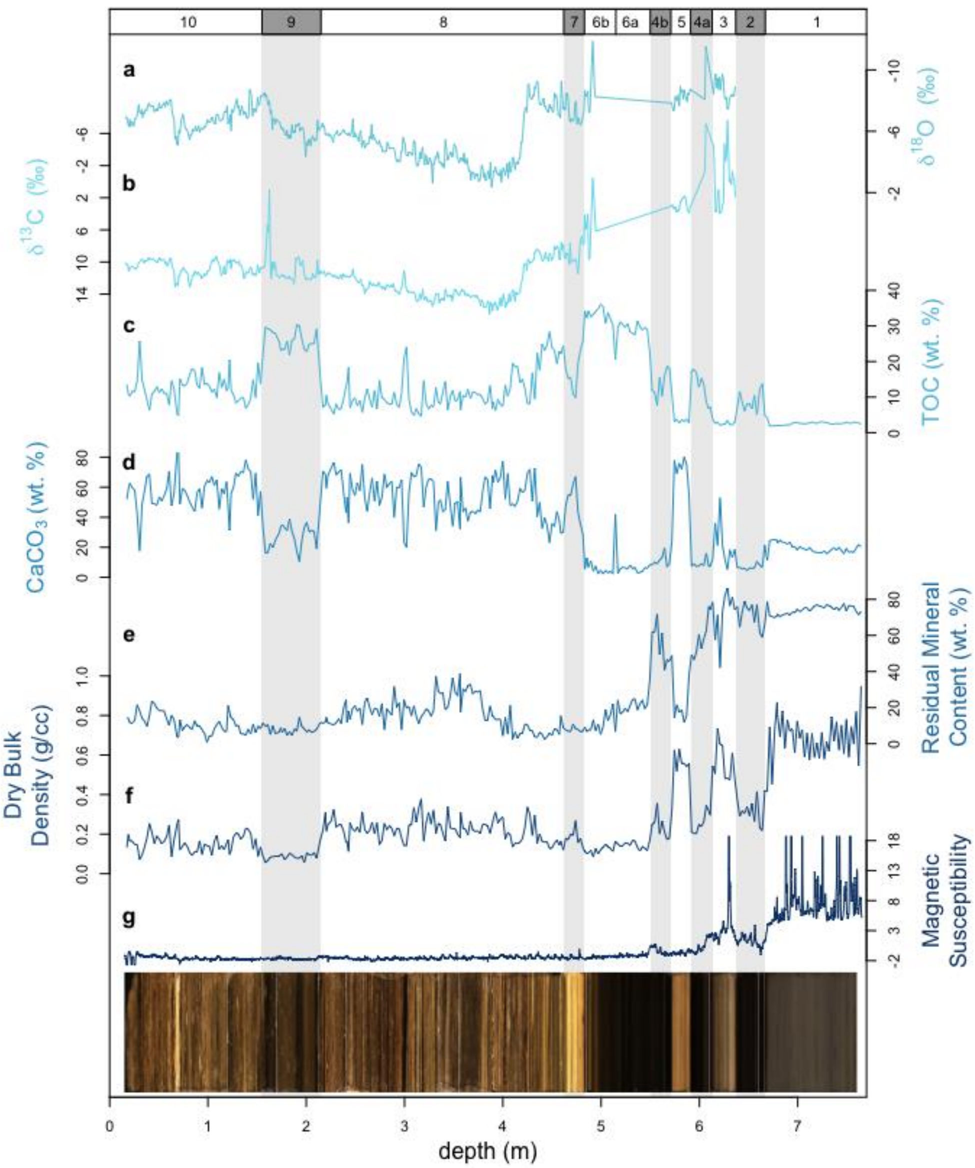

Figure 6. Bulk sediment properties and isotopic data for the C/D composite core. a, oxygen isotope values (‰, VPDB), b, carbon isotope values (‰, VPDB), c, total organic carbon content (wt. %), d, calcium carbonate content, e, residual mineral content (%), f, sediment dry bulk density (g/cm^3), and g, magnetic susceptibility (S.I.). Bottom: high resolution linescan image of the core. Unit identification labels along the top axis delineate the lithologic units discussed in the text.

2.4.6 Unit 4 (6.13-5.91, 5.71-5.5 mblf) and unit 5 (5.91-5.71 mblf)

Unit 4 has a unique expression in the C/D core, in that it is interrupted by a carbonate-rich interval (unit 5) that is not observed in any other transect cores. As such, in core C/D we subdivide this deposit into subunit 4a (6.13-5.91 mblf, 21.15-20.2 ka) and subunit 4b (5.71-5.5 mblf, 19.1-18.0 ka). Both subunits appear black to very dark grey and contain elevated levels of Ti, Si, and residual mineral matter, moderate organic content, and low carbonate content.

Unit 5 (5.91-5.71 mblf, 20.2-19.1 ka) consists of yellow to light tan carbonate and shows mm- to cm-scale laminations. The contacts at the base and top of unit 5 are abrupt and clean. The sediment is low in organic content and contains a small residual mineral component. Unit 5 is not a coring artefact because it is replicated in both the C and D cores, but its absence in all other transect cores suggests anomalous depositional conditions that apparently affected a relatively small portion of the basin.

In the other deep-water cores, unit 4 (e.g., ~21-18 ka) is a single, uninterrupted interval with similar sedimentology that spans less than 0.5 m. In the intermediate water cores this interval is associated with up to 2 m of deposition, which is likely a function of their proximity to the glacial outwash fans and suggests that a large proportion of clastic mineral material was deposited in nearshore locations. Unit 4 marks the final observation of glacially generated clastic inputs reaching the basin's depocenter.

2.4.7 Unit 6 (5.5-4.82 mblf)

Unit 6, from 18.0-14.6 ka, is an interval of sustained high organic content with very low carbonate and low levels of clastic indicators (Ti, Si, MS, residual mineral matter) indicating that glaciers had retreated upvalley behind moraine-dammed lakes. While the bulk sediment properties remain stable throughout unit 6, the appearance of the sediments undergoes a distinct shift. Unit 6a (5.5-5.17 mblf) consists of banded layers that are several cm thick and range from black to dark grey. The transition to unit 6b at 5.17 mblf (16.2 ka) is characterized by a shift to dark grey sediments with cm to sub-cm-scale laminations, > 80% organic matter, and a smoother, gelatinous consistency compared to unit 6a. Around 4.96 mblf (15.6 ka), occasional lighter tan banding occurs but the carbonate content remains low. Plant macrofossils are relatively sparse from 18-15.6 ka. A sample from 5.17 mblf equivalent depth in unit 6a yields a C/N value of 6.2 suggesting high algal content and consistent deep-water conditions. Unit 6 in the other deep-water cores has a similar character and appearance as in C/D. This unit is not apparent in intermediate water cores A-15 and B-15, wherein all the high-organic, low-carbonate sediments also have high mineral content.

2.4.8 Unit 7 (4.82-4.37 mblf)

Unit 7, from 14.6-13.0 ka, consists of bright yellow to light tan sediments with alternating smooth to laminated texture and a gelatinous consistency similar to that of unit 6b. It contains moderate to high carbonate, low to moderate organic content, and low mineral content. Unit 7 is similar in appearance in the other deep-water cores where radiocarbon ages indicate it persisted until ~12.6 ka. The facies associated with unit 7 is absent in the intermediate water cores. The entire time interval is missing from B-15 according to an unconformity bracketed by ages of 15.3 and 9.66 ka. In A-15, this interval is associated with dark, organic-rich sediment and an unconformity in Drive 2 (D2) at 94 cm is bracketed by ages of 16.45 and 13.7 ka.

2.4.9 Unit 8 (4.37-2.12 mblf)

Unit 8, from 13.0-4.5 ka, is compositionally similar to unit 7 with moderate to high carbonate and low to moderate organic content, but the sediments are medium to dark brown, coarsely banded and show a distinctly mottled texture. Mineral content is slightly elevated and variable. Unit 8 has a similar appearance in all the deep-water cores and is the first unit with abundant visible mollusks/ostracods, suggesting that bioturbation and mixing may explain the mottled texture.

Several dated unconformities indicate that carbonate deposition associated with unit 8 is only partially captured in the intermediate and shallow water sites. In A-15 and B-15, carbonate overlies sediment that is high in both TOC and mineral content, whereas in the shallow water G-15 core it overlies dark red to dark grey coarse sand that is almost entirely minerogenic. Radiocarbon ages directly above the following unconformities document increases in lake level and resumed sedimentation after lowstands: 9.66 ka in B-15 D3 68 cm, 8.31 ka in G-15 D2 80 cm, 7.08 ka in A-15 D2 88 cm, and 7.02 ka in G-15 D1 88 cm.

2.4.10 Unit 9 (2.12-1.58 mblf)

Unit 9, from 4.5-2.55 ka, is marked by a distinct transition to dark brown and smoothly laminated sediments with a similar appearance and gelatinous consistency as unit 6b. It contains high organic content and low carbonate and mineral content. Mollusks remain abundant. In addition to the C/D core, this unit can be identified in the deep-water cores H-15 and E-15, all three of which are located in 8-9 m of water today, but is not apparent in the westernmost transect core, I-15, which is in 6.6 m of water. Unit 9 is also absent in the intermediate water cores but there is no stratigraphic or radiocarbon evidence for a corresponding unconformity.

A brief (<10 cm) interval resembling reworked material and rip up clasts is present in the middle of unit 9 in core D-15 from 1.9-1.97 mblf (3.9-4.1 ka); two other overlapping drives from the C/D core site also capture the reworked interval but it instead spans 20-30 cm. Potentially coeval reworked sediments are observed in cores E-15 and H-15 but are located at the base of unit 9 rather than the middle. This interval has been tentatively attributed to disturbance from tectonic activity in the basin (Weidhaas 2017) although little is known about past tectonic activity in this region.

2.4.11 Unit 10 (1.58-0.15 mblf)

Unit 10, from 2.55-0.23 ka, contains high carbonate and low to moderate TOC and is present in all transect cores except F-15. It ranges from light yellow to medium brown in color, with textures varying from mottled to banded with frequent mollusks.

Sediments in F-15, the shallowest core site, span the same time interval as unit 10 but differ markedly in appearance and composition. The lowermost unit (>1.94 ka) is coarse black sand with abundant mollusks, overlain unconformably by a black organic-rich unit from 0.71-0.665 ka, followed by an uppermost mixed carbonate and organic-rich unit. Radiocarbon ages directly above the following unconformities in F-15 document increases in lake level and resumed sedimentation after lowstands: 0.71 ka in F-15 D1 44 cm and 0.54 ka in F-15 D1 33 cm.

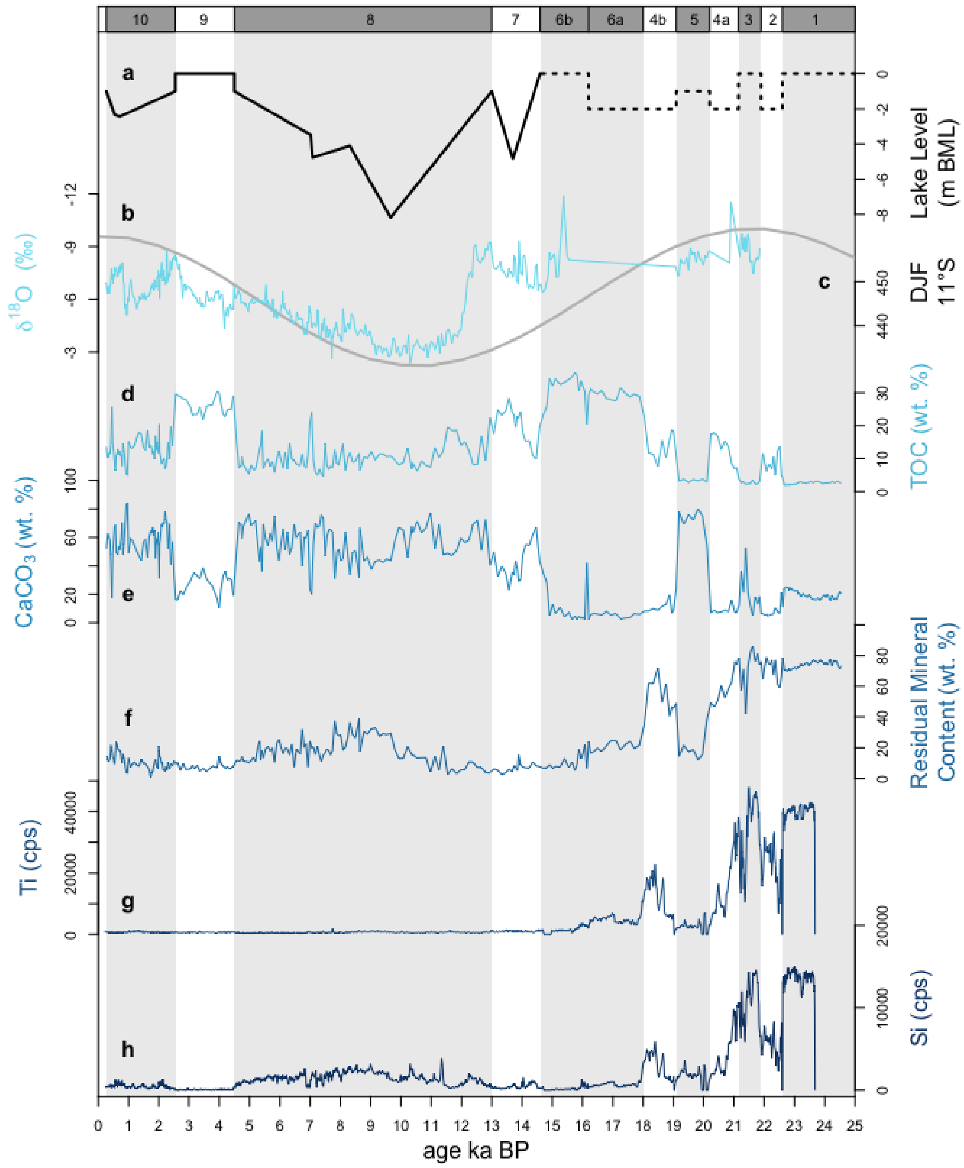

Figure 7. Lake Junín proxy data over the past 25 ka. a, lake level curve with dashed line indicating lake level inferred from stratigraphy and solid line indicating lake level inferred from unconformities, b, oxygen isotope values (‰, VPDB), c, summer insolation for Dec-Jan at 11°S, carbon isotope values (‰, VPDB), d, total organic carbon content (wt. %), e, calcium carbonate content (wt. %), f, residual mineral content (wt. %), g, Ti (cps), and h, Si (cps).

2.5 Discussion

2.5.1 Sedimentology of the Lake Junín transect cores

There is no evidence of major unconformities or erosional surfaces in the Lake Junín C/D composite core. The transitions between units are generally distinct and horizontal and the high density of radiocarbon ages do not indicate any prolonged intervals of discontinuous sedimentation. Most of the sediment units described for the C/D core have clearly identifiable equivalents in the other three deep water cores that were recovered in ~6-9 m of water (Figure 5). These units are of similar thickness and the radiocarbon ages are remarkably consistent among all four cores. Therefore, we assume that the C/D composite core captures the complete deglacial and Holocene sequence and is reflective of depocenter conditions across a large portion of the lake.

In contrast, the intermediate water cores differ markedly in appearance, length, and composition. Of the ~9 m of sediment recovered in A-15 and B-15, the lower ~7 m are mineral-rich (30-80% residual mineral content) with moderate and variable organic matter content and moderate to low carbonate content (Figure 5). The sediments are generally dark with gradual transitions between poorly defined units. The upper ~2 m of carbonate-rich sediment in each core sits unconformably above a clastic unit, indicating prolonged episodes of exposure and erosion during the late deglacial to early-Holocene. The shallow water cores G-15 and F-15 span only 2 m and 1 m, respectively, and preserve several unconformities indicating these locations were sub-aerially exposed more often than they were submerged. Dark, clastic-rich sediment in G-15 intermittently covers short intervals dating to the deglacial and early Holocene before transitioning to upper carbonate-rich sediments, while the clastic and organic-rich sediments in F-15 span only the last 2 ka (Figure 5).

2.5.2 Interpretation of clastic sediment inputs to proglacial Andean lakes

Previous studies in the tropical Andes have established that the primary control on the delivery of clastic sediment to proglacial alpine lakes is the extent of up-valley ice cover (Abbott et al. 2003; Rodbell et al. 2008; Stansell et al. 2005). Glacially eroded clastic sediment yield is greatest during times of advancing ice and reduced during periods of glacial retreat, in part because of the short response time of precipitation-sensitive tropical glaciers to changes in mass balance (Kaser et al. 2003). While active erosion by growing glaciers generates higher sediment flux, the ice melt and increased runoff during periods of glacier recession also yield a transient sediment discharge, leading to a temporal offset in sediment flux during this paraglacial sediment phase (Church and Ryder 1972; Rodbell et al. 2008). However, for small, warm-based tropical glaciers this time lag is expected to be brief, as the constant melting of basal ice and resultant water drainage limits the amount of clastic material accumulating beneath the glacier. Furthermore, the close proximity between Lake Junín and catchment glaciers, as well as the paternoster, moraine-dammed lakes that serve as local sedimentary traps up-valley, limits the amount of fine-grained sediment buildup and storage on the landscape and makes the Junín record especially sensitive to initial ice retreat. As such, we assume that any lag between the initiation of glacier retreat and subsequent decrease in sediment yield occurs well within the century-scale uncertainty of our age model and is thus negligible to our interpretations.

Seltzer et al. (2000) demonstrated the strong coupling between ice extent and deposition of glacial flour in Lake Junín during the last glacial cycle based on the sediment magnetic susceptibility and established that clastic sediment input is limited to intervals during which paleoglaciers are present in the basin. XRF count rates of erosional elements such as redox-insensitive titanium have also been demonstrated as effective, high-resolution proxies for glacial erosion of bedrock and lithogenic sediment transfer to lakes related to glacier mass turnover (Bakke et al. 2009). Counts of Ti and Si were used to demonstrate the rapid retreat of glaciers in the Junín basin in response to reduced precipitation during the Dansgaard-Oeschger (DO) warmings of the last glacial period (Woods et al. 2020). In the current study, MS and scanning XRF data backed by lower resolution residual mineral content of the bulk sediment provide a record of relative changes in paleoglacier mass balance during the last deglaciation. Accordingly, the large decrease in MS, Ti and Si values in the C/D core at 18 ka and the continued low levels thereafter indicates the cessation of glacially eroded clastic inputs to the depocenter and suggests that glaciers had fully retreated behind the up-valley moraine-dammed lakes (Figure 7, Figure 8).

Precipitation amount and lake level variations can also control clastic inputs to lakes independent of glaciers. These processes continued to play a role at Junín after the final deglaciation of the catchment, evidenced by the low to moderate and variable levels of residual mineral matter throughout the late deglacial and Holocene in the deep-water cores. This influence is especially apparent in the intermediate and shallow water cores more proximal to the mineral sediment source, which show highly elevated residual mineral content well after glaciers had disappeared from the basin.

These clastic inputs were likely sourced from nearby poorly consolidated alluvial fan material, and/or the sub-aerial exposure and erosion of previously submerged deposits following decreases in lake level. It is likely that a majority of clastic sediment fell out of suspension within the first several km of the lake shore, and only the finer-grained material continued to reach the depocenter. The differences in magnitude and timing of mineral inputs across the transect cores reveals the importance of water depth and proximity to the shoreline in controlling clastic sedimentation throughout the lake basin.

2.5.3 Interpretation of organic matter and carbonate content in Lake Junín sediments

Visibly prominent in the Junín record during the last glacial period is a series of dark, organic-rich sediment layers that coincide with DO interstadials and are interpreted to reflect episodes of peat accumulation during lake lowstands (Woods et al. 2020). This facies is also observed during the deglacial interval. Units 2 and 4, which contain 20-40% organic matter and 60-80% mineral matter, display abundant visible macrofossils and are rich in partially degraded plant material. Unit 6a is otherwise similar but contains 70-80% organic content and 20% mineral content owing to the cessation of glacial inputs by that time (Figure 6). These layers are interpreted as peat-rich sediment deposits following studies of the modern vegetation and soil characteristics of ecosystems in this region of the Andes.

Cushion peatlands, known in South America as bofedales, are a type of high-altitude wetland restricted to elevations above 3800 m that are characterized by a variety of cushion-forming plant species underlain by soil with high organic carbon content (Squeo et al. 2006; Fonkén 2014). Owing to their porous nature and dense growth structure, cushion peatlands serve a regulatory function in the local hydrologic cycle by storing runoff and suppressing evaporation (Earle et al. 2003). As such, they are sensitive to physical disturbances and hydrologic changes (Earle et al. 2003; Squeo et al. 2006; Hartman et al. 2016). Dry periods tend to diminish the protective vegetation cover, reducing the water storage capacity of the underlying soil and leading to increased erosion (Schittek et al. 2012). A study looking at human disturbance to peatlands in the Junín National Reserve and surrounding areas observed dried out cushions and physical evidence of peat erosion when peatlands are drained, resulting in lower organic matter content of the peatland soil samples (Salvador et al. 2014).

The appearance and characteristics of the organic-rich layers in the deep-water cores from Lake Junín suggest they are derived from erosion of the surrounding peatlands during dry intervals, rather than *in situ* peat formation in the lake depocenter. Attempts at radiocarbon dating bulk sediments from the peat-rich intervals resulted in near-complete dissolution of the samples after exposure to 1M NaOH during pretreatment and yielded a dark brown solution indicative of strong leaching of soil humics (Olsson 1986), consistent with a study suggesting that degree of humification is a good indicator for identifying Andean peatland sediments (Salvador et al. 2014). Furthermore, the upper and lower boundaries of the peat-rich sediment layers are distinct suggesting that root structures did not develop *in situ* that might otherwise blur the stratigraphic transitions. As such, we suggest these layers were deposited during intervals of lower lake level that resulted in drying of peatlands surrounding the lake margins and enhanced erosion of the underlying soils.

In contrast, units 6b and 9 also contain elevated organic matter content (60-85%), but they instead have a gelatinous consistency, display visible banding and occasional laminations and contain fewer macrofossils. These units are interpreted to reflect predominantly algal organic matter deposition during lake highstands. This interpretation is supported by C/N ratios of bulk sediment, wherein $C/N > 20$ suggests a greater proportion of terrestrial source inputs, while $C/N < 10$ suggests greater aquatic source inputs (Meyers and Teranes 2001). All ten samples from the last 25 ka have C/N values < 20, indicating no occurrences of exclusively terrestrially sourced organic matter. However, samples associated with units 2 and 4a (peat layers) have C/N values of 12.9 and 10.6, respectively, suggesting mixed terrestrial and aquatic inputs, whereas a C/N value of 6.2 associated with unit 6b suggests dominantly aquatic organic inputs.

Finally, high authigenic carbonate content is observed during interglacial intervals when the influx of glacial silt is cut off (Seltzer et al. 2000; Chen et al. 2020; Hatfield et al. 2020). Owing to the Paleozoic-Mesozoic marine limestones and dolostones comprising the majority of bedrock in the Junín watershed (Cobbing et al. 1981), all major input streams to the lake are supersaturated with respect to carbonate (Flusche et al. 2005). The carbonate-rich sediments of the late deglacial and Holocene also contain variable levels (~20-60%) of organic content that likely reflects a mix of terrestrially and aquatically sourced organic matter.

2.5.4 Lake level curve

A lake level curve was developed for Junín (Figure 7) by integrating facies changes identified in the deep-water cores with the character and timing of stratigraphic transitions and erosional unconformities at intermediate to shallow water coring sites. Lake level estimates are referred to in meters below modern level (m BML) in July/August 2015 when the cores were recovered. Because the level of Lake Junín varies on seasonal to interannual timescales today (Flusche et al. 2005) and is further modified by water storage and release associated with the Upamayo Dam (Martin et al. 2001), the lake levels suggested here should be considered relative estimates rather than absolute values. For intervals where the lake level estimate is pinned to an unconformity, the depth of the unconformity in the sediment core was added to the water depth at that coring location.

The stepwise shape of the curve from ~14-25 ka reflects the absence of unconformities that can be linked to the units in the deep-water cores, and lake level changes during this interval are instead inferred from sedimentological indicators of the depositional setting and regional hydroclimate. Glacial silt units 1 and 3 indicate glacial advance and regionally wetter conditions, suggesting the lake level may have been as high as modern (0 BML) during their deposition. In contrast, the peat-rich sediments of units 2 and 4 suggests the lake lowered enough to dry out the cushion peatlands surrounding the lake margins, allowing for enhanced erosion of the underlying soils. We cannot know precisely how much the lake dropped, and the intermediate and deep-water core sites did remain submerged, but conditions were likely relatively drier compared to the intervals before and after the peat-rich units. As such, we suggest a tentative estimate of 2 m BML for units 2 and 4 based on the range of lake level variations today (Flusche et al. 2005; Martin et al. 2001). The residual mineral content suggests ice was still present in the watershed but likely at a reduced extent because glacially eroded inputs tail off sharply after the end of unit 4 (Figure 7).

The interim period of carbonate deposition associated with unit 5 indicates possible seasonal lowering of lake level that resulted in concentration of solutes, but not enough to cause peat accumulation, so a lake level of 1 m BML is estimated. Unit 6 is split into two subunits based on the appearance and texture of the organic-rich sediments. The dark, crumbly, and macrofossil-rich sediments of unit 6a resembles the peat layers of units 2 and 4 and is therefore also assigned a lake level estimate of 2 m BML. In contrast, the gelatinous texture and sparse macrofossils of unit 6b suggests algal origins for the organic matter and a possible highstand that may have inhibited carbonate deposition, so a lake level of 0 m BML is estimated.

The first major dated unconformity occurs during unit 7. The entire time interval is missing from B-15 according to an unconformity bracketed by ages of 15.3 and 9.66 ka. In A-15, the interval is associated with dark, organic-rich sediment and an unconformity bracketed by ages of 16.45 and 13.7 ka suggests that lake level rose above 4.83 m BML by 13.7 ka.

Unit 8, which spans most of the Holocene, contains several unconformities in the intermediate and shallow water cores. Radiocarbon ages directly above the following unconformities document increases in lake level and resumed sedimentation after lowstands: above 8.18 m BML after 9.66 ka (B-15), above 4.1 m BML after 8.31 ka (G-15), above 4.77 m BML after 7.08 ka (A-15), and above 3.48 m BML after 7.02 ka (G-15).

Unit 9 resembles unit 6b in that it contains laminated, organic-rich sediments with a gelatinous texture that is likely of algal origin. The fact that this sedimentology is absent in the intermediate water cores (Figure 5) but there is no evidence for a corresponding unconformity suggests that a depositional environment with deeper water was required for its formation. As such, we assign a lake level of 0 m BML. In unit 10, radiocarbon ages directly above the following unconformities in shallow water core F-15 document increases in lake level and resumed sedimentation after lowstands: above 2.44 m BML after 0.71 ka, and above 2.33 m BML after 0.54 ka.

2.5.5 The local LGM and deglaciation of the Junín watershed (25 – 18 ka)

Unit 1 captures the final phase of the LLGM, when glacial advances resulted in a large pulse of homogenous fine-grained silt with nearly 80% mineral content. The timing of this sediment pulse is consistent with the advanced positions of terminal moraines in the Junín basin (to within 10 km of the modern shoreline) that date to 34-22 ± 6.4 ka (Smith et al. 2005), and a mean age of 25.1 ka (SD 4.0) for groups of LGM moraines from several other localities throughout tropical Peru and Bolivia (Mark et al. 2017).

The Junín record is notable for its association with an early onset of deglaciation indicated by declines in MS and Ti in the sediment record beginning ~22.5 ka (Figure 8) (Seltzer et al. 2000; Seltzer et al. 2002; Woods et al. 2020) as well as moraines associated with retreating ice margins beginning around ~21 ka (Smith et al. 2005). Early deglaciation in the tropical Andes was initially linked to early warming (Seltzer et al. 2002) indicated by limited evidence from an Antarctic ice core temperature record that preceded NH warming by several thousand years (Blunier et al. 1998). This stands in contrast to moraine records from many mid- to high-latitude sites that place the onset of NH deglaciation around 19-20 ka (Clark et al. 2009). Moraine records from elsewhere in Peru also indicate that deglaciation was underway by ~20 ka (Shakun et al. 2015; Bromley et al. 2016; Smith and Rodbell 2010), before the end of the global LGM and before the onset of the deglacial CO_2 rise ~18 ka

(Marcott et al. 2014). Subsequent Antarctic ice core records indicate the magnitude of warming was modest before 18 ka (WAIS Divide Project Members et al. 2015), so the trigger for early tropical deglaciation remains unclear (Shakun et al. 2015) and may vary regionally.

More recently, the early onset of deglaciation in the Junín region was attributed to drying because the initial reductions in clastic inputs to Lake Junín coincide with peat layers indicating lower lake level (Woods et al. 2020). According to this interpretation, the sediments of units 2 and 4 are associated with intervals of drought that resulted in reductions in both paleoglacier mass balance and the size of Lake Junín. These drought episodes are interrupted by mineral-rich sediments in unit 3 indicating a glacial readvance at Junín from ~22-21 ka (Figure 7). Notably, the millennial scale dry events in the Junín record from ~23-18 ka are also observed in a speleothem from Pacupahuain cave, only ~25 km from Junín (Kanner et al. 2012). The evidence for drought implies that regional forcing related to reductions in SASM strength initially drove the early deglaciation at Junín prior to global temperature forcing. This deglacial variability is absent in other South American speleothems, which show stable values from the LGM until the development of Heinrich Stadial 1 (Deininger et al. 2019). This may be a function of their lower temporal resolution through this interval, or the dry events may have been localized to a relatively limited region of the high elevation Andes.

The final observation of elevated mineral inputs and Ti levels at Junín is associated with the unit 4b peat interval (~19-18 ka). A radiocarbon age of 18.7 ka directly above an apparent unconformity in G-15 suggests that lake level may have dropped as low as 4.24 m BML before this time, and the overlying sand-rich sediments point to a higher-energy, shoreline depositional setting consistent with continued lower lake level thereafter. Given the apparently dry conditions at Junín, the clastic inputs from 19-18 ka may have been associated with either a glacial standstill or retreat and continued erosion of alluvial fan material. A review of cosmogenic nuclides ages from Peru and Bolivia suggests a mean age of 18.9 ka (SD of 0.5) for post-LGM boulders associated with moraine abandonment in the region (Mark et al. 2017). The end of unit 4b marks the final deglaciation ~18 ka, after which any remnant glaciers in the Junín basin were restricted to elevations > 4250 masl behind moraine-dammed lakes. As such, deglaciation of the Junín basin was relatively rapid, from 22.6-18 ka according to our age model, and took place amid relatively cold conditions at high latitudes of both hemispheres (Figure 8) (WAIS Divide Project Members et al. 2015a; Andersen et al. 2006; Svensson et al. 2008), although higher elevation valleys in the southern tropical Andes remained glaciated after this time.

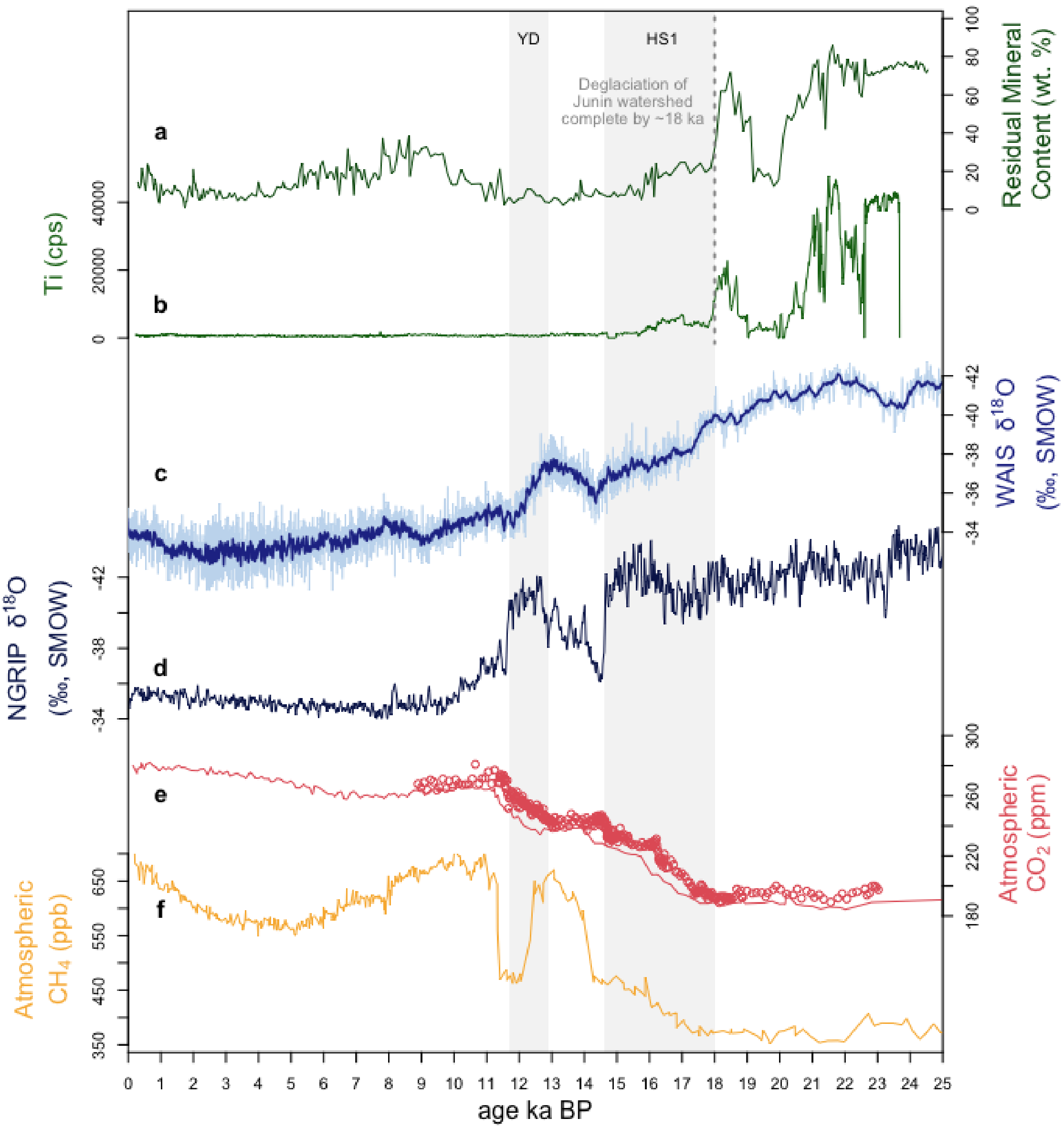

Figure 8. Deglaciation of the Junín watershed. Deglaciation was largely complete by ~18 ka, before the increase in global temperature and rise in atmospheric greenhouse gas levels. a, Junín residual mineral content, b, Junín Ti levels, c, Antarctic ice core $\delta^{18}O$ values (WAIS Divide Project Members, 2013), d, Greenland ice core $\delta^{18}O$ values (Svensson et al., 2008), e, CO_2 concentration from EPICA (line) (Lüthi et al., 2008) and WAIS Divide (circles) (Marcott et al., 2014), f, CH_4 concentration from EPICA (Loulergue et al., 2008). Grey shaded bars indicate the Younger Dryas and Heinrich Stadial 1.

2.5.6 Heinrich Stadial 1 (18-14.6 ka)

The interval from 18-14.6 ka broadly coincides with Heinrich Stadial 1, a period of cooler sea surface temperatures in the North Atlantic (Bard et al. 2000), cooler surface temperatures over Greenland (Andersen et al. 2006; Svensson et al. 2008; Rasmussen et al. 2014), rising temperatures in the Southern Hemisphere (WAIS Divide Project Members et al. 2015a), and a major reduction in AMOC strength (McManus et al. 2004). Numerous records indicate drier conditions in the northern tropics (Wang et al. 2001; Peterson et al. 2000; Escobar et al. 2012, Deplazes et al. 2013), and wetter conditions throughout much of southern tropical South America (Cruz et al. 2005; Arz et al. 1998; Placzek et al. 2006; Portilho-Ramos et al. 2017; Wang et al. 2004; Mosblech et al. 2012), consistent with a southward ITCZ shift that is predicted for this period (Schneider et al 2014; McGee et al. 2014).

In the Junín record, H1 is associated with unit 6, a broad interval of highly elevated organic matter content that is notable for several reasons. First, unit 6 is the first organic-rich interval with minimal clastic inputs reaching the depocenter, suggesting the Junín watershed is mostly deglaciated by 18 ka. Second, the dark, macrofossil-rich sediments of unit 6a (18-16.2 ka) suggest peat accumulation and lower lake level during the first half of H1, whereas the laminated, algal-rich sediments of unit 6b (16.2-14.6 ka) suggest higher and more stable lake level thereafter. Finally, it is important to note that there is no evidence for unconformities during this interval.

The available high-resolution records from the South American monsoon domain reveal a complex spatial and temporal expression of H1 (Figure 9). The major decrease in AMOC strength that persists across all of H1 coincides, with nearly identical timing, to the increase in Fe/Ca ratios observed in Amazon Fan sediments in the equatorial Atlantic that suggests a sustained precipitation increase in the Andes (Zhang et al. 2017). Speleothems from sites in northeast, central, and southeast Brazil display lower $\delta^{18}O$ values at the onset of H1 (Stríkis et al. 2015; 2018; Cruz et al. 2005; Novello et al. 2017) indicating a widespread increase of monsoon precipitation in the region of the South Atlantic Convergence Zone (SACZ), although there is a double-plunge structure observed in two records from Brazil suggesting a brief return to drier conditions in mid-H1 (Stríkis et al. 2015; Novello et al. 2017). In contrast, speleothems from the western Amazon do not show a pronounced negative excursion, with El Condor cave indicating stable $\delta^{18}O$ values and Cueva del Diamante actually showing an increase in $\delta^{18}O$ across H1 (Cheng et al. 2013). Pacupahuain Cave in central Peru displays an abrupt positive $\delta^{18}O$ excursion before terminating in the middle of H1 (Kanner et al. 2012).

While an increase in precipitation at the beginning of H1 (~18 ka) is implied by some of the above records, several glacial and lacustrine records from the Andes indicate a delayed onset of wetter conditions with a major climatic shift closer to 16 ka. To the south of Junín on the Altiplano (15.5°S to 22.5°S), the giant paleolake Tauca (52,000 km^2) developed during H1 with the transgression beginning around 18 ka, but the highest stand was synchronous with H1a dating to ~16.5-14.5 ka, (Sylvestre et al. 1999; Placzek et al. 2006; Blard et al. 2011; 2009). Major glacial readvances or standstills are recorded around 16-15 ka in the surrounding valleys, coeval with the highstand (Blard et al. 2011; Placzek et al. 2013; Martin et al. 2018; 2020). Other valleys in Peru and Bolivia also provide moraine evidence for glacial advances during H1 (Smith et al. 2008; Blard et al. 2009; 2011) with a mean cosmogenic nuclide age of 16.1 ka (SD 1.1) (Mark et al. 2017).

The observation of glacial advances throughout the tropical Andes during H1, when Junín was mostly deglaciated, is not surprising given its elevation. Lake Junín, at 4100 masl, has maximum headwall elevations of 4700 masl, making it more sensitive to ELA shifts than the other glaciated systems which have summit elevations ranging from ~5300 to ~6500 masl. The Antarctic ice core indicates warmer temperatures during H1 than any time in the 18-50 ka interval (WAIS Divide Project Members et al. 2013), suggesting that Southern Hemisphere warming may explain why Junín remained deglaciated after 18 ka.

The timing of lake level changes at Junín appears roughly consistent with the moisture conditions on the Altiplano. The lake remained lower during the first half of H1 (unit 6a, 18-16.2 ka), followed by lake level increase during the second half (unit 6b, 16.2-14.6 ka). The magnitude of the precipitation increase over the Altiplano was likely much greater and has been attributed to a southward shift of the Bolivian High drawing in additional moisture from the SACZ as well as rainfall amplification in the center of paleolake Tauca (Martin et al. 2018). The reason for the delayed onset of wetter conditions in the Andes is unclear given the large decrease in AMOC strength at the onset of H1 (McManus et al. 2004), which is expected to produce a relatively rapid southward shift of the ITCZ (McGee et al. 2014). Interestingly, the Cariaco Basin record also indicates an abrupt southward ITCZ shift at ~16.2 ka based on optical sediment lightness (Deplazes et al. 2013), which is nearly identical to the timing of wetter conditions at Junín. It is notable that the coldest temperatures in the Greenland ice core were reached from ~16-14.5 ka (Andersen et al. 2006; Svensson et al. 2008), suggesting the greatest inter-hemispheric temperature contrast occurred during the second half of H1 (Figure 9). This may have drawn the ITCZ further southward and contributed to the observed moisture pattern.

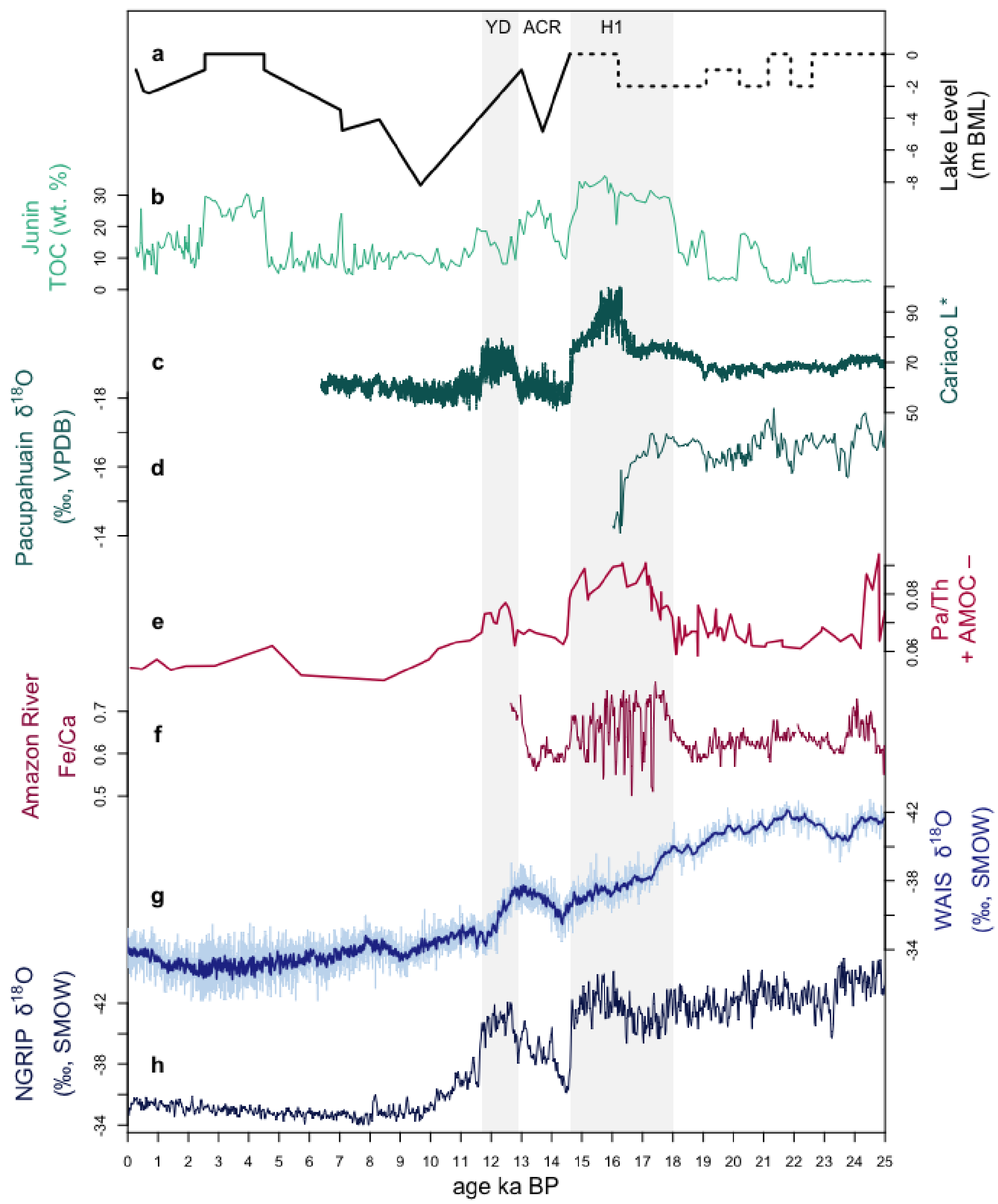

Figure 9. Different moisture patterns during Heinrich Stadial 1. Records from Lake Junín, Cariaco Basin, and Pacupahuain Cave indicate drier conditions in South America during the first half of Heinrich Stadial 1 and wetter conditions during the second half. a, Junín lake level, b, Junín TOC content with peat accumulation initially, followed by an organic-rich unit of algal origin suggesting a highstand, c, Caricao Basin sediment lightness indicates the ITCZ was further south during the second half of H1 (Deplazes et al., 2013), d, Pacupahuain Cave $\delta^{18}O$ (Kanner et al., 2012), e, AMOC strength indicated by Pa/Th ratios (McManus et al., 2004), f, Amazon Fan Fe/Ca (Zhang et al., 2017), g, Antarctic ice core $\delta^{18}O$ (WAIS Divide Project Members, 2013), g, NGRIP ice core $\delta^{18}O$ (Svensson et al., 2008).

2.5.7 The Antarctic Cold Reversal (14.6 – 13.0 ka)

The ACR is a period of cooling in the SH, from 14.7-13 ka based on an Antarctic $\delta^{18}O$ stack (Pedro et al. 2011) that interrupted the warming trend during deglaciation. Many regions of the Andes saw a large glacial advance during the ACR (Rodbell et al. 2009; Jomelli et al. 2014; Mark et al. 2017), a response that was common to both the northern and southern tropical Andes. Simulations suggest the advance occurred in response to cold SSTs in the SH (Jomelli et al. 2014), in line with a compilation of marine and terrestrial records indicating cooling from low to high latitudes across the SH (Pedro et al. 2016). There is no evidence for glacial readvance in the Junín sediment record, and moraines in the upper valleys of the Junín watershed are all older than the ACR (Smith et al. 2005a; Smith et al. 2005b) suggesting the cooling was insufficient to support glacial advance at more moderate elevations such as the Junín watershed with headwalls of ~4700 m. Antarctic ice cores indicate that temperatures during the ACR still remained warmer than they were during MIS 2 and 3 (WAIS Divide Project Members et al. 2013).

The ACR interval is termed the Bølling-Allerød (BA) interstadial in the NH, where it was associated with abrupt warming of ~10°C in Greenland (Buizert et al. 2014). Numerous speleothem records indicate reduced SASM strength during this time (Cruz et al. 2005; Mosblech et al. 2012; Novello et al. 2017; Stríkis et al. 2015; 2018; Cheng et al. 2013), suggesting in-phase behavior with the North Atlantic region and consistent with proxy evidence for increased AMOC strength at the BA transition (McManus et al. 2004). The Junín record is in fairly good agreement with the hydrologic pattern indicated by these terrestrial records: the increase in carbonate content around 14.6 ka may be an initial response to drier conditions that facilitated carbonate ion saturation, and an unconformity in core A-15 points to a major drop in lake level prior to ~13.7 ka, in agreement with the speleothem evidence for reduced SASM strength. These results are also consistent with the near complete disappearance of Lake Tauca between 14-13 ka (Blard et al. 2011; Martin et al. 2020). The $\delta^{18}O$ values from Lake Junín are more positive at the onset of the ACR and show a slight decreasing trend thereafter, broadly consistent with the timing of the unconformity, although they remain fairly negative especially compared to the early Holocene. This may in part reflect reduced evaporation under regionally cooler temperatures.

2.5.8 The Younger Dryas (12.9-11.7 ka)

The Younger Dryas (YD) is associated with abrupt cooling in the NH (Alley 2000) and a slowdown of AMOC, although to a lesser degree than during H1 (McManus et al. 2004; Lynch-Stieglitz 2017). Cooling was greatest in the North Atlantic and smaller in regions further away, resulting in an estimated global mean cooling of 0.6°C (Renssen et al. 2018; Shakun and Carlson 2010). The combined North Atlantic cooling and AMOC configuration during the YD has been linked to a southward shift of the ITCZ (Peterson et al. 2000; Portilho-Ramos et al. 2017; Haug et al. 2001), although hydroclimate records from tropical South America show a complex spatial and temporal expression during the YD. The highstand of Altiplano paleolake Coipasa (32,000 km^2) was tentatively dated to 13-11 ka initially (Placzek et al. 2006), with subsequent dating improvements placing this wet interval from 12.5-11.9 ka (Blard et al. 2011) and 12.9-11.8 ka (Martin et al. 2020), roughly synchronous with the timing of the YD. Lake level estimates from Lake Titicaca based on carbon isotope transfer functions indicate lake level as high as modern or a slight lowering during the YD, depending on method (Rowe et al. 2002). Wetter conditions at Titicaca are also supported by a minimum of benthic diatom abundance and maximum of freshwater diatoms from 13-11.5 ka (Baker et al. 2001). In the central Andes of Peru, well-dated moraines indicate a significant but short-lived glacial advance at the onset of the YD, followed by retreat throughout much of the remainder (Rodbell et al. 2009). Integrated moraine ages and lake sediment data from the Cordillera Blanca, Peru also indicate the YD was a phase of retreating ice margins, possibly due to a shift to drier conditions (Stansell et al. 2017) and/or progressive warming (Jomelli et al. 2014).

In the Junín sediment record the onset of the YD coincides with the beginning of unit 8, characterized by high carbonate content and the development of a distinctly mottled texture. This stratigraphy continues into the early Holocene, such that the YD is not associated with a unique facies in the Junín sediments. The $\delta^{18}O$ record from Lake Junín, on the other hand, indicates that major changes in SASM strength and P-E balance occurred during the YD. Negative $\delta^{18}O$ values persist from ~13-12.4 ka, suggesting wetter conditions in the first half of the YD. A sharp, ~5‰ increase in $\delta^{18}O$ values occurs from 12.4-11.7 ka, after which positive and relatively stable values persist through 9 ka, indicating a drier early Holocene (Figure 10). A very similar positive excursion is also observed in nearby Andean $\delta^{18}O$ records from Lake Pumacocha (Bird et al. 2011), the Huascaran ice core (Thompson et al. 1995), and unpublished isotope data from the Piuray paleolake outcrop (M. Abbott, personal communication), although the shift instead occurs after the YD according to those age models which are not as well constrained as the new Junín age model. The excursion is also seen in a pair of speleothems (El Condor and Diamante) from the western Amazon, where it occurs after ~12.5 ka (Cheng et al. 2013) (Figure 10).

The unmistakable similarity of this isotopic trend among multiple records suggests a common forcing mechanism, but the inconsistent timing among records precludes any robust attribution. The Pumacocha age model is poorly constrained during this interval, relying on a single basal radiocarbon age of ~11.6 ka, and the Huascaran ice core age model tunes the isotopic excursion to the timing of the YD in the layer-counted GRIP and GISP2 ice cores in Greenland. As such, neither of these age models can be considered reliable during this interval. The speleothem age models are more robust, with four U/Th ages spanning from 10.2-13.9 ka for Diamante and seven U/Th ages spanning from 10.58-13.4 ka for El Condor. Similarly, the Lake Junín age model incorporates seven radiocarbon ages from 10.25-13.9 ka. The age model for the 1996 core from Lake Junín also suggests an earlier onset to the isotopic excursion (Seltzer et al. 2000).

The YD in the tropical Andes is clearly complex, with hydroclimate records from the Altiplano consistently indicating wetter conditions, whereas the $\delta^{18}O$ records discussed here show a major, progressive drying with uncertain timing. The stronger chronologies and closer timing of the isotopic excursion in the Junín and speleothem records suggests that it may have occurred during the YD rather than the early Holocene as previously thought. If correct, this suggests an opposite moisture pattern in central and northern Peru compared to the Altiplano, but there is no obvious climatic forcing at this time that explains the drying. As pointed out by Bird et al. (2011), the isotope excursion is not clearly linked to precessional forcing because it occurs more rapidly compared to the gradual changes in insolation, and this would be true regardless of the precise timing of the event. Additional well-dated and moisture-sensitive records spanning this interval would help in characterizing the timing and geographic pattern of the YD in the tropical Andes.

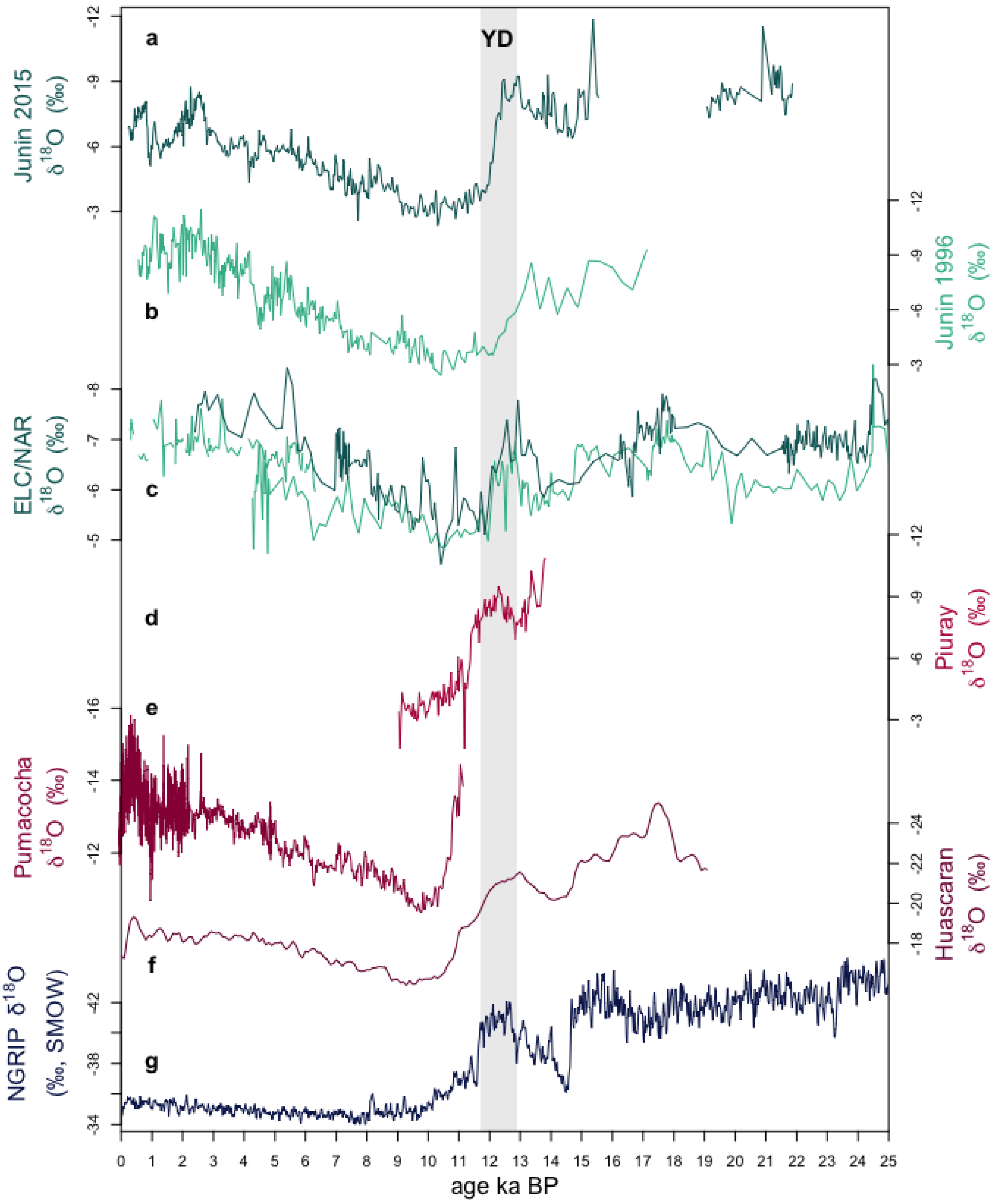

Figure 10. Timing of the early Holocene isotopic excursion. Stable isotope records from South America document an abrupt positive shift in $\delta^{18}O$ values that occurs sometimes between the Younger Dryas and early Holocene, but the timing is widely disputed. a, Lake Junín core collected in 2015, b, Lake Junín core collected in 1996 (Seltzer et al., 2000), c, speleothems from the western Amazon (El Condor Cave (ELC) is lighter green, Diamante Cave (NAR) is darker green) (Cheng et al., 2013), d, Piuray paleolake outcrop (M. Abbott, personal communication), e, Lake Pumacocha (Bird et al., 2011), f, Huascaran ice core (Thompson et al., 1995), and g, Greenland ice core (Svensson et al., 2008).

2.5.9 Hydroclimate trends during the Holocene

The main feature of Andean isotopic records during the Holocene is the long-term decrease in $\delta^{18}O$ values that follows insolation (Bird et al. 2011; Seltzer et al. 2000; Kanner et al. 2013; Bustamante et al. 2016; Thompson et al. 1995; Abbott et al. 1997), indicating a gradual strengthening of the SASM and increased convection upstream (Vuille et al. 2012). This decline is also observed in speleothems from lower elevation sites in western Amazonia (van Breukelen et al. 2008) and southeast Brazil (Cruz et al. 2005).

The Junín lake level reconstruction is consistent with the isotopic evidence for a weaker monsoon in the early to mid-Holocene, with several unconformities in the intermediate and shallow water cores during that time. The most severe lowstand occurred before 9.66 ka when lake level dropped as much as 8 m BML, with additional unconformities suggesting more moderate reductions in lake level (~4 m BML) until 7.02 ka. This evidence for aridity is consistent with enhanced evaporation inferred by pairing the closed-basin, evaporation-sensitive Junín $\delta^{18}O$ record with that of Lake Pumacocha, a nearby open-basin system with short (<1 year) residence time that records the $\delta^{18}O$ of local precipitation (Bird et al. 2011). The $\delta^{18}O$ signature of modern lake water at Junín is ~6‰ more enriched than precipitation (Flusche et al. 2005), reflecting the effects of evaporation and residence time. The persistence of these effects throughout the Holocene is confirmed by the positive offset in Junín $\delta^{18}O$ values relative to Pumacocha $\delta^{18}O$ values. Notably, this offset is larger (~6‰) from 10.5-5 ka than it is after 5 ka (~4 ‰), suggesting a stronger evaporative influence during the early Holocene when the SASM was weaker.

The timing of Holocene lake level changes in the Andes has been the subject of considerable debate, along with the question of whether they can be explained by a single precession cycle (Abbott et al. 1997; 2003; Bird et al. 2011; Baker et al. 2001; Rowe et al. 2003). The observed aridity at Lake Junín, where the lowest lake levels occurred prior to 7 ka, is in agreement with dry conditions at Lake Chochos, Peru (7°S) from 9.5-7.3 ka (Bush et al. 2005) and a diatom record from Lake Pacucha (13°S) indicating a lowstand formed around 10 ka with a slight deepening after 8.3 ka (Hillyer et al. 2009). Other records suggest a delayed development of dry conditions, with greater lake level reductions during the mid-Holocene. A lowstand is identified at Lake Titicaca (16°S) from 7-4 ka based on seismic profiling (Seltzer et al. 1998) and sediment $\delta^{13}C$ (Rowe et al. 2003), and from 8.5-5 ka based on the fraction of shallow water diatoms (Baker et al. 2001), and Taypi Chaka KKota, Bolivia (16°S) shows a dry event from 6-2.4 ka (Abbott et al. 2003). Lake Pacucha (13°S) shows generally low and fluctuating lake levels until 5 ka with wetter conditions thereafter (Hillyer et al. 2009).

In general, more northerly Andean sites including Junín seemed to experience drying earlier, consistent with insolation forcing, whereas more southerly sites in the Altiplano region lagged behind the Holocene insolation minimum and instead show drier conditions during the mid-Holocene. It is notable that the mid-Holocene lowstand does not have a clear counterpart in the available isotope records that reflect SASM strength over a large region of continental South America. The records are generally in agreement that wetter conditions occurred sometime after ~5 ka (Thompson et al. 2006; Bird et al. 2011; Baker et al. 2001). The Junín lake level reconstruction is consistent with this trend, with an apparent highstand from 4.5-2.5 ka. Century-scale climatic events affecting SASM strength have been described in detail elsewhere (Bird et al. 2011; Bustamante et al. 2016; Kanner et al. 2013) and may account for some minor discrepancies between the Junín lake level curve and $\delta^{18}O$ record, but the overall Holocene trends in lake level, $\delta^{18}O$ values and insolation are consistent suggesting that precessional forcing of SASM strength is the major first-order control on Holocene P-E balance at Lake Junín.

Table 2. Radiocarbon ages for the Junín C/D composite core

UCI AMS#	Core-Drive	Core depth (cm)	Total depth (m)	Material	^{14}C age (BP)	±1σ	Median age (cal BP)	95% prob. lower range	95% prob. upper range
164796	C15-D1	6-7	0.215	charcoal	330	35	390	305	475
201049	C15-D1	50-51	0.655	charcoal	630	60	605	535	675
164797	C15-D2	16-17	0.980	charcoal	1815	20	1760	1710	1820
164798	C15-D3	16-19	1.470	charcoal	2275	25	2320	2170	2350
209665	C15-D3	23-24	1.610	charcoal	2510	35	2590	2490	2740
164802	D15-D3	16-19	1.875	charcoal	3440	25	3690	3620	3830
201050	D15-D3	19-21	1.900	charcoal	3900	80	4320	4090	4530
164803	D15-D3	39-42	2.105	charcoal	3990	45	4470	4300	4780
209668	D15-D3	44-45	2.145	charcoal	4060	70	4570	4420	4820
164799	C15-D6	9-12	2.830	charcoal	5775	25	6580	6500	6640
164800	C15-D6	56-59	3.300	charcoal	6915	30	7740	7680	7820
193150	1D-2H-2	10-13	3.430	charcoal	7310	90	8120	7970	8320
193151	1D-2H-2	21-22	3.530	charcoal	7645	50	8440	8380	8540
193101	D15-D6	41-42	3.805	plant macrofossil	8730	150	9790	9500	10190
201051*	C15-D7	10-11	3.840	charcoal	9100	230	10250	9560	11050
201052	C15-D7	21-23	3.890	charcoal	9145	50	10300	10200	10500
201053	C15-D7	31-33	3.990	charcoal	9670	120	11000	10650	11250
209666*	C15-D7	70-71	4.375	plant macrofossil	11670	230	13500	13100	14100
209667	C15-D7	81-83	4.490	plant macrofossil	11940	70	13750	13600	14000
193098	C15-D7	90-91	4.575	plant macrofossil	11860	130	13700	13450	14000
209669	D15-D7-1	42-44	4.640	plant macrofossil	12070	90	13900	13750	14150
201054	C15-D8	11-12.5	4.810	plant macrofossil	12500	45	14750	14350	15050
172568	1C-2H-1	35-36	4.850	plant macrofossil	12605	35	15000	14750	15150
201055*	C15-D8	16-17	4.855	plant macrofossil	12940	270	15450	14450	16250
201056*	C15-D8	21-22	4.905	plant macrofossil	13540	300	16350	15500	17250
193099	C15-D8	28-29	4.975	plant macrofossil	13200	40	15850	15700	16050
164801	C15-D8	51-54	5.215	plant macrofossil	13320	70	16000	15800	16250
193146	1C-2H-1	95-96	5.640	plant macrofossil	15670	80	18900	18750	19100
164804	D15-D8	41-44	5.665	plant macrofossil	15705	45	18950	18800	19100
193102	D15-D8	46-47	5.705	plant macrofossil	15740	120	19000	18750	19300
201057	D15-D8	48-50	5.730	plant macrofossil	15540	140	18800	18500	19100
193103*	D15-D8	62-64	5.870	plant macrofossil	16550	220	19950	19500	20500
193104	D15-D8	65-66	5.895	plant macrofossil	16675	45	20100	19950	20300
201058*	D15-D8	67-68	5.915	plant macrofossil	16150	420	19500	18650	20500
193147	1C-2H-1	127-128	5.950	plant macrofossil	16940	60	20400	20200	20600
193105	D15-D8	78-79	6.025	plant macrofossil	15420	60	18700	18550	18800
193106	D15-D8	83-84	6.075	plant macrofossil	17490	80	21100	20900	21400
193100	C15-D9	68-69	6.365	plant macrofossil	18100	60	21900	21700	22200
193148	1C-2H-2	19-20	6.375	plant macrofossil	18065	50	21900	21700	22100
164805	D15-D9	12-14	6.390	plant macrofossil	18055	45	21900	21700	22100
193149	1C-2H-2	44-45	6.610	plant macrofossil	18495	50	22400	22300	22500
164806	D15-D9	36-38	6.630	plant macrofossil	18660	60	22500	22400	22700
181187	1C-2H-2	47-48	6.640	plant macrofossil	18850	60	22700	22500	22900
193107**	D15-D9	41-42	6.675	plant macrofossil	13910	35	16850	16650	17050
201059	D15-D9	41-42	6.675	plant macrofossil	18715	45	22600	22400	22700

Note: asterisks denote ages excluded from the age model. * = large error (> 200 yrs), ** = major reversal.

Table 3. Radiocarbon ages for the Junín transect cores

UCI AMS#	Core-Drive	Core depth (cm)	Total depth (m)	Material	^{14}C age (BP)	±1σ	Median age (cal BP)
180969	A15-D1	72-74	0.930	plant macrofossil	3605	15	3910
180970	A15-D2	40-41	1.455	plant macrofossil	4425	15	5010
180971	A15-D2	85-86	1.905	plant macrofossil	6190	15	7080
180972	A15-D2	89-90	1.945	plant macrofossil	11870	25	13700
172556	A15-D2	97-98	2.025	plant macrofossil	13620	40	16450
180973	A15-D3	56-57	2.615	plant macrofossil	14845	25	18200
180974	A15-D4	68-69	3.735	plant macrofossil	17330	35	20900
180975	A15-D4	71-72	3.765	plant macrofossil	17295	30	20900
172557	A15-D5	13-14	4.185	plant macrofossil	17220	45	20800
209660	B15-D2	21.5-22.5	1.070	charcoal	3750	60	4110
209661	B15-D2	29-30.5	1.150	charcoal	3880	45	4310
193097	B15-D3	65-67	2.210	plant macrofossil	8725	25	9660
180976	B15-D3	69-70	2.245	plant macrofossil	12815	20	15300
180977	B15-D4	28-29	2.535	plant macrofossil	12990	25	15550
180978	B15-D4	92-93	3.175	plant macrofossil	13330	80	16050
180979	B15-D4	95-96	3.205	plant macrofossil	13365	25	16100
172558	B15-D6	48-50	4.440	plant macrofossil	15130	40	18500
180980	B15-D6	73-74	4.685	plant macrofossil	15900	30	19150
180981	B15-D6	77-78	4.725	plant macrofossil	15570	25	18850
172559	B15-D7	79-80	5.745	plant macrofossil	17180	45	20700
180982	B15-D8	9-10	6.045	plant macrofossil	13115	25	15700
209662	B15-D8	42-43	6.375	plant macrofossil	18240	1110	22000
209663	B15-D8	48-49_1	6.435	plant macrofossil	18080	110	22000
209664	B15-D8	48-49_2	6.435	plant macrofossil	18290	130	22200
172560	B15-D8	93-95	6.890	plant macrofossil	18805	50	22700
209670	E15-D2	64-65	1.625	charcoal	2230	30	2230
209671	E15-D2	70.5-72	1.690	charcoal	2340	45	2360
209672	E15-D2	78-79	1.765	charcoal	2670	80	2790
209673	E15-D3	60-61	2.435	charcoal	3920	40	4350
209674	E15-D4	31-32	2.895	charcoal	5030	80	5770
209675	E15-D5	30-31	3.685	charcoal	6850	90	7690
209676	E15-D5	72-73	4.105	charcoal	9000	190	10100
209677	E15-D6	68-70	5.070	charcoal	10750	170	12700
209678	E15-D6	94-95	5.325	charcoal	12430	320	14600
209679	E15-D7	10.5-12	5.490	plant macrofossil	13260	70	15950
209680	E15-D7	17.5-18.5	5.560	charcoal	13750	480	16650
172561	E15-D7	89-91	6.280	plant macrofossil	16745	45	20300
172562	E15-D8	50-51	6.885	plant macrofossil	18780	60	22700
193096	F15-D1	30-31	0.495	plant macrofossil	540	20	540
180983	F15-D1	34-35	0.535	plant macrofossil	705	15	665
181171	F15-D1	42-43	0.615	plant macrofossil	810	15	710
181172	F15-D1	45-46_1	0.645	plant macrofossil	2000	70	1940
181173	F15-D1	45-46_2	0.645	plant macrofossil	2265	20	2250
181174	G15 D1	50-51_1	0.685	plant macrofossil	4420	20	5000
181175	G15 D1	50-51_2	0.685	plant macrofossil	4170	20	4720
181176	G15 D1	52-53	0.705	plant macrofossil	4390	20	4940

Table 3 (continued)

181177	G15 D1	53.5-54.5	0.720	plant macrofossil	4360	15	4920
181178	G15 D1	55-56	0.735	plant macrofossil	4480	15	5190
172563	G15 D1	84-86	1.030	plant macrofossil	6135	25	7020
181179	G15 D1	90-91	1.085	plant macrofossil	7615	20	8400
181180	G15 D2	78-79	1.665	plant macrofossil	7485	20	8310
209681	G15 D2	81-82	1.695	plant macrofossil	9775	45	11200
181181	G15 D3	23-25	1.820	plant macrofossil	15350	60	18700
209682	H15 D3	11-12	1.775	charcoal	2470	70	2550
209683	H15 D3	46-47	2.125	charcoal	3060	80	3260
209684	H15 D5	20.5-21.5	3.470	charcoal	5650	80	6440
209685	H15 D6	32-33	4.585	charcoal	9130	330	10300
209686	H15 D7	7.5-8.5	5.340	charcoal	10610	80	12650
209687	H15 D7	52-53.5	5.790	charcoal	13290	520	15950
172564	H15 D8	26-28	6.530	plant macrofossil	16520	40	19950
209688	H15 D8	64-65	6.905	plant macrofossil	18400	360	22300
172565	H15 D8	91-92	7.175	plant macrofossil	18530	50	22400
209689	I15 D3	8-9	1.885	charcoal	4910	110	5660
209690	I15 D7	6-8	5.470	charcoal	11010	440	12900
209691	I15 D7	45-46	5.855	plant macrofossil	12870	360	15300
209692	I15 D7	53-54	5.935	plant macrofossil	13550	110	16350
172566	I15 D8	40-42	6.810	plant macrofossil	17020	100	20550
172567	I15 D8	91-92	7.315	plant macrofossil	18945	50	22900

3.0 Andean drought and glacial retreat tied to Greenland warming during the last glacial period

3.1 Introduction

Variations in Atlantic Meridional Overturning Circulation (AMOC) during the last glacial cycle drove abrupt changes in the thermal gradient of the North Atlantic sector, altering the interhemispheric distribution of tropical heat, the mean position of the intertropical convergence zone (ITCZ), and trade wind strength (Henry et al. 2016; McGee et al. 2018; Portilho-Ramos et al. 2017). South American low-latitude paleoclimate proxy records are sensitive to high-latitude forcing via the strength of the South American summer monsoon (SASM), which increased during cold stadial periods such as Heinrich events (Arz et al. 1998; Kanner et al. 2012; Wang et al. 2004; Baker et al. 2001), and weakened during the abrupt warmings recorded in Greenland ice cores associated with Dansgaard-Oeschger (DO) interstadials (Cheng et al. 2013; Zhang et al. 2017; Kanner et al. 2012).

Large fluctuations in Andean paleolake levels have been documented on the Bolivian Altiplano in association with the Younger Dryas and Heinrich events 1 and 2 (Placzek et al. 2006; Blard et al. 2011; Baker et al. 2001), and Andean glacier advances or stillstands have been linked to these wet events in some cases (Martin et al. 2018). Less is known about the effects of the shorter duration DO cycles on precipitation anomalies and on the mass balance of tropical Andean glaciers. Although some studies proposed a causal link between local glacier fluctuations and the sedimentary record of Lake Titicaca (Fritz et al. 2010), well-dated continuous records are necessary to test this hypothesis. Much of the paleoclimatic evidence documenting these rapid changes in tropical South American hydroclimate relies on the interpretation of $\delta^{18}O$ variations in speleothems from the Amazon Basin and surrounding regions (Cheng et al. 2013; Kanner et al. 2012; Wang et al. 2004). Similarities among speleothem $\delta^{18}O$ records reflect the regional impact of variations in convective activity and upstream rainout in the core monsoon region of Amazonia (Vuille and Werner 2005). However, speleothem records from several localities do not reveal a tight coupling between independent proxies of local precipitation amount and the $\delta^{18}O$ of that precipitation ($\delta^{18}O_{precip}$) (Ward et al. 2019; Wortham et al. 2017), indicating that upstream factors other than the amount effect (Dansgaard 1964) may dominate

$\delta^{18}O_{precip}$ at some locations. The inability to isolate local precipitation variations from the composite $\delta^{18}O$ signal (Lee et al. 2009; Konecky et al. 2019) makes it difficult to assess the specific impact of abrupt Arctic warming on water availability and glacial mass balance in the tropical Andes, and it highlights the need for $\delta^{18}O$-independent records of hydroclimate.

Here we present a sediment record from a high elevation lake in the central Peruvian Andes that records lake level fluctuations as well as changes in paleoglacier mass balance. We show that the DO interstadials between 50 and 15 ka, which are recorded isotopically both in Greenland ice cores (Andersen et al. 2006; Svensson et al. 2008) and speleothem $\delta^{18}O$ from Pacupahuain Cave in the upper Amazon Basin (Kanner et al. 2012), were associated with rapid and large reductions in Andean precipitation amount recorded by multiple independent proxies in Lake Junín sediments. Many of these perturbations were sufficient to deglaciate the adjacent portion of the eastern Andean cordillera up to at least 4700 masl and profoundly shrink Lake Junín, Peru's second largest lake located at 4100 masl and ~25 km from Pacupahuain Cave (Figure 11). This record documents the unambiguous impact on glacier mass balance and hydroclimate of the climatic teleconnection linking the Atlantic meridional thermal gradient with the strength of the SASM over the past 50 ka.

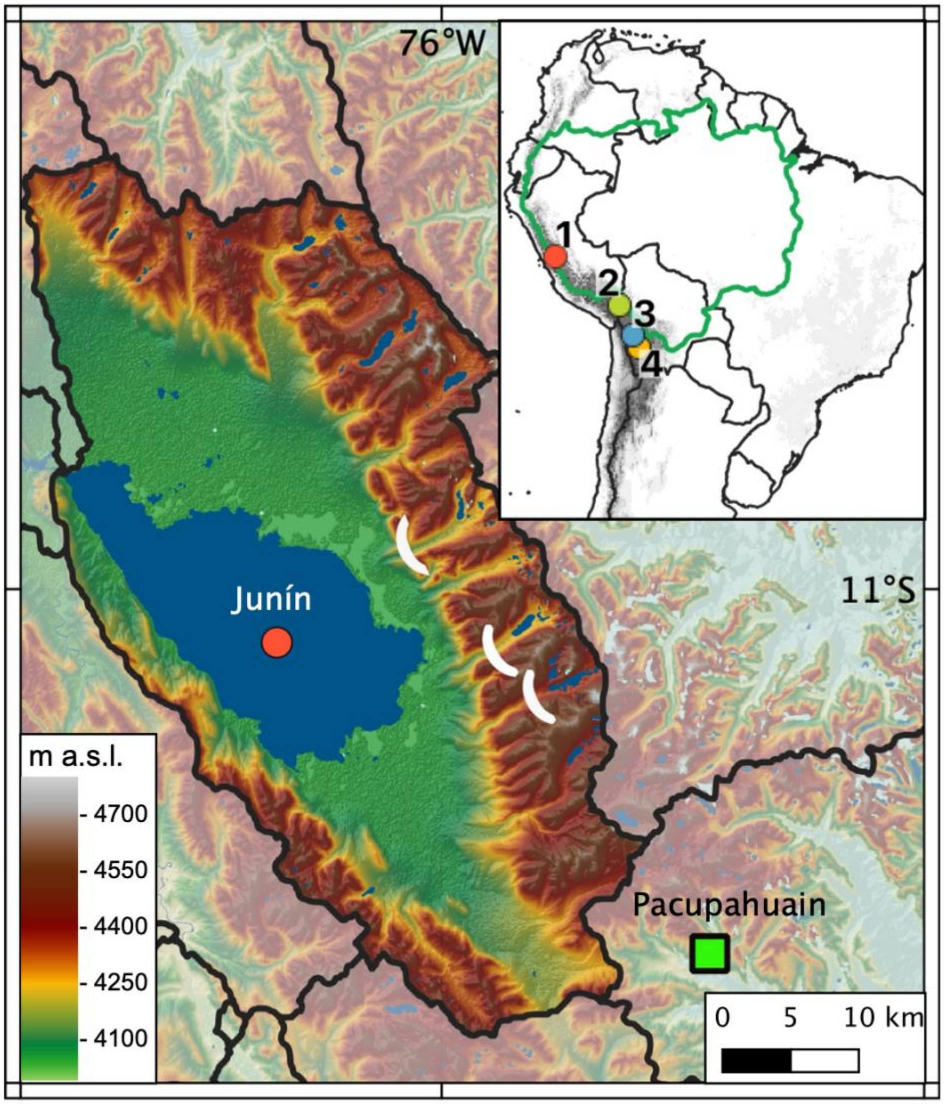

Figure 11. Location of the Lake Junín drainage basin and Pacupahuain cave. White ellipses in valleys east of Lake Junín indicate the mapped downvalley extent of glaciers during the local Last Glacial Maximum (Smith et al. 2005). Inset map: green line indicates the Amazon drainage basin, and circles indicate Andean records discussed in the text: 1. Junín, 2. Lake Titicaca, 3. Paleolake Tauca, 4. Salar de Uyuni.

3.2 Methods

3.2.1 Chronology

Samples and standards for radiocarbon age determination were chemically pretreated, vacuum sealed and combusted at University of Pittsburgh according to standard protocols (https://sites.uci.edu/keckams/files/2016/12/aba_protocol.pdf), and graphitized and dated by accelerator mass spectrometry at the W.M. Keck Carbon Cycle AMS facility at the University of California, Irvine. Radiocarbon samples obtained from off-splice core sections were assigned stratigraphically equivalent splice depths; development of the splice is detailed elsewhere (Hatfield et al. 2020). Radiocarbon age measurements with errors and median calibrated age estimates are reported in Table 4. An age model was constructed based on 79 radiocarbon ages spanning the upper 17.6 m of sediment. The IntCal 13 calibration curve (Reimer et al. 2013) was used to calibrate all dates <50,000 cal yr BP, and the CalPal2007_Hulu calibration curve (Weninger and Jöris 2008) was used for those >50,000 cal yr BP. Bayesian age-depth modeling was performed using the R software package Bacon v. 2.3 (Blaauw and Christen 2011) with the following settings: acc.mean = 25 yr cm^{-1}, acc.shape = 1.5, mem.strengh = 4, mem.mean = 0.7, and thick = 5 cm.

Initial age model test runs indicated that in some instances the mean age estimates were biased toward outliers at the expense of clusters of more consistent dates. Therefore, dates that fell outside of the model's 95% confidence interval were excluded prior to final age model construction if they also met other criteria, such as small sample mass (<1 mg) or low CO_2 gas yield (<10 Torr) when a larger sample was available from the same interval, or if a reversal was evident based on multiple surrounding dates. In addition, the two oldest measured dates that are within the IntCal 13 calibration range (UCIAMS# 193160, 193169) would imply that sedimentation rates from ~45-50 ka were higher than any other portion of the record, including the LGM. We suggest these two ages are erroneously young and warrant exclusion. The stratigraphy does not indicate a change in sedimentation regime during this interval, and there is a pair of older dates between them (calibrated using the CalPal2007_Hulu curve) that are in close stratigraphic and chronologic agreement. Finally, sample 201045 yielded the largest lab error and is closest to the limits of the radiocarbon method, and it represents an age reversal of several thousand years in the context of three underlying samples. Dates excluded from the final age model are marked by an asterisk in Table 4. Calibrated median ages and

95% probability ranges are rounded to the nearest 5 yr for ages <1,000, the nearest 10 yr for 1,000-10,000, the nearest 50 yr for 10,000-20,000, and the nearest 100 yr for >20,000.

3.2.2 Physical analysis of sediment cores

Bulk density was determined from the air-dried mass of 1 cm^3 samples taken every 2.5 cm above 6.665 m and every 8 cm below 6.665 m. Total organic and inorganic carbon (TOC, TIC) was measured on samples taken every 2.5 cm above 6.665 m and every 4 cm below 6.665 m. Total carbon (TC) was determined by combusting samples at 1000°C using a UIC 5200 automated furnace, and analyzing the resultant CO_2 using a UIC 5014 coulometer at Union College. Similarly, TIC was determined by acidifying samples using an Automate acidification module and measuring the resultant CO_2 by coulometry at Union College. We calculated weight percentage TOC from TOC=TC-TIC. We measured the biogenic silica ($bSiO_2$) content of a total of 65 samples obtained randomly from all facies present in the sediment core. Siliciclastic flux ($Flux_{clastic}$, Equation 1) was calculated as:

$$Flux_{clastic} = SR * (BD - ((BD * TOM) + (BD * TCC))) \qquad (1)$$

where SR is bulk sedimentation rate (cm yr^{-1}), BD is bulk density (gm cm^{-3}), TOM is the weight fraction organic matter of the bulk sediment, and TCC is the weight fraction $CaCO_3$ of the bulk sediment. We calculated TOM from TOC (%)/44 to reflect the molar ratio between plant cellulose $(C_6H_{10}O_5)n$ and TOC (%), and we calculated TCC from TIC (%)/12 to reflect the molar ratio between TIC (%) and $CaCO_3$. Because of the presence of both authigenic and detrital $CaCO_3$ in the sediment core, the removal of all $CaCO_3$ in the estimation of $Flux_{clastic}$ results in an underestimation of the total detrital flux during intervals of high clastic input, and this, in turn, reduces the amplitude of change in clastic flux between intervals of high and low glacigenic sediment input. While we do not explicitly remove the bSiO2 in the calculation of $Flux_{clastic}$, the average weight percentage $bSiO_2$ for all 65 samples facies samples is 0.92 ± 1.12% (±1σ), and thus is negligible. XRF scanning was performed at the LacCore XRF Lab, University of Minnesota-Duluth Large Lakes Observatory using a Cox Analytical ITRAX with a Cr tube, 5 mm resolution, and 15 second dwell time.

3.3 Results

3.3.1 Lake setting and glacial connection

Lake Junín (11°S) is a seasonally closed-basin lake located between the eastern and western cordilleras of the central Peruvian Andes (Fig. 1). With a surface area of ~280 km^2 and a seasonally variable water depth of ~8-12 m, Lake Junín is especially sensitive to changes in precipitation-evaporation balance (P-E). The watershed occupies the Puna grasslands ecoregion where groundwater-fed peatlands (*bofedales)*, characterized by organic-rich sediment, occupy the shallow water lake margins. Glacial outwash fans and lateral moraines form the basin's eastern and northern edges (Figure 11), and ^{10}Be exposure ages from these moraines indicate they span multiple glacial cycles (Wright 1983; Smith et al. 2005), but at no time during at least the last 50 ka has the lake been overridden by glacial ice (Smith et al. 2005). Thus, Lake Junín is ideally situated to record the last glacial cycle in the adjacent eastern cordillera. During the local last glacial maximum (LLGM; ~28.5-22.5 ka) alpine glaciers descended from headwall elevations as high as ~4700 masl to end moraine positions ~4160 masl, within several km of the modern shoreline (Smith et al. 2005). Whereas glaciers in the inner tropics of the Andes are especially temperature sensitive because of sustained precipitation year-round, glaciers in the outer tropics, such as those at the latitude of the Junín basin, experience greater seasonality of precipitation and are twice as sensitive to changes in precipitation as those in the inner tropics (Sagredo et al. 2014; Kaser 2001). The Junín region receives most of its moisture through the SASM during the austral summer (DJF) with less than 7% falling during the winter (JJA), making variations in the SASM a principal driver of changes in paleoglacier mass balance.

Most records of glaciation in the tropical Andes rely on moraine exposure ages to infer the timing and extent of advances (Smith et al. 2005; Shakun et al. 2015; Martin et al. 2018). However, such records are limited by age uncertainties of ~±5%, an unknown temporal relationship between the timing of moraine stabilization and ice advance, and the tendency for larger advances to erase evidence of prior glacial cycles. Continuous proxy records from well-dated glacier-fed lakes such as Junín can compensate for such limitations, with clastic sediment flux and high-resolution XRF scans being well-established proxies for glacial erosion of bedrock that, in turn, reflect relative changes in paleoglacier activity and mass balance (Bakke et al. 2009; Rodbell et al. 2008). Accordingly, final deglaciation of the Junín watershed was nearly complete by 18 ka and was marked by a near total cessation of clastic sediment input to the lake (Rodbell et al. 2008; Seltzer et al. 2000).

3.3.2 Sedimentary context

The Junín sediment cores were obtained from the lake depocenter (Figure 11) in 8.2 m of water. The age model for the last 50 ka (cal yr BP, 1950 *CE*) is based on 79 radiocarbon measurements from terrestrial macrofossils and charcoal (Figure 12, Table 4). Sediment deposited from 50-22.5 ka is dominated by fine-grained glacial flour characterized by high Ti and Si counts per second (cps), high density, and low total organic carbon (TOC) (Figure 12). Glacigenic sediment input to Lake Junín was especially high and devoid of plant macrofossils from 28.5-22.5 ka, which corresponds to the age of moraines deposited during the maximum extent of ice in the last 50 ka in the adjacent eastern cordillera (Smith et al. 2005), according to ^{10}Be ages recalculated based on updated production rates and scaling factors (Heyman et al. 2016). The scaling procedure applied here (Heyman et al. 2016) yields ^{10}Be ages that are compatible within ±2% with those that would be obtained using local tropical Andes ^{10}Be production rates (Martin et al. 2015; Kelly et al. 2015).

Glacigenic sediment deposition was punctuated by a series of distinct 1 to 20 cm-thick peat layers (Figure 12) containing 5-35% TOC with abundant macrofossils that are similar to the sediment accumulating today in the fringing peatlands. These peat layers span intervals from ~25-500 years based on mean sedimentation rates and are interpreted to reflect lake low stands when surrounding peatlands encroached toward the center of the lake, forming a record of repeated water level fluctuations of up to ±8 m. There is no sedimentary or radiocarbon evidence for unconformities within age model precision, which indicates that while these peat layers represent considerably lower water level, the drill site remained submerged, at least seasonally, for the duration of our record. Today Lake Junín overflows during the summer wet season and there is no evidence of shoreline features above modern lake level. Sediment deposited after ~20 ka reveals a rapid decline in clastic input, evidenced by the low values of Ti, Si, bulk density, and siliciclastic flux. The near-complete loss of the clastic signal does not imply reduced precipitation after 20 ka, but rather reflects a different sedimentary environment wherein glaciers had retreated behind up valley moraine-dammed lakes that served as local sediment traps. During the late glacial, the sedimentary regime shifted to a lake increasingly dominated by authigenic $CaCO_3$ with frequent laminations (Figure 13). The occasional fine-grained organic-rich intervals <20 ka contain few plant macrofossils and record autochthonous (algal) productivity; these intervals do not resemble the dark, crumbly, and macrofossil-rich peats that punctuate the 20-50 ka interval of the core.

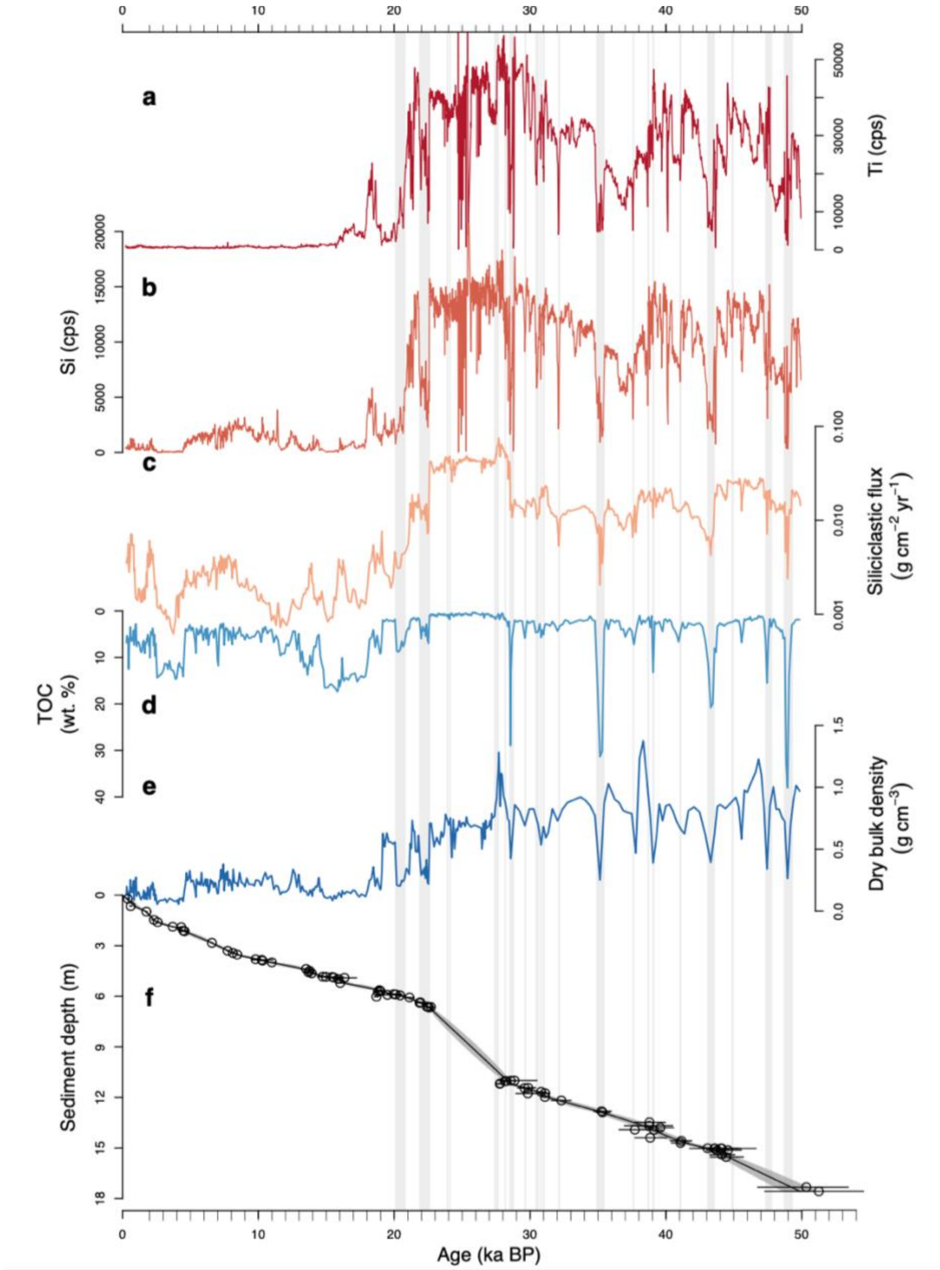

Figure 12. Physical and geochemical sediment properties from the Junín drill core. The similar XRF profiles of a, Ti and b, Si indicate both elements primarily represent clastic inputs, with slight differences attributable to different bedrock mineralogy and grain size. c, Siliciclastic sediment flux (log scale). d, Total organic carbon (TOC). e, Dry bulk density. f, Bacon age-depth model of 79 AMS radiocarbon ages on terrestrial macrofossils; error bars denote 95% probability range for calibrated ages. Ages excluded from the age model are listed in the supplemental. Grey vertical bars show the distribution of peat layers.

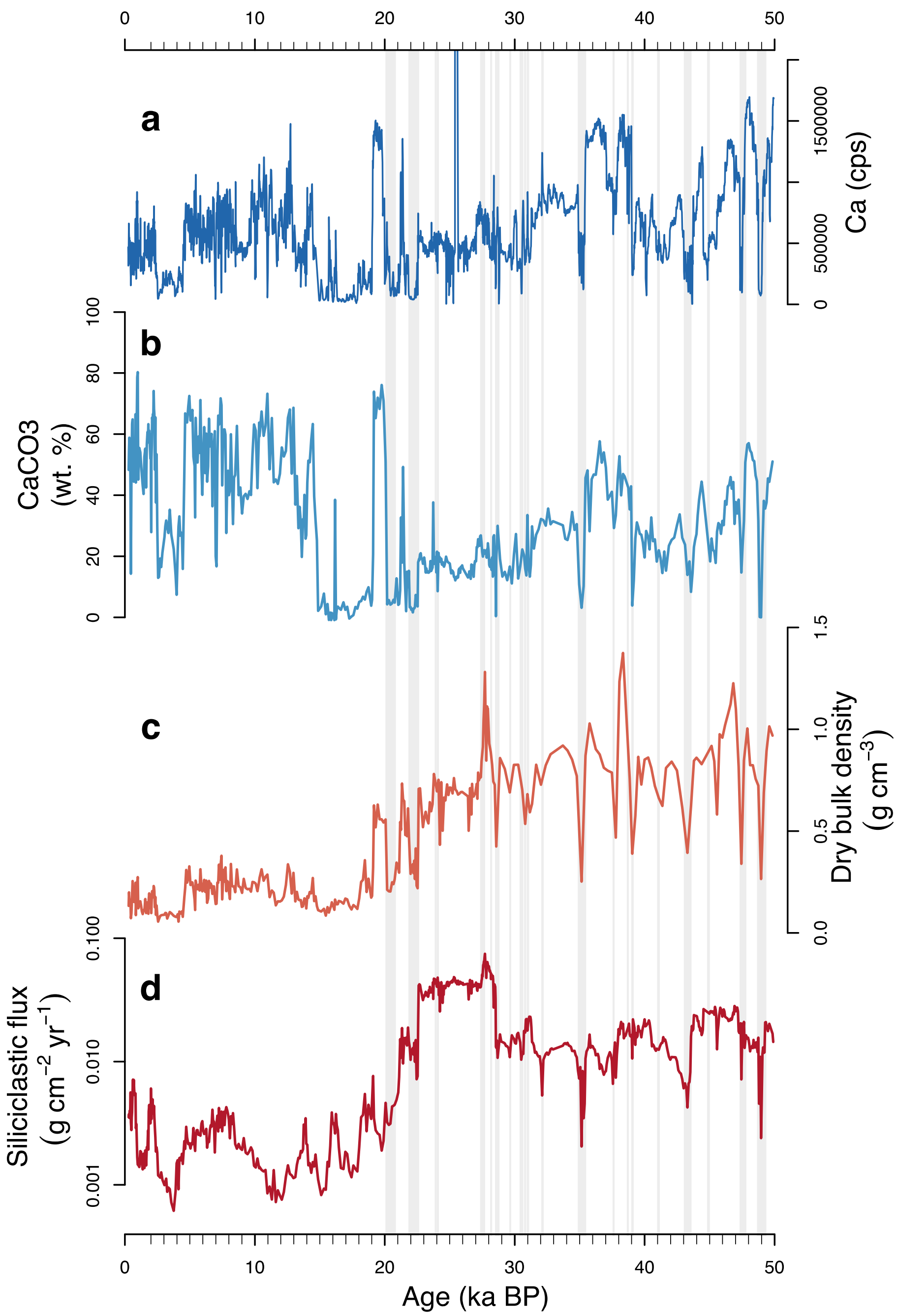

Figure 13. Variable carbonate content of Junín sediments. The carbonate content reflects different processes during glacial versus interglacial periods. Elevated $CaCO_3$ from 20-50 ka indicates glacially-generated detrital inputs derived from the extensive limestone bedrock in the valleys surrounding the lake. During the late-glacial and Holocene, when glaciers are no longer present in the watershed, authigenic precipitation of fine-grained calcite dominates the sedimentary record[1]. a, Calcium (cps) from scanning XRF closely resembles b, sedimentary $CaCO_3$ content (wt. %). c, dry bulk density. d, siliciclastic flux.

3.3.3 Synchronous changes in lake level and paleoglacier extent

The Junín record exhibits a reduced input of glacigenic sediment during DO interstadials 4-13 (Figure 15), with all but two of these intervals marked by enhanced peat accumulation, associated higher TOC, and lower density (Figure 12). Similar but less pronounced changes appear to be associated with DO interstadials 2 and 3. However, the timing of these latter events coincides with the period of rapid clastic sedimentation during the LLGM, an interval that is devoid of datable macrofossils and therefore has less robust age control. Declines in siliciclastic sediment flux indicate that simple dilution effects were not responsible for the reductions in glacigenic sediment concentration. The timing of DO interstadials was thus marked by widespread glacial retreat and lake level lowering up to ~8 m, within the chronologic uncertainty of our age model (Figure 14). The absence of evidence for lowered lake level during complete and final deglaciation of the Junín catchment (~20-15 ka), when regional warming drove snowlines to rise 300-600 m (Seltzer et al. 2000; Smith et al. 2005), indicates that the level of Lake Junín is especially sensitive to precipitation amount rather than variations in temperature. The close association between low lake stands and reduced glacial sediment flux during DO events suggests that these reductions in paleoglacier mass balance were primarily driven by decreases in precipitation. The declines in lake level associated with the DO events noted here corroborates evidence of water level reductions associated with DO interstadials 11, 10, and 8 at 1360 masl in southern Peru (14°S) (Urrego et al. 2010), and evidence for millennial scale fluctuations in nearshore terrigenous inputs to Lake Titicaca that may be linked to DO events (Fritz et al. 2010). The documented changes in hydroclimate in the Junín region may thus have affected a large region of the westernmost Amazon Basin, which is consistent with the Fe/Ca record of Amazon River discharge (Zhang et al. 2017) (Figure 15). Relative to Altiplano lake records (Baker et al. 2001; Placzek et al. 2006), Junín most strongly records dry (DO) events, whereas the Altiplano records are more sensitive to wet (Heinrich) events. Thus, the records appear to be biased toward recording hydroclimatic perturbations that contrast the most with their respective background states; namely, more arid on the Altiplano and more humid in the Junín region.

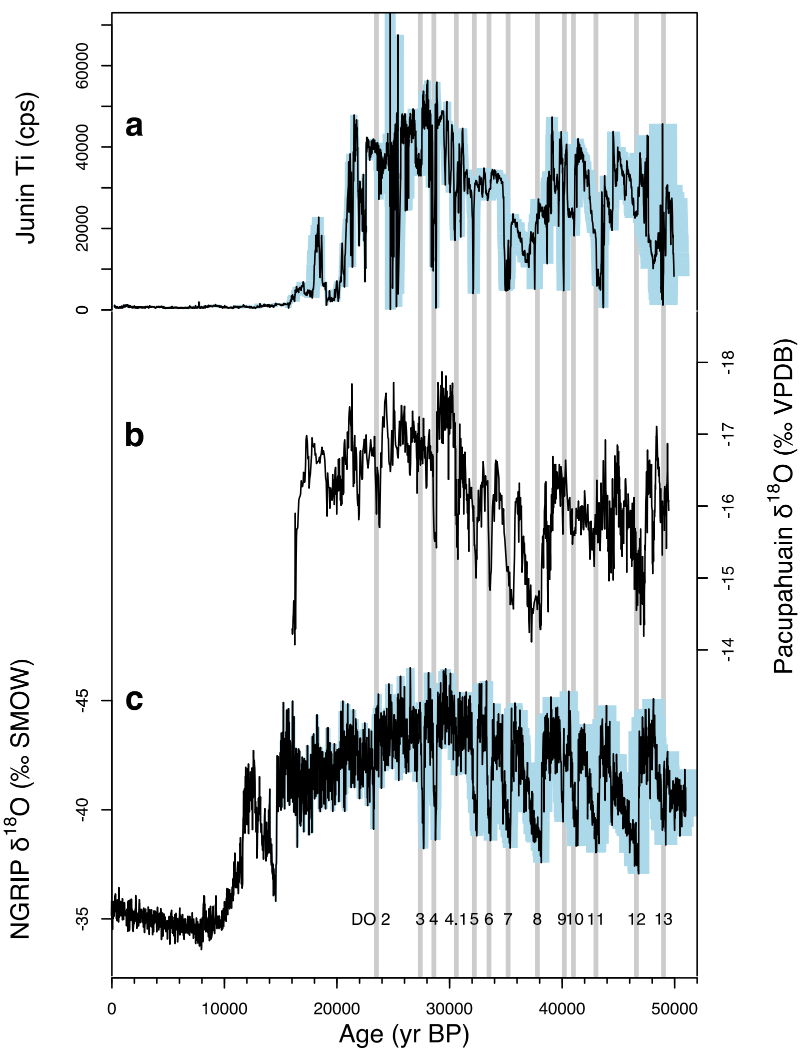

Figure 14. The timing of Dansgaard-Oeschger (DO) interstadials, as recorded by decreases in glacigenic sediment flux to Lake Junín and increases in the $\delta^{18}O$ value of the NGRIP ice core record, overlap within the age model chronological uncertainties. Continuous error estimates are not available for the Pacupahuain speleothem time series, but the 2σ errors for individual ^{230}Th ages are small, ranging from ±40 to ±150 years. a, NGRIP $\delta^{18}O$ based on the GICC05 timescale (black line) and the maximum counting error (blue shaded region), which should be regarded as 2σ as discussed in Andersen et al. (2006). b, Pacupahuain speleothem $\delta^{18}O$ (Kanner et al. 2012). c, Lake Junín Ti counts per second (cps) (black line) and age model 95% confidence interval (blue shaded region) based on the Bacon age model discussed in the text. Numbered grey vertical lines indicate DO interstadials.

3.4 Discussion

On millennial timescales, multiple independent proxies measured on Junín sediments bear a strong correspondence to the precisely-dated speleothem $\delta^{18}O$ records from both the nearby Pacupahuain Cave (Kanner et al. 2012) and from El Condor Cave (Figure 15), a lower elevation site (800 masl) in the western Amazon Basin of northern Peru (Cheng et al. 2013). This concurrence indicates that regional monsoon strength was a first-order control on all records. While downcore changes in clastic sediment inputs at Junín are indicative of relative, rather than absolute, changes in precipitation, they record an entirely local signal. The observed similarity with nearby speleothems suggests that $\delta^{18}O_{precip}$, which has been interpreted to reflect upstream convection and rainout (Vuille and Werner 2005; Wang et al. 2017; Kanner et al. 2012), also reflects some degree of variable local precipitation amount in the tropical Andes. However, the magnitude and duration of Junín's response to individual DO events is often not to scale with that of Pacupahuain, only 25 km away. For example, DO interstadials 11 and 13 register as profoundly dry intervals at Junín but only minimally so in Pacupahuain, contrary to the signal that would be predicted by a simple amount effect (Dansgaard 1964). A similar mismatch occurs during DO interstadial 8, which is a relatively weak dry period at Junín with moderate reductions in Ti and Si and only a multi-decadal interval of peat accumulation, yet DO 8 in the Pacupahuain record is marked by the most positive $\delta^{18}O$ excursion in the entire speleothem sequence, lasting nearly a millennium. These observations indicate that the local moisture response at Junín can be disproportional to, and possibly even decoupled from, the $\delta^{18}O$ signal that is thought to be recording millennial-scale SASM intensity. This confirms earlier work showing that atmospheric transport of water vapor from the tropical Atlantic across the Amazon lowlands involves numerous isotopic controls, in addition to precipitation amount, which influence the $\delta^{18}O_{precip}$ signal of geologic archives (Konecky et al. 2019; Lee et al. 2009; Wang et al. 2017).

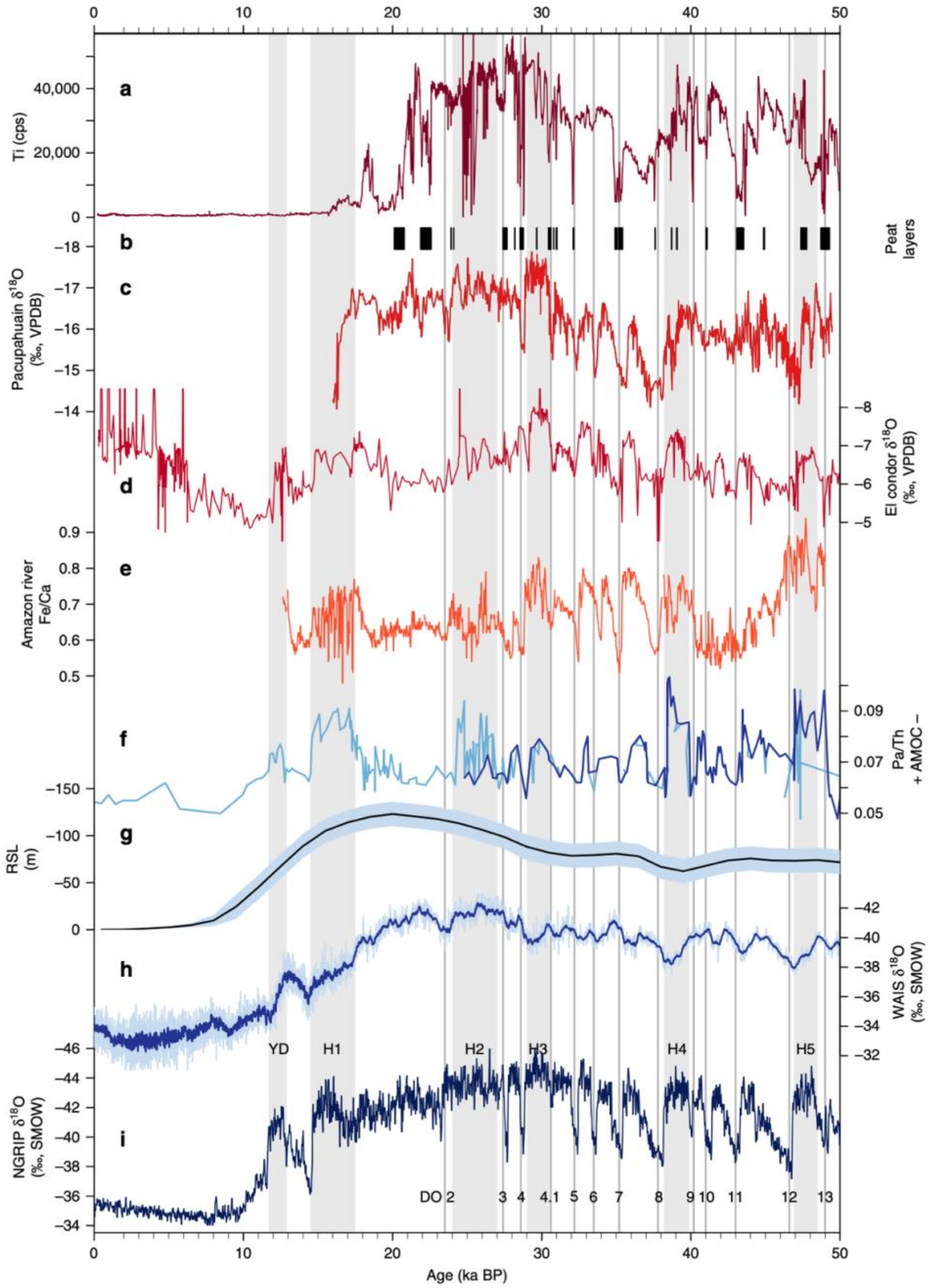

Figure 15. Comparison of regional and global proxy paleoclimatic records. a, Junín glaciation (Ti). b, Junín low stands (peat layers). c, Pacupahuain speleothem $\delta^{18}O$ (Kanner et al. 2012). d, El Condor speleothem $\delta^{18}O$ (Cheng et al. 2013). e, Amazon Discharge (Zhang et al. 2017). f, Atlantic Meridional Overturning Circulation (AMOC) strength (dark blue curve is Pa/Th data reported in (Henry et al. 2016), and light blue curve is a compilation of previously reported Pa/Th records as presented in (Henry et al. 2016). g, Relative sea level (Waelbroeck et al. 2002). h, WAIS Divide ice core $\delta^{18}O$ (WAIS Divide Project Members, 2013). i, NGRIP ice core $\delta^{18}O$ (Andersen et al. 2006). Vertical grey boxes denote the Younger Dryas and Heinrich stadials H1-H5, and numbered vertical lines are Dansgaard-Oeschger (DO) warming events 2-13.

The early onset of deglaciation in the central Peruvian Andes, ~22.5 ka based on lake sediment records (Seltzer et al. 2002), is consistent with moraine ages that reflect retreating ice margins at this time (Shakun et al. 2015; Smith et al. 2005). This onset was several millennia prior to the onset of global deglaciation as recorded by sea level rise (Waelbroeck et al. 2002) (Figure 15), and was initially interpreted as evidence for early tropical warming because of the lack of evidence for drying at this time (Seltzer et al. 2002). The Junín peat record, however, reveals that two prolonged droughts, lasting a total of ~1300 yr, occurred in quick succession (22.5-21.9 ka and 20.8-20.1 ka), just prior to the onset of warming ~20 ka in the high latitudes of the Southern Hemisphere (WAIS Divide Project Members et al. 2013) (Figure 15). We suggest that these prolonged dry intervals, which resemble Junín's response to DO events, were responsible for the early onset of glacial retreat in this region of the tropical Andes. These abrupt reductions in precipitation at Junín are evident, though subtle, in the Pacupahuain record, yet they do not appear as pronounced individual excursions in AMOC (Henry et al. 2016) or Amazon discharge (Zhang et al. 2017) (Figure 15). It is notable, however, that the latter two records indicate that the period from ~24 to 19 ka was characterized by a relatively strong AMOC and overall drier conditions in the Amazon Basin, respectively. These observations, along with records of tropical Atlantic mixed layer depth (Portilho-Ramos et al. 2017), indicate that the 24-19 ka interval was not marked by the large southward ITCZ displacements that characterized Heinrich events 2 and 1, and this may explain why Junín experienced extended droughts and early deglaciation during this interval. Alternately, modeling studies have pointed to a thermodynamically-driven contraction of the tropical rainbelt associated with global cooling during the global LGM (McGee et al. 2014), which may have contributed to reductions in SASM rainfall and early deglaciation in the tropical Andes.

The significant disruption to glaciers and hydroclimate in the tropical Andes in response to perturbations in the meridional temperature gradient of the North Atlantic documented here demonstrates the sensitivity of tropical P-E balance to Northern Hemisphere climatic shifts. There are multiple possible scenarios for regional hydroclimatic change in the Amazon Basin in response to 21st century warming. One scenario posits that accentuated warming in the Arctic will result in a northward shift in the mean position of the ITCZ (Lee and Wang 2014; Broecker and Putnam 2013), while another projects a stable mean position of the ITCZ, but reductions in both width and strength (Byrne et al. 2018). Past changes in the hemispheric thermal gradient are an imperfect analog for future change, however. For example, the attendant increase in AMOC strength documented during warm interstadials is not expected to accompany future CO_2-induced warming (Gregory et al. 2005), and changes in ITCZ position could be superimposed (Broecker and Putnam 2013) on enhanced tropical precipitation that is projected by some models (Held and Soden 2006). Nevertheless, a northward shift in the thermal equator remains likely given faster heating of the Northern Hemisphere, and this scenario is consistent with a multimodel ensemble of simulations which projects regional drying of Amazonia and much of the tropics (Neelin et al. 2006). This would lead to significant reductions in P-E in the tropical Andes with impacts on glaciers, water supplies, hydropower, and agriculture in a region inhabited by tens of millions of people.

Table 4. Radiocarbon ages for the Junín cores

UCI AMS#	Core	Mean depth (cm)	Total depth (m)	Material	^{14}C age (BP)	±1σ	Median age (cal BP)	95% prob. lower range	95% prob. upper range
164796	C15-D1	6-7	0.215	charcoal	330	35	390	305	475
201049	C15-D1	50-51	0.655	charcoal	630	60	605	530	675
164797	C15-D2	16-17	0.980	charcoal	1815	20	1760	1710	1820
164798	C15-D3	16-19	1.470	charcoal	2275	25	2320	2170	2350
209665	C15-D3	23-24	1.610	charcoal	2510	35	2590	2490	2740
164802	D15-D3	16-19	1.875	charcoal	3440	25	3690	3620	3830
201050	D15-D3	19-21	1.900	charcoal	3900	80	4320	4090	4530
164803	D15-D3	39-42	2.105	charcoal	3990	45	4470	4300	4780
209668	D15-D3	44-45	2.145	charcoal	4060	70	4570	4420	4820
164799	C15-D6	9-12	2.830	charcoal	5775	25	6580	6500	6640
164800	C15-D6	56-59	3.300	charcoal	6915	30	7740	7680	7820
193150	1D-2H-2	10-13	3.430	charcoal	7310	90	8120	7970	8320
193151	1D-2H-2	21-22	3.530	charcoal	7645	50	8440	8380	8540
193101	D15-D6	41-42	3.805	plant macrofossil	8730	150	9790	9500	10200
201051	C15-D7	10-11	3.840	charcoal	9100	230	10250	9560	11050
201052	C15-D7	21-23	3.890	charcoal	9145	50	10300	10200	10500
201053	C15-D7	31-33	3.990	charcoal	9670	120	11000	10650	11200
209666	C15-D7	70-71	4.375	charcoal	11670	230	13500	13100	14050
209667	C15-D7	81-83	4.490	plant macrofossil	11940	70	13750	13600	14000
193144*	1C-2H-1	7-8	4.570	plant macrofossil	10850	150	12750	12550	13050
193098	C15-D7	90-91	4.575	plant macrofossil	11860	130	13700	13450	14000
209669	D15-D71	42-44	4.640	charcoal	12070	90	13900	13750	14150
201054	C15-D8	11-12.5	4.810	charcoal	12500	45	14750	14350	15058
172568	1C-2H-1	35-36	4.850	plant macrofossil	12605	35	15000	14750	15150
201055	C15-D8	16-17	4.855	plant macrofossil	12940	270	15450	14450	16250
193145	1C-2H-1	39-40	4.890	plant macrofossil	13000	200	15550	15000	16150
201056	C15-D8	21-22	4.905	plant macrofossil	13540	300	16350	15500	17250
193099	C15-D8	28-29	4.975	plant macrofossil	13200	40	15850	15700	16050
164801	C15-D8	51-54	5.215	plant macrofossil	13320	70	16000	15800	16250
193146	1C-2H-1	95-96	5.640	plant macrofossil	15670	80	18900	18750	19100
164804	D15-D8	41-44	5.665	plant macrofossil	15705	45	18950	18800	19100
193102	D15-D8	46-47	5.705	plant macrofossil	15740	120	19000	18750	19300
201057	D15-D8	48-50	5.730	plant macrofossil	15540	140	18800	18500	19100
193103	D15-D8	62-64	5.870	plant macrofossil	16550	220	19950	19500	20500
193104	D15-D8	65-66	5.895	plant macrofossil	16675	45	20100	19950	20300
201058	D15-D8	67-68	5.915	plant macrofossil	16150	420	19500	18650	20500
193147	1C-2H-1	127-128	5.950	plant macrofossil	16940	60	20450	20200	20600
193105	D15-D8	78-79	6.025	plant macrofossil	15420	60	18700	18550	18800
193106	D15-D8	83-84	6.075	plant macrofossil	17490	80	21100	20900	21400
193100	C15-D9	68-69	6.365	plant macrofossil	18100	60	21900	21700	22200
193148	1C-2H-2	19-20	6.375	plant macrofossil	18065	50	21900	21700	22100
164805	D15-D9	12-14	6.390	plant macrofossil	18055	45	21900	21700	22100
193149	1C-2H-2	44-45	6.610	plant macrofossil	18495	50	22400	22300	22500
164806	D15-D9	36-38	6.630	plant macrofossil	18660	60	22500	22400	22700
181187	1C-2H-2	47-48	6.640	plant macrofossil	18850	60	22700	22500	22900
193107*	D15-D9	41-42	6.675	plant macrofossil	13910	35	16850	16650	17050
201059	D15-D9	41-42	6.675	charcoal	18715	45	22600	22400	22700
181189	1B-4H-1	126-127	10.999	charcoal	24720	740	28900	27700	30500

Table 4 (continued)

193161	1B-4H-1	127-128	11.009	charcoal	24540	200	28600	28100	29000
201037	1B-4H-1	130-131	11.039	plant macrofossil	24120	100	28100	27900	28500
201038	1B-4H-1	130-131	11.039	charcoal	24210	80	28200	28000	28500
193162	1B-4H-1	143-145	11.174	plant macrofossil	23730	100	27800	27600	28000
181190	1D-5H-1	21-22	11.194	plant macrofossil	23680	110	27800	27600	28000
193163	1B-4H-2	16-17	11.429	charcoal	25680	170	29900	29400	30400
181191	1D-5H-1	48-49	11.444	plant macrofossil	25480	190	29600	29100	30200
193164	1B-4H-2	40-41	11.669	plant macrofossil	26550	170	30800	30500	31100
172616	1D-5H-1	78-79	11.749	plant macrofossil	27100	230	31100	30800	31400
181192	1B-4H-2	50-51	11.769	charcoal	25650	410	29800	29000	30700
193153	1D-5H-1	101-102	11.979	plant macrofossil	27090	140	31100	30900	31300
181193	1B-4H-2	91-93	12.184	plant macrofossil	28390	230	32300	31600	33000
181194	1D-5H-2	36-37	12.819	charcoal	31370	330	35300	34700	36000
193154	1D-5H-2	43-44	12.889	plant macrofossil	31460	230	35300	34800	35900
181195	1D-5H-2	102-103	13.479	plant macrofossil	34280	470	38800	37700	40000
193155*	1D-5H-2	102-103	13.479	plant macrofossil	27420	150	31300	31100	31500
193165	1B-5H-1	91-93	13.684	plant macrofossil	34320	730	38800	37000	40500
181196	1D-5H-2	134-135	13.799	charcoal	35050	430	39600	38700	40600
193166	1B-5H-1	110-113	13.919	charcoal	33460	430	37700	36600	38700
201039	1B-5H-1	113-114	13.939	charcoal	34620	250	39100	38600	39700
201040*	1B-5H-1	133-134	14.139	charcoal	32960	220	37000	36400	37900
181199*	1B-5H-1	136-139	14.179	plant macrofossil	17930	110	21700	21400	22000
193167	1B-5H-2	8-10	14.398	plant macrofossil	34330	490	38800	37700	40000
193156	1D-6H-1	51-54	14.578	plant macrofossil	36540	430	41100	40300	41900
201041	1B-5H-2	38-41	14.703	plant macrofossil	36440	310	41100	40400	41700
172569	1B-5H-2	71-72	15.023	plant macrofossil	39270	500	43100	42400	44000
181200	1B-5H-2	72-73	15.033	plant macrofossil	40460	840	44000	42900	45500
181201	1B-5H-2	72-73	15.033	plant macrofossil	39860	630	43600	42700	44700
181197	1D-6H-1	96-97	15.033	charcoal	40550	680	44100	43100	45300
181198	1D-6H-1	96-97	15.033	plant macrofossil	39800	1530	43600	41800	46600
201042	1B-5H-2	81-83	15.128	plant macrofossil	41070	560	44600	43600	45600
201043	1B-5H-2	83-84	15.143	plant macrofossil	40160	490	43800	43000	44700
201044	1B-5H-2	108-111	15.403	plant macrofossil	40560	520	44100	43200	45100
193157	1D-6H-1	147-148	15.538	plant macrofossil	40930	730	44400	43300	45700
193158*	1D-6H-2	8-11	15.683	plant macrofossil	35780	570	40400	39300	41500
193159*	1D-6H-2	34-36	15.938	plant macrofossil	18810	70	22700	22500	22900
193160*	1D-6H-2	107-110	16.665	plant macrofossil	41200	1300	44700	42800	47400
201045*	1B-6H-1	111-112	17.145	charcoal	49800	1600	55500	50200	57300
201046	1B-6H-1	129-130	17.325	charcoal	46700	1500	50300	46800	53400
201047	1B-6H-2	7-10	17.574	plant macrofossil	47400	1600	51300	47300	54500
193168	1B-6H-2	8-9	17.574	plant macrofossil	52600	3000	–	–	–
201048*	1B-6H-2	10-11	17.594	plant macrofossil	36640	730	41100	39900	42300
193169*	1B-6H-2	44-45	17.934	plant macrofossil	43300	960	46600	45100	48800
172570	1D-7H-1	82-84	17.994	plant macrofossil	>50800		–	–	–
172617	1D-7H-2	134-136	20.014	charcoal	>53400		–	–	–

4.0 Monsoon strength and glaciation in the tropical Andes during MIS 15-12

4.1 Introduction

Low latitude climate systems, including tropical monsoons, play a key role in regulating global energy fluxes through their interaction with large-scale atmospheric circulation, and the resultant surface winds and water vapor transport affect climate in tropical and extra-tropical regions. One such system, the South American Summer Monsoon (SASM), is a major source of precipitation and heat to the Amazon lowlands today that also sustains water resources and mountain glaciers in the Andean highlands. Our ability to characterize climate dynamics in this region requires insight from paleoclimate research into the mechanisms driving long term changes in hydroclimate, but only a limited number of records documenting precipitation and temperature trends in tropical South America are available from previous glacial and interglacial cycles and their interpretations remain uncertain. Some records show large variations in tropical climate signatures on glacial/interglacial scales (Torres et al. 2013; Harris and Mix 1999; Groot et al. 2011; Fritz et al. 2007), indicating a sensitivity to global temperature and/or ice volume. In other records precession appears to be the dominant form of long-term variability (Cruz et al. 2005; Burns et al. 2019), although the disparate responses during some glacial periods suggest that precessional scale changes in insolation are more influential during interglacials (Kanner et al. 2012; Govin et al. 2014). Depending on the time period in question, these independent forcings may reinforce or counteract each other, with regionally varying effects on the precipitation-evaporation (P-E) balance.

From a thermodynamic standpoint, colder glacial climates should be associated with less humidity, and a recent review finds that glacial periods were associated with drying across large regions of the tropics (McGee 2020). At the same time, preferential cooling of the Northern Hemisphere during peak glacials is expected to result in a southward shift of the tropical rainbelt, leading to hemispheric asymmetries in precipitation patterns (Donohoe et al. 2013; McGee et al. 2014). These uncertainties are reflected in studies from tropical South America, which disagree as to whether glacial periods were overall wetter or drier compared to interglacials. Proxy evidence suggests warm and dry interglacial periods on the Bolivian Altiplano (Hanselman et al. 2011; Fritz et al. 2007) and in the northern Colombian Andes (Torres et al. 2013), and cold and wet conditions during peak glacial intervals. In contrast, sediment from the western equatorial Atlantic indicates that in the Amazon Basin, glacials were instead somewhat drier than interglacials (Harris and Mix 1999), and a speleothem record suggests reduced convection and moisture recycling resulted in drier conditions in Amazonia during the last glacial period compared to a wetter Holocene (Wang et al. 2017). The discrepancies in records from South America may be related to uncertain proxy interpretations, or they may reflect true regional variability in moisture distribution arising from competing influences on tropical hydroclimate over long timescales. Additionally, millennial to multi-millennial scale changes in monsoon strength arising from variations in ocean/atmosphere circulation are superimposed on orbital scale changes and may alter regional climate signatures.

Our understanding of long-term trends in tropical South American climate is hampered by the limited number of well-dated records that span multiple glacial/interglacial cycles, such that most of our interpretations are based on observations from the Holocene and Marine Isotope Stages (MIS) 2/3. Yet even during the past 800 ka, the interval after which the global climate system had largely completed the mid-Pleistocene transition (MPT) from dominant 41 kyr to 100 kyr glacial cycles, substantial glacial and interglacial diversity is observed in terrestrial and marine records from both hemispheres (Lang and Wolff 2011; Past Interglacials Working Group of PAGES 2016). Differences in greenhouse gas (GHG) concentration, ice sheet configuration, sea level, and other factors lead to variable regional climate responses, and highlight the need for additional multi-proxy paleolimnology studies from the tropics (Escobar et al. 2020). The aim of this study is to explore how monsoon strength and glaciation in the tropical Andes responded to climate forcing on orbital and multi-millennial timescales, and to understand how the patterns and magnitude of climate variability centered around half a million years ago compare to those during the Holocene and last glacial period. Here we present a high-resolution climate record from Lake Junín in the Peruvian Andes spanning two glacial cycles from MIS 15 to MIS 12 (~620-420 ka), an interval that precedes the abrupt increase in interglacial intensity that occurred near the MIS 12/11 transition (~420 ka) known as the mid-Brunhes event (MBE) (Jouzel et al. 2007). As such, this interim period between the MPT and the MBE coincides with major reorganizations of the global climate system and has less well-defined character and smaller amplitude ice volume variations relative to the past 400 ka (Figure 16).

MIS 15 and 13 are long interglacials that were globally cooler than the Holocene, and they underwent larger amplitude precessional cycles owing to greater eccentricity (Laskar et al. 2004). MIS 14 was the mildest glacial of the past 800 ka in terms of the global ice volume signature, whereas MIS 12 was large and comparable to the last glacial period (Lisiecki and Raymo 2005). Our results indicate considerably different responses of P-E balance and glaciation at Junín during each of these intervals and highlight the sensitivity of tropical Andean climate to relatively small differences in global boundary conditions.

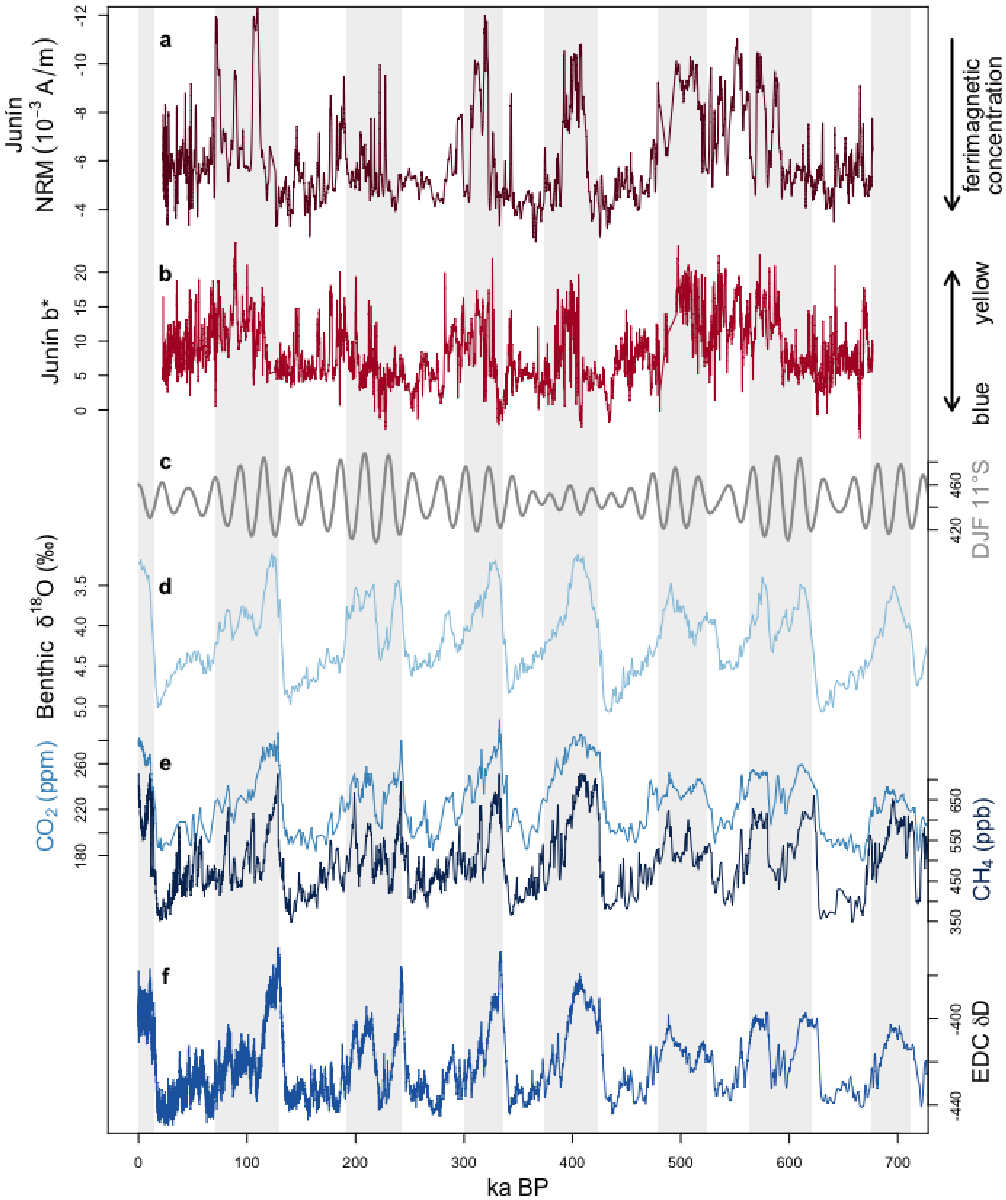

Figure 16. Global glacial/interglacial cycles of the past 700 kyr. Changes in a, ferrimagnetic concentration (Hatfield et al., 2019) and b, sediment color from Lake Junín track the 100 kyr pacing of glacial/interglacial cycles. c, summer insolation (Dec-Jan) for 11°S (Laskar et al., 2004), d, LR04 benthic stack $\delta^{18}O$ values (Lisiecki & Raymo, 2005), e, atmospheric CO_2 (Lüthi et al., 2008, light blue) and CH_4 (Loulergue et al., 2008, dark blue) concentrations, and f, Antarctic temperature based on ice core δD (Jouzel et al., 2007). Data in a and b are plotted on the age model of Hatfield et al. (2020), which differs slightly from the age model for MIS 12-15 used in this paper. Gray shaded bars indicate interglacial periods based on the Marine Isotope Stage boundaries of the LR04 benthic stack.

4.1.1 Study location and modern climate

Lake Junín (11°S, 76°W, 4100 masl, Figure 17) occupies an intermontane basin known as the Junín Plain between the eastern and western cordilleras of the Peruvian Andes, dammed at its northern and southern ends by coalescing glacial outwash fans (Wright 1983). The watershed is currently unglaciated, but moraines dating to previous glacial cycles indicate that glaciers repeatedly advanced to within several km of the lake depocenter in the past (Smith et al. 2005). The lake's surface area of ~280 km^2 occupies roughly a third of the watershed, and a dense perimeter of fluctuating wetlands and peatlands surrounds the lake margins. A maximum depth of 15 m was noted by Seltzer et al. (2000), although the deepest measurement obtained during the 2015 field season was 8.8 m, reflecting substantial seasonal to interannual variations in lake level. Surface water inputs contribute ~60% of total water input to the lake and the rest comes from direct precipitation (Flusche et al. 2005). Stream discharge measured during the dry season was ~8% of that measured during the wet season in 2001-2002, consistent with unpublished rainfall data from 1916-1988 for La Oroya, Peru indicating that a majority of precipitation to the Junín region is received during the austral summer with less than 7% falling during austral winter (Servicio Nacional de Meteorologia e Hidrologia del Peru, Ministeria del Ambiente). Total annual precipitation is around 900 mm/yr.

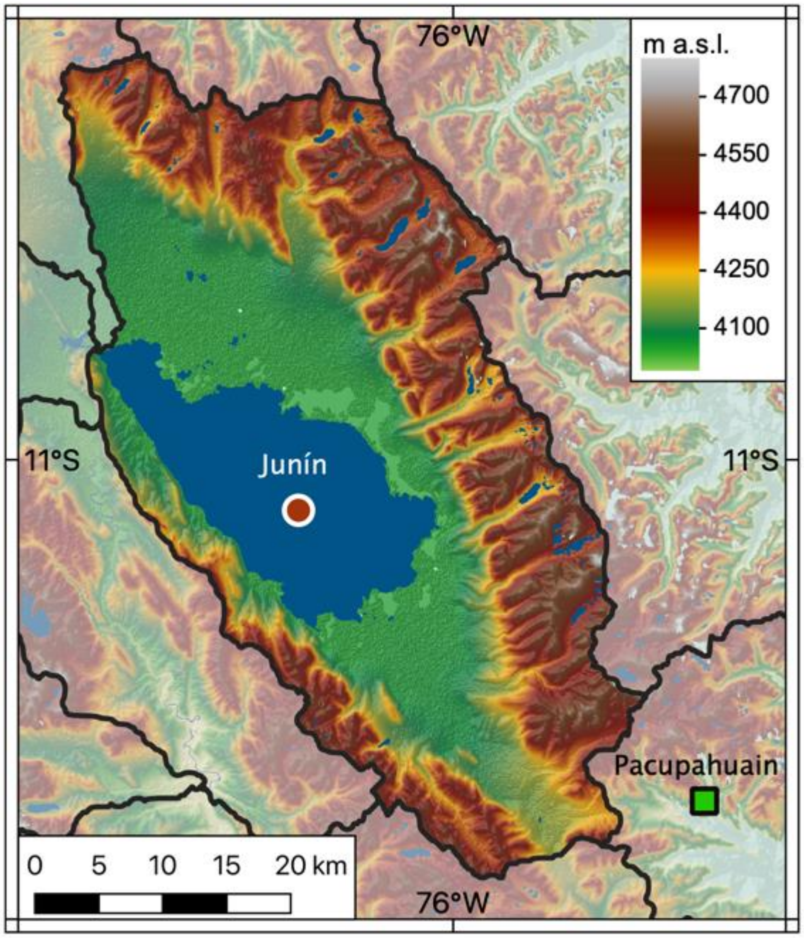

Figure 17. The Lake Junín watershed in the central Peruvian Andes.

4.1.2 Sedimentology

The stratigraphy of Lake Junín reflects both climatic and hydrologic variations. The sediments are characterized by alternating grey detrital silts with variable carbonate content and high magnetic concentrations deposited during cold intervals when piedmont glaciers in the eastern valleys are in advanced positions, and authigenic carbonate silts deposited during warm intervals when glaciers have retreated up valley behind moraine-dammed lakes that cut off detrital inputs (Seltzer et al. 2000; Rodbell et al. 2008), a pattern than holds over the past ~700 ka (Figure 16) (Chen et al. 2020; Hatfield et al. 2020). Peat layers consisting of partially decomposed macrofossil fragments are interspersed within the glacial silts and are interpreted as episodes of low lake stands when the fringing peatlands dried out and contributed organic-rich material to the lake (Woods et al. 2020). Fine-grained organic-rich muds lacking macrofossils deposited during the last deglaciation likely reflect in-lake algal productivity.

All major streams and springs flowing into Lake Junín are supersaturated with respect to Ca^{2+} and HCO_3^-, consistent with waters that dissolve limestone bedrock (Flusche et al. 2005). The lake today does not preserve calcite in its sediments because of the construction of the Upamayo Dam ca. 1932 that diverts acid mine drainage into the lake (Rodbell et al. 2014). Prior to this, the majority of calcite in Junín sediments likely precipitated from the water column as a result of algal productivity that seasonally changes the alkalinity, and/or seasonal lake level declines that concentrate solutes. The similarities in Holocene calcite sedimentation in Lake Junín across a series of transect cores from varying depositional environments (Weidhaas 2017) suggest it is a fairly uniform basin-wide process. In some areas of the lake calcite may also precipitate onto the stems of rooted macrophytes such as *Chara* spp. (Seltzer et al. 2000); this is likely less common in the deeper parts of the lake, but shallow water *Chara* calcite may get reworked and deposited into deep water environs.

4.1.3 Interpretation of bulk sediment properties and scanning XRF data

Previous studies in the tropical Andes have established that the primary control on the delivery of clastic sediment to proglacial alpine lakes is the extent of up-valley ice cover (Abbott et al. 2003; Rodbell et al. 2008; Stansell et al. 2005). Seltzer et al. (2000) demonstrated the strong coupling between ice extent and deposition of glacial flour in Lake Junín during the last glacial cycle based on the sediment magnetic susceptibility (MS) and established that clastic sediment input is limited to intervals during which paleoglaciers are present in the basin. X-Ray Fluorescence (XRF) count rates of erosional elements such as redox-insensitive titanium have also been demonstrated as effective, high-resolution proxies for glacial erosion of bedrock and lithogenic sediment transfer to lakes related to glacier mass turnover (Bakke et al. 2009). Here, scanning XRF counts of Ti are backed by lower resolution residual mineral content of the bulk sediment to provide a record of relative changes in paleoglacier mass balance during past glacial periods.

4.1.4 Controls on $\delta^{18}O$ values at Lake Junín

In South America, moist air masses originating from the tropical Atlantic are transported landward by the easterly trade winds and contribute to the development of deep convection and precipitation over the continent associated with the SASM during the austral summer wet season (DJF) (Zhou and Lau 1998), and this moisture is further transmitted to the high elevation Andes via the Low Level Jet. The $\delta^{18}O$ of precipitation in the tropics is often interpreted to reflect precipitation amount based on the correlation between higher monthly precipitation and lower $\delta^{18}O$ values observed at tropical weather stations (Dansgaard 1964). As such, the $\delta^{18}O$ value of SASM precipitation primarily reflects convective activity and rainout in the Amazon Basin core monsoon region at least on seasonal and interannual timescales (Vuille et al. 2003; Lee and Fung 2008), although this effect becomes weaker further inland towards western South America (Vimeux et al. 2005). Therefore, a primary control on the $\delta^{18}O$ of precipitation reaching Junín is SASM intensity upstream, which is the basis underlying paleoclimate interpretations from the region (Seltzer et al. 2000; Bird et al. 2011; Kanner et al. 2012). Observational and modeling studies have demonstrated additional influences on tropical South American $\delta^{18}O$ values, including moisture trajectories (Vimeux et al. 2005), cloud type (Konecky et al. 2019), changes in the seasonality of precipitation (Liu and Battisti 2015), and the degree of transpiration/recycling (Salati et al. 1979; Martinelli et al. 1996); the relative importance of these effects varies with region and timescale but they are generally thought to be of secondary importance compared to SASM intensity.

Stream waters in the Junín watershed today have $\delta^{18}O$ values between -13 and -15‰ (Flusche et al. 2005), consistent with precipitation-weighted annual mean $\delta^{18}O$ values for the region in IAEA station data and models (Vuille et al. 2003). Lake Junín is large, shallow and well-mixed enough to average out shorter term seasonal isotopic variations, and thus to a first order incorporates the isotopic composition of mean annual precipitation. However, the lake water $\delta^{18}O$ is between -7 and -10‰ (Flusche et al. 2005), reflecting a large evaporative influence. This modern-day isotopic relationship is mirrored in the Junín Holocene record, wherein carbonate $\delta^{18}O$ values decrease from the early to late Holocene as austral summer insolation increases, interpreted as a gradual strengthening of the SASM (Seltzer et al. 2000). A similar overall trend in $\delta^{18}O$ from nearby open basin lakes (Bird et al. 2011) and speleothems (Kanner et al. 2013) suggests a common precipitation source among these sites in the central Peruvian Andes. However, the $\delta^{18}O$ values from Junín are 4-6‰ more positive and this offset is greatest during the early Holocene insolation minimum, suggesting evaporative enrichment of lake waters was more pronounced under a weak monsoon and highlighting the sensitivity of Lake Junín to local P-E balance.

4.2 Materials and methods

4.2.1 Chronology

An initial age model was developed for the ~95 m composite core record based on U-Th dating of authigenic $CaCO_3$ that was deposited during interglacial periods (Chen et al. 2020), making Lake Junín one of the few long tropical records to establish an independent radiometric chronology. Since the initial set of 174 U-Th measurements yielded a high degree of scatter, rigorous geochemical screening criteria were applied to identify samples that may have been influenced by detrital contamination and/or post-depositional alteration. This process returned 72 "passing" U-Th ages that serve to anchor several interglacial periods within the past ~700 kyr. The U-Th ages of Chen et al. (2020) were subsequently incorporated into a second age model based on the relative paleointensity record from Junín (Hatfield et al. 2020), which is best resolved and most continuous in sediments containing glacially eroded clays. This age model used the normalized remanence ratio (NRM/ARM_{slope}) to provide a continuous record of paleomagnetic field intensity variability for alignment to a well-dated reference stack. While the radiometric and paleomagnetic age models for Junín differ by several thousand years in some intervals, the mean ages of each model fall within the other model's 95% confidence intervals (Hatfield et al. 2020). Together, the radiometric and paleomagnetic chronologies provide an independent chronological framework that confirms that the sequence of glacial and interglacial periods recorded in the sediments extends through at least MIS 16.

The typical spacing of 1-4 m between dates, however, implies intervals of ~10-40 kyr with minimal age control. The section spanning MIS 13-15 in particular would benefit from additional chronologic information, as three U-Th ages from approximately the same depth (70.93-71.19 m) simultaneously date to MIS 13, 14, and 15, and their calculated error estimates do not overlap (Chen et al. 2020). Furthermore, the low concentration of magnetic minerals throughout this carbonate-rich section precludes the selection of paleomagnetic tie points, such that the nearest ones fall within the glacial sediments associated with MIS 12 and 16 (Hatfield et al. 2020). Variable sedimentation rates between glacial and interglacial periods cannot easily be captured with this resolution of age control. Fortunately, Junín's stratigraphy and geochemistry display a characteristic response to certain long-term global climate fluctuations as documented during the well-dated past 50 kyr (Seltzer et al. 2000; Woods et al. 2020), namely a glacial/interglacial shift from fine-grained clays to carbonates, and summer insolation forcing of monsoon strength, and thus $\delta^{18}O$ values. These well-established relationships allow for the selection of additional tie points which are incorporated into a modified age model (Figure 18, Table 5).

Three prominent precession cycles are apparent in our $\delta^{18}O$ data during MIS 15, characterized by a smaller-larger-smaller amplitude pattern and followed by a fourth, lower-amplitude cycle with a distinct tapered/asymmetrical shape (Figure 20). The structure of these $\delta^{18}O$ variations closely resembles the eccentricity-modulated precession signal that characterizes local summer insolation (DJF, 11°S) during MIS 15. The depths associated with peak monsoon intensity/insolation were assigned based on the midpoint between the descending and ascending arms of the $\delta^{18}O$ curves. Two additional tie points, based on the boundaries between MIS 11/12 and MIS 15/16 in the LR04 benthic stack (Lisiecki and Raymo 2005), were aligned to the respective carbonate/silt transitions in the Junín stratigraphy. The large depth uncertainty of ± 20 cm assigned to tie point LR04-1 reflects the termination of Ti inputs in the middle of a dark organic unit (i.e. dark organic sediments extend for ~20 cm in both directions), and delayed onset of elevated carbonate content. For tie point LR04-2, the smaller depth uncertainty of ± 1 cm reflects the sharp stratigraphic transition in the core images associated with the shift from Ti-rich to and $CaCO_3$-rich sediment (Figure 19).

Since the age uncertainty in the LR04 benthic stack is estimated as 4 kyr for 0-1 ma, values at least this large were assigned to the tie points used here. The insolation tie points were assigned smaller age uncertainties, because aligning the Junín data directly to local summer insolation is preferable to "double tuning," or tuning to another proxy record such as the benthic stack that is itself tuned to insolation curves (Blaauw 2012).

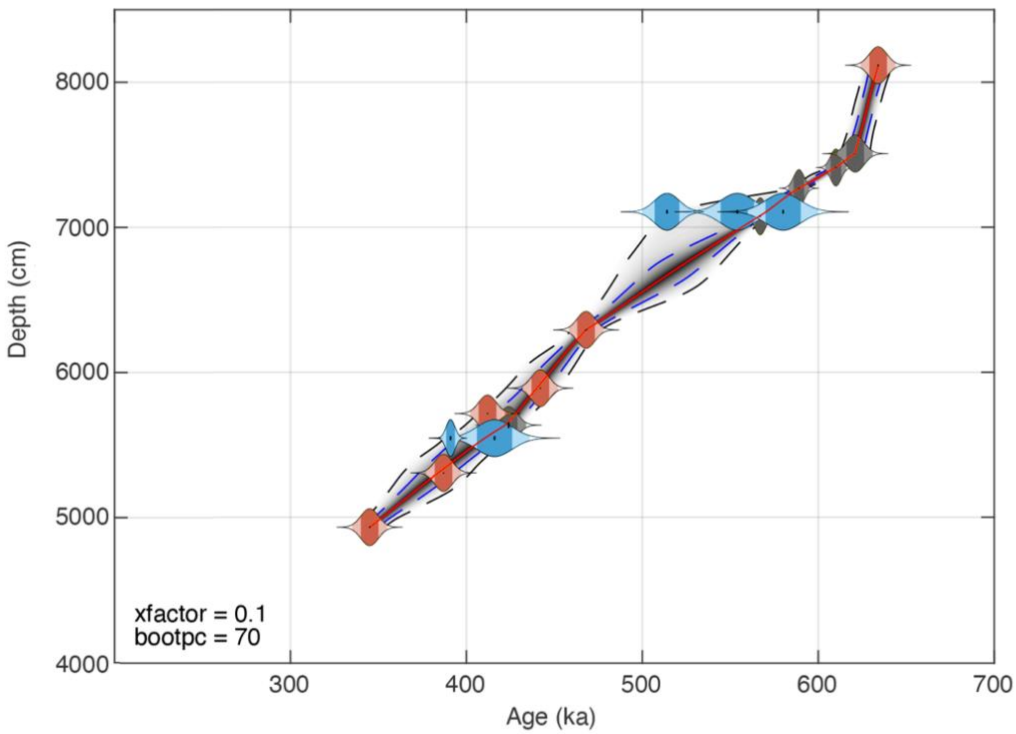

Figure 18. Modified age-depth model for the older portion of the Junín record, based on a combination of U/Th ages (blue), relative paleointensity (red), and tie points (black). The age model was created using the MATLAB package Undatable.

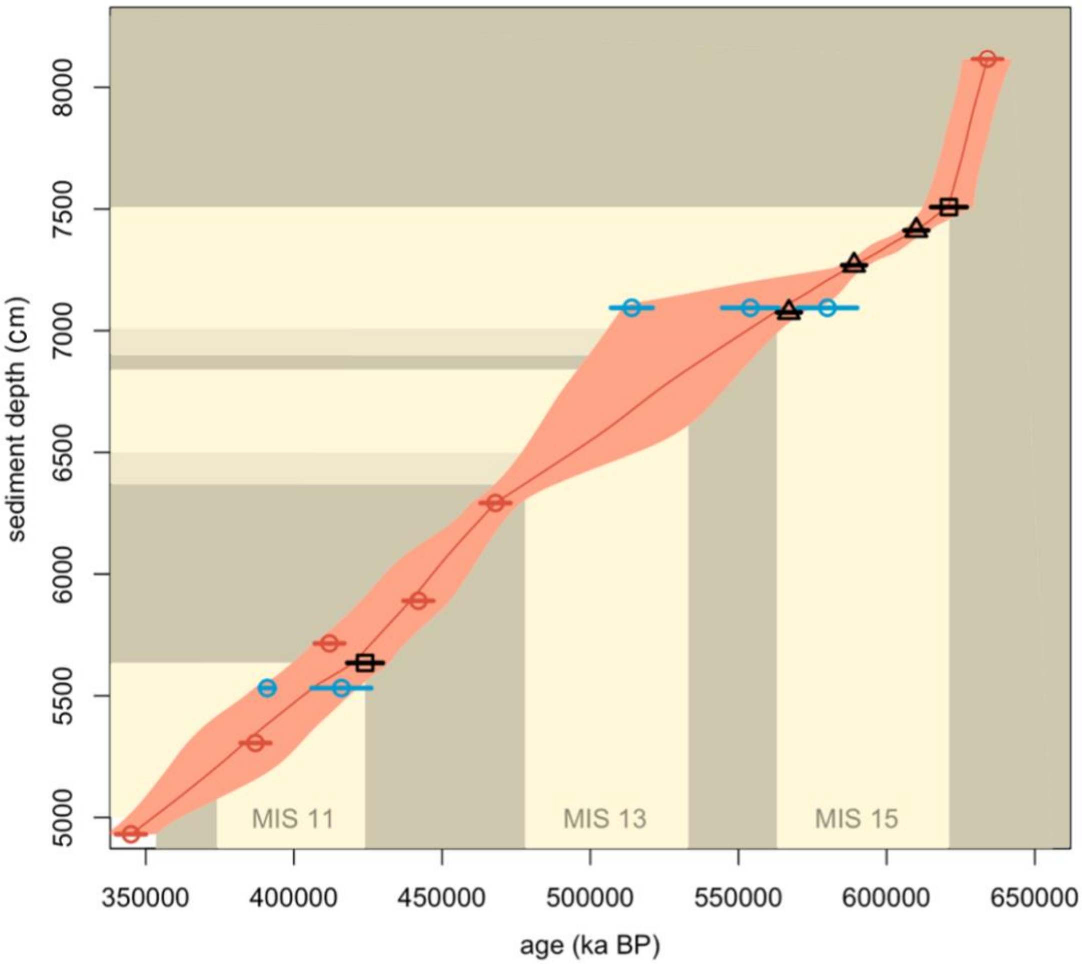

Figure 19. Age model for MIS 15-12 and glacial/interglacial stratigraphy. U/Th ages (blue circles), relative paleointensity points (red circles), and tie points based on insolation (black triangles) and the LR04 benthic stack (black squares). Vertical bars correspond to the timing of marine isotope stages according to LR04 (light tan is interglacials, dark tan is glacials), and horizontal bars delineate the Junín facies, with light tan showing carbonate, dark tan showing glacial silts, and medium tan showing intermediate facies that are harder to classify (e.g. containing organics and silts).

Table 5. Tie points used in the modified age-depth model for MIS 12-15

Tie Point	Age (ka)	Age error (ka)	Depth (m)	Depth error (m)	Notes
Insol-1	567	2-4	70.750	0.04	
Insol-2	589	2-4	72.690	0.04	
Insol-3	610	2-4	74.120	0.04	
LR04-1	424	4-6	56.350	0.20	MIS 11/12 boundary
LR04-2	621	4-6	75.077	0.01	MIS 15/16 boundary

4.2.2 Bulk sediment and geochemical analysis

Bulk density was determined from the air-dried mass of 1 cm^3 samples taken every 8 cm. Total organic and inorganic carbon (TOC, TIC) was measured on samples taken every 4 cm. Total carbon (TC) was determined by combusting samples at 1000°C using a UIC 5200 automated furnace, and analyzing the resultant CO_2 using a UIC 5014 coulometer at Union College. Similarly, TIC was determined by acidifying samples using an Automate acidification module and measuring the resultant CO_2 by coulometry at Union College. We calculated weight percentage TOC from TOC=TC-TIC. We calculated total carbonate content from TIC (%)/12 to reflect the molar ratio between TIC (%) and $CaCO_3$, and total organic matter (TOM) content from TOC (%)/44 to reflect the molar ratio between TOC (%) and organic matter. The percent residual mineral matter was estimated by subtracting carbonate content and TOM from 100.

Stable oxygen and carbon isotopes were measured on bulk carbonates every 2 cm. Samples were measured via a Thermo Gas Bench II connected to a Thermo Delta Advantage mass spectrometer in continuous flow mode at Union College. Reference standards (LSVEC, NBS-18, and NBS-19) were used for isotopic corrections, and to assign the data to the appropriate isotopic scale using linear regression. The following values were used for $\delta^{13}C$ and $\delta^{18}O$ respectively: LSVEC: -46.6‰, -26.7‰; NBS-18: -5.014‰, -23.2‰; and NBS-19: +1.95‰, -2.2‰. The combined uncertainty (analytical uncertainty) for $\delta^{13}C$ is ± 0.03‰ (VPDB) and $\delta^{18}O$ is ± 0.05‰ (VPDB), based on 11 NBS-19 standards over 3 analytical sessions. XRF scanning was performed at the LacCore XRF Lab, University of Minnesota-Duluth Large Lakes Observatory using a Cox Analytical ITRAX with a Cr tube, 5 mm resolution, and 15 second dwell time.

4.3 Results

4.3.1 MIS 15 (75-70.3 m)

An abrupt transition from dark grey glacial silt to carbonate-rich sediment at 75 m (~620 ka) marks the onset of MIS 15. $CaCO_3$ content remains elevated (60-90 wt. %) and Ti levels remain low for the duration of this interglacial (Figure 20). Carbonate $\delta^{18}O$ values range from -3 to -18‰ (VPDB) and $\delta^{13}C$ values range from 16 to 0‰ (VPDB). $\delta^{18}O$ and $\delta^{13}C$ values covary (r=0.93) throughout MIS 15 (Figure 21).

The intervals with more negative $\delta^{18}O$ values (-13 to -18‰) are associated with creamy yellow to light gray massive facies (Figure 22), wherein the absence of laminations likely reflects the deposition of homogeneous, nearly pure carbonate (averaging 85 wt. % but as high as 96 wt. %), with very low TOC content (generally < 3 wt. %). Intervals with more positive $\delta^{18}O$ values (> -12‰) are associated with finely banded carbonate facies that range in color from yellow-tan to reddish and greenish, interspersed with occasional organic-rich layers with TOC content in the range of 5-20%.

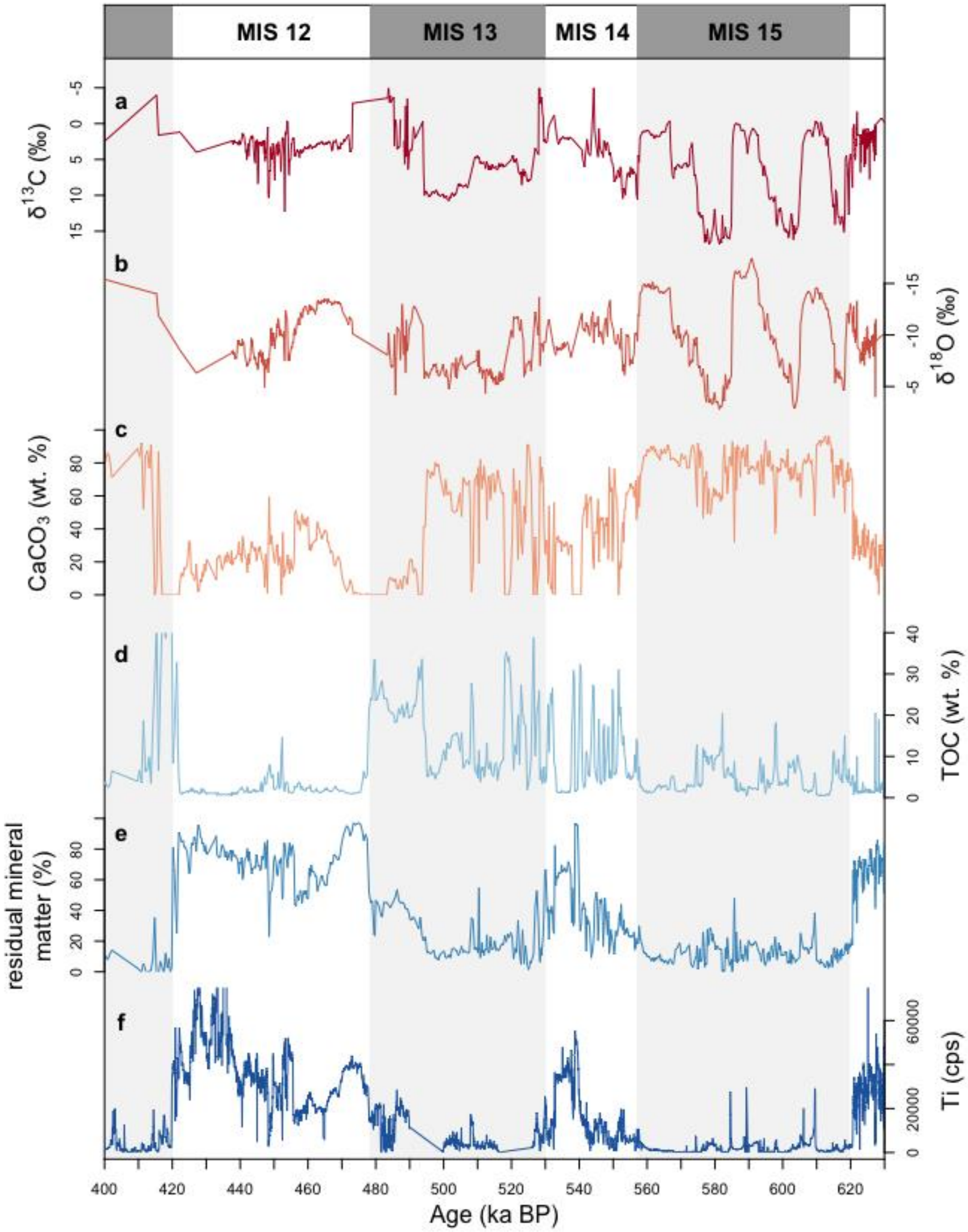

Figure 20. Proxies from Lake Junín during MIS 12-15 show large differences between glacial and interglacial periods. a, $\delta^{13}C$ and b, $\delta^{18}O$ values measured on authigenic carbonates, c, calcium carbonate content, d, total organic carbon content, e, residual mineral matter, and f, XRF Ti counts.

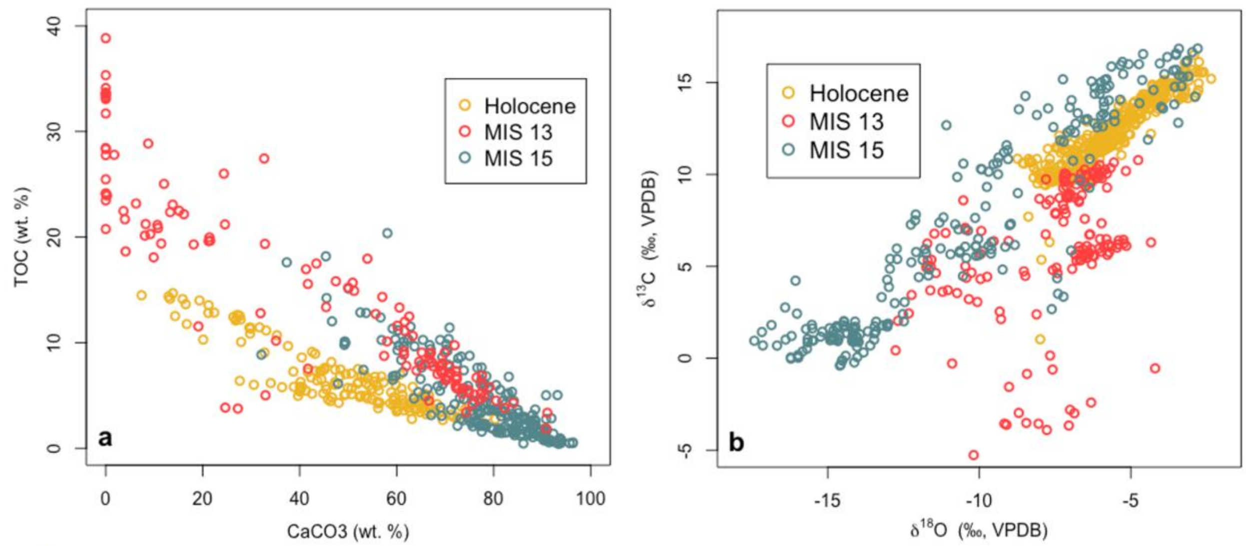

Figure 21. Differences in stable isotope values and carbon content among interglacials. a, all three interglacials are characterized by highly elevated carbonate content; MIS 13 is unique in that it displays intervals with much higher TOC content and minimal carbonate during the early and late phases of this interglacial period. b, the $\delta^{18}O$ and $\delta^{13}C$ values of authigenic carbonates are highly correlated during the Holocene (r=0.90) and MIS 15 (r=0.93), reflecting the impacts of residence time and evaporation. The correlation during MIS 13 is weaker (r=0.43) due to scatter in a subset of samples that coincide with the intervals of highly elevated TOC content.

4.3.2 MIS 14 (70.3-68.4 m)

The transition from MIS 15 to MIS 14 (70.3 m) at Lake Junín is marked by a moderate decline in $CaCO_3$ content, increase in TOC, and moderate increase in Ti levels indicating enhanced erosion from advancing glaciers (Figure 20). Light grey sediments with occasional banding early on give way to medium to dark grey, banded silts interspersed with thicker and more frequent peat layers (Figure 22). Carbonate $\delta^{18}O$ values exhibit a smaller range (-6 to -13‰) and greater short-term variability compared to the previous interval. A sharp increase in Ti values at 68.8 m (~538 ka) initiates a ~0.4 m deposit of homogenous, light grey/tan silt that represents local glacial maximum conditions. High clastic inputs persist until the abrupt onset of deglaciation at 68.4 m (~533 ka), immediately followed by further peat deposition marking a low lake stand.

The sequence of alternating glacial silt and peat during the first half of MIS 14 resembles the changes documented at Junín during MIS 3 associated with DO cycles, wherein increased input of glacigenic silt coincides with enhanced monsoon precipitation during Greenland stadials, and reduced silt flux indicates glacial retreat during dry interstadials coupled with peat deposition revealing low lake level (Woods et al. 2020). During both glacial periods, the peat layers contain 5-35% TOC and range in thickness from 1 to 20 cm, although most of the MIS 14 peats fall in the higher ends of these ranges. During MIS 3 the peats are frequently separated by 10-70 cm of glacial silts, compared with ≤ 30 cm during MIS 14, and Ti counts associated with the glacial silt units during MIS 14 are considerably lower compared to those of MIS 3, owing in part to the higher average TOC content during MIS 14.

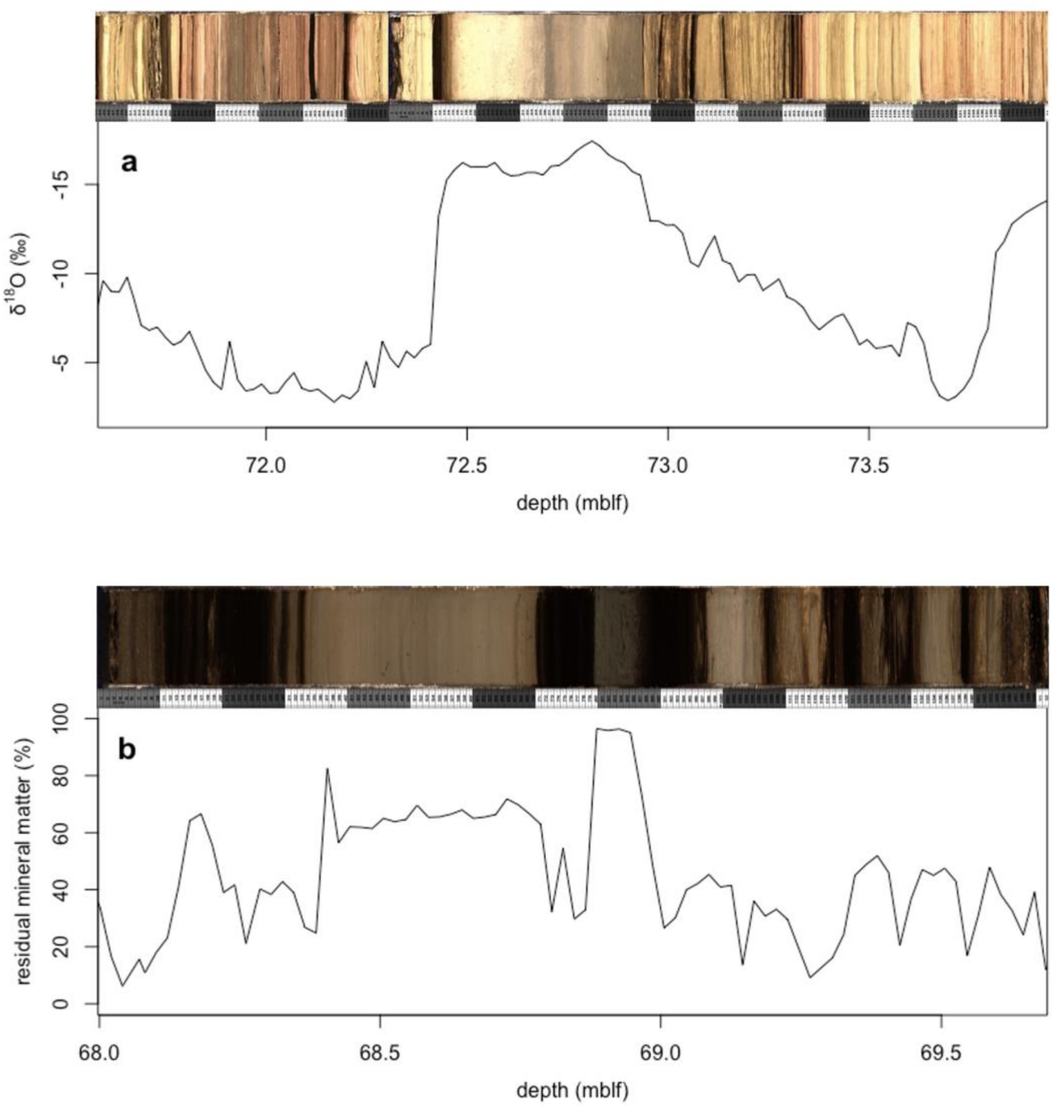

Figure 22. High resolution line-scan images of sediment cores that are representative of interglacial and glacial facies. Top: overlapping cores 1E-15H-1 and 1C-24H-1 from MIS 15. More negative $\delta^{18}O$ values (a) coincide with light-colored massive carbonates, whereas more positive values coincide with banded to laminated carbonates. Bottom: core 1E-14H-1 from MIS 14. Higher residual mineral content (b) coincides with tan to grey glacial silts, and lower mineral content coincides with dark, organic-rich peat layers.

4.3.3 MIS 13 (68.4-63.7 m)

MIS 13 differs markedly from MIS 15 – the sediments are darker, more organic-rich with TOC consistently >5%, and more variable in $CaCO_3$ content, such that there is not a clearly delineated transition from MIS 14 to MIS 13. A series of 1-10 cm-thick peat layers from 68.4-67.3 m (~533-520 ka) resembles those deposited during early MIS 14. Above 67.3 m (520 ka) the sediments develop finer laminations and $CaCO_3$ content stabilizes between 50-80%, indicating more typical interglacial conditions during mid-MIS 13. An abrupt decrease in $CaCO_3$ content at 65 m (494 ka) marks the onset of a dark, organic-rich deposit with moderate clastic content and no visible stratigraphy, that abruptly terminates at 63.7 m (~478 ka). Ti levels are elevated compared to MIS 15 (Figure 20).

The $\delta^{18}O$ values span -5 to -12‰ and $\delta^{13}C$ values span 10 to -5‰, indicating a smaller amplitude of isotopic variability compared to MIS 15. Isotopic values are more variable during early and late MIS 13 and fairly stable during mid-MIS 13, and there is more scatter in the relationship between $\delta^{18}O$ and $\delta^{13}C$ values (r=0.43) compared to MIS 15 (Figure 21).

4.3.4 MIS 12 (63.7-56.5 m)

The transition to MIS 12 is marked by an abrupt shift from a thick TOC-rich unit to dark grey glacial silts indicating glacier expansion. From 63.7-61.8 m (~478-460 ka) the sediments appear massive with some subtle variation in color but consistent texture, and Ti inputs increase and then decrease gradually. From 61.8-59 m (460-440 ka) the sediments develop more frequent banding with several intervals containing slightly elevated TOC content; Ti inputs remain elevated and also variable. Above 59 m (440 ka), Ti inputs increase to levels nearly double those seen during late MIS 14, and residual mineral matter also increases but to a lesser degree; the sediments again become massive with very low TOC content until 56.5 m (420 ka). This interval represents peak glacial expansion and is followed by an abrupt decline in Ti at 420 ka and a major increase in TOC content (>40 wt. %) that marks the termination of this glacial period (Figure 20). The $\delta^{18}O$ values span -6 to -13‰ and $\delta^{13}C$ values span 12 to 0‰. The facies changes described here are summarized in Table 6.

Table 6. Interpretation of facies and bulk sediment properties

Facies	Lake level	Context	Observed during MIS
Peat layers (elevated TOC content)	Low	Expansion and erosion of surrounding peatlands	12, 13, 14, 15
Banded/layered carbonates	Medium to low	Lower lake level allowing increased terrigenous inputs	13, 15
Massive carbonates	High	Minimal terrigenous inputs resulting in homogenous sediment	15
Glacial silts (elevated Ti and residual mineral matter)	Medium to high	Colder and/or wetter conditions enabling glacier advance or stand still	12, end of 13, 14

4.4 Discussion – interglacial periods

4.4.1 Differences in monsoon strength and P-E balance among interglacials

MIS 13 and 15 show stratigraphic and geochemical characteristics that separate them from each other and from the Holocene, indicating distinctly different P-E balance and lake hydrology among interglacial periods at Junín. Precessional-scale isotopic variability is prominent during MIS 15, with an overall range in $\delta^{18}O$ values that is ~3 times larger than it is during the Holocene (Figure 23), consistent with the enhanced amplitude of precessional cycles owing to the MIS 15 eccentricity maximum (Laskar et al. 2004). Insolation maxima coincide with very negative $\delta^{18}O$ values (< -12‰) that are not observed during the Holocene or MIS 13, suggesting episodes of greatly enhanced monsoon strength. Similarly, the massive unlaminated carbonate facies that correspond to these intervals are unique to MIS 15 and suggest relatively high and stable lake levels in a well-mixed water column prevailed for millennia, with minimal inputs of nearshore/terrigenous material (Table 6, Figure 22).

Periods of lower summer insolation during MIS 15 are associated with more positive $\delta^{18}O$ values and the corresponding finely-banded sediments contain increased TOC and mineral matter. These facies likely reflect a shifting balance between calcite production, variations in aquatic and terrestrial organic matter inputs, and terrigenous detrital inputs, which suggests shallower and more variable lake level (Table 6, Figure 22). The sediments also intermittently display reddish and greenish coloring, which is not seen during MIS 13 or the Holocene. Red to green color intensity changes in the carbonate facies of Lake Junín have been suggested to result from post-depositional diagenesis (Chen et al. 2020). According to this interpretation, reddish sediments reflect carbonates containing iron-bearing minerals and organic matter deposited under oxygenated conditions; continued degradation of organic matter after burial would eventually lower the pH of local pore fluids such that they reduce the surrounding sediments and shift the color toward a greenish hue (Chen et al. 2020). This interpretation is consistent with higher $\delta^{18}O$ values (-3 to -12‰) suggesting a weaker SASM, as the fluctuations in local water table that would facilitate such color intensity changes are more likely during times of somewhat lower lake level. Still, $CaCO_3$ content remains high (>60%) and only thin peat layers form (with TOC generally <10%) indicating relatively stable sedimentation and only short duration (multi-decadal) low stands.

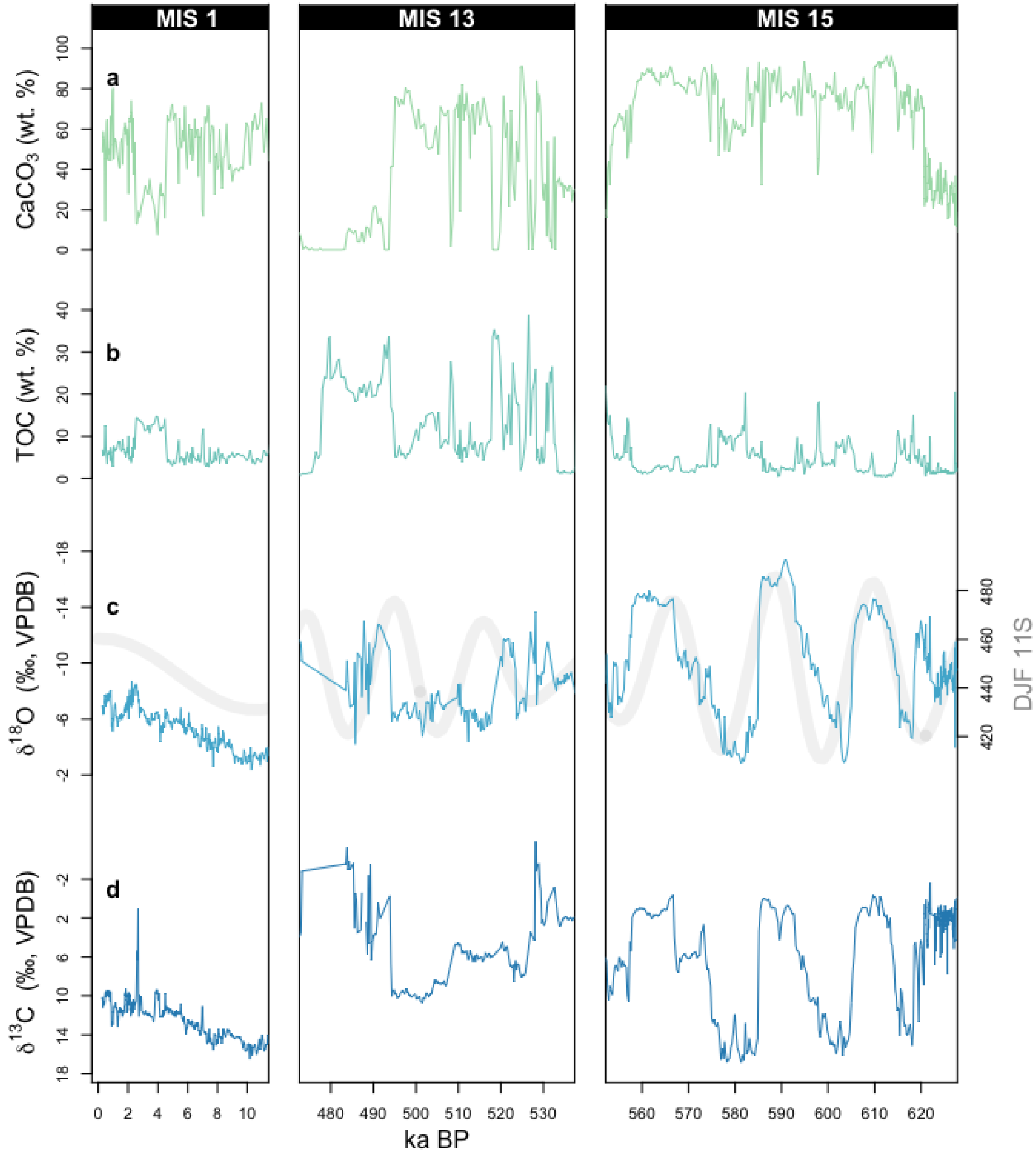

Figure 23. Side-by-side comparison of Junín proxies during the three interglacial periods discussed in the text. a, carbonate content, b, total organic carbon content, c, carbonate δ^{18}O values, and d, carbonate δ^{13}C values.

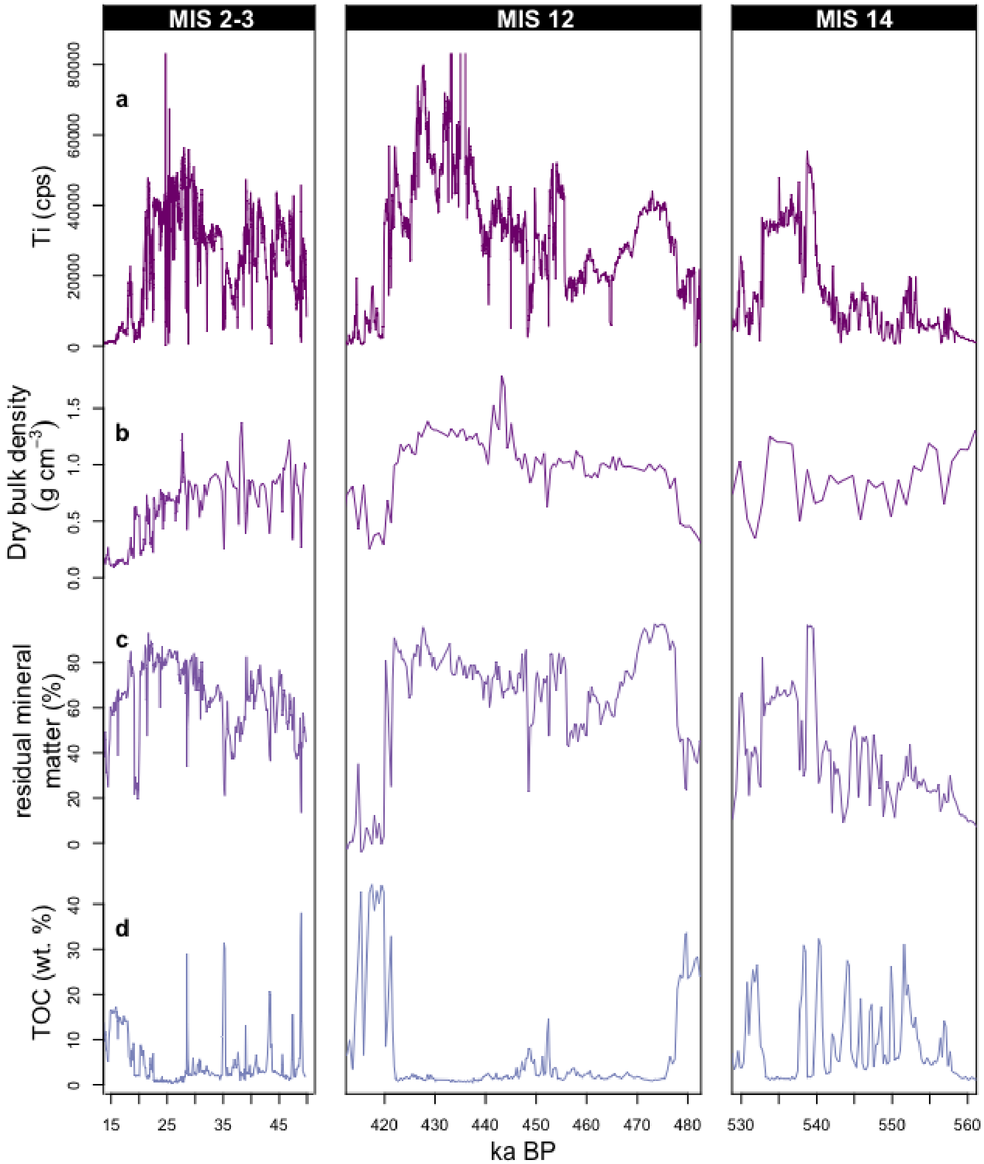

Figure 24. Side-by-side comparison of Junín proxies during the three glacial periods discussed in the text. a, Ti counts, b, dry bulk density, c, residual mineral matter, and d, total organic carbon content.

Conditions were cool and dry at Junín during much of MIS 13. A precession signal is only weakly apparent in the $\delta^{18}O$ and $\delta^{13}C$ data despite fairly large amplitude variations in local summer insolation, and the overall range in $\delta^{18}O$ values is reduced compared to MIS 15 (Figure 23). Sediments during the middle of MIS 13 (~495-515 ka) resemble the finely-banded intervals of MIS 15 and the Holocene in terms of $CaCO_3$ and TOC content, suggesting lake level fluctuations associated with medium to low stands, and the $\delta^{18}O$ values in this section overlap with the late Holocene (-5 to -8‰) (Figure 23). In contrast, the rest of MIS 13 appears more arid and cooler than either the Holocene or MIS 15 based on the sedimentology. Early-MIS 13 (~515-530 ka) contains multiple thick peat layers indicating persistent millennial-scale droughts, and the 20-kyr-long interval of elevated TOC during late-MIS 13 (~495-475 ka) suggests even more protracted dry conditions. Elevated Ti counts and mineral content during these arid intervals suggests possible erosional inputs from glacier presence in the watershed during early and late MIS 13 (Figure 20). Two ^{10}Be cosmogenic exposure ages from the eastern side of the Junín watershed (515 ±26 ka and 486 ±26 ka) (Smith et al. 2005) may support glacier presence during MIS 13, although they could date to MIS 12 and MIS 14, respectively, within dating errors.

MIS 13 and 15 stand out for displaying a weak interglacial signature in many global records compared to the interglacials of MIS 1-11. Ice core records indicate relatively cool conditions with CO_2 levels below ~260 ppm (Figure 25) (Lüthi et al. 2008), and higher global ice volume (Lisiecki and Raymo 2005); MIS 13 was slightly colder than MIS 15 according to these records, but the overall difference is subtle. It is therefore notable that these interglacials are so different from each other in the Junín record. During MIS 15, the Junín $\delta^{18}O$ record is antiphased with that from Sanbao Cave (31°N) in the northern tropics of China (Cheng et al. 2016), consistent with long-term north/south shifts of the tropical rainbelt related to precession (Figure 25). Given this relationship, the lack of a precession signal in the Junín $\delta^{18}O$ data during MIS 13 is unexpected. The overall shape of the $\delta^{18}O$ record during MIS 13 does show a reasonably close similarity, however, with the XRF-based molybdenum record from Cariaco Basin (10°N) (Gibson and Peterson 2014) (Figure 25). Molybdenum is enriched in sediments that accumulate under anoxic conditions in association with northward ITCZ shifts. The record indicates a more northerly ITCZ during the middle of MIS 13 from ~515-495 ka when Junín $\delta^{18}O$ values are more positive, and a more southerly ITCZ during early and late MIS 13 when $\delta^{18}O$ values are generally more negative, suggesting long term shifts in ITCZ position unrelated to precession may have been controlling SASM strength during this interglacial.

However, this scenario is at odds with our interpretation based on Junín's stratigraphy, which instead suggests drier conditions during early and late MIS 13 based on high TOC content and visible peat accumulation. This suggests a possible decoupling of SASM strength from actual hydroclimate conditions at Junín. A decoupling between $\delta^{18}O$ values and non-$\delta^{18}O$-based proxies for local moisture conditions has been noted during the Holocene for several localities in interior South America (Wortham et al. 2017; Ward et al. 2019), but not for Andean sites.

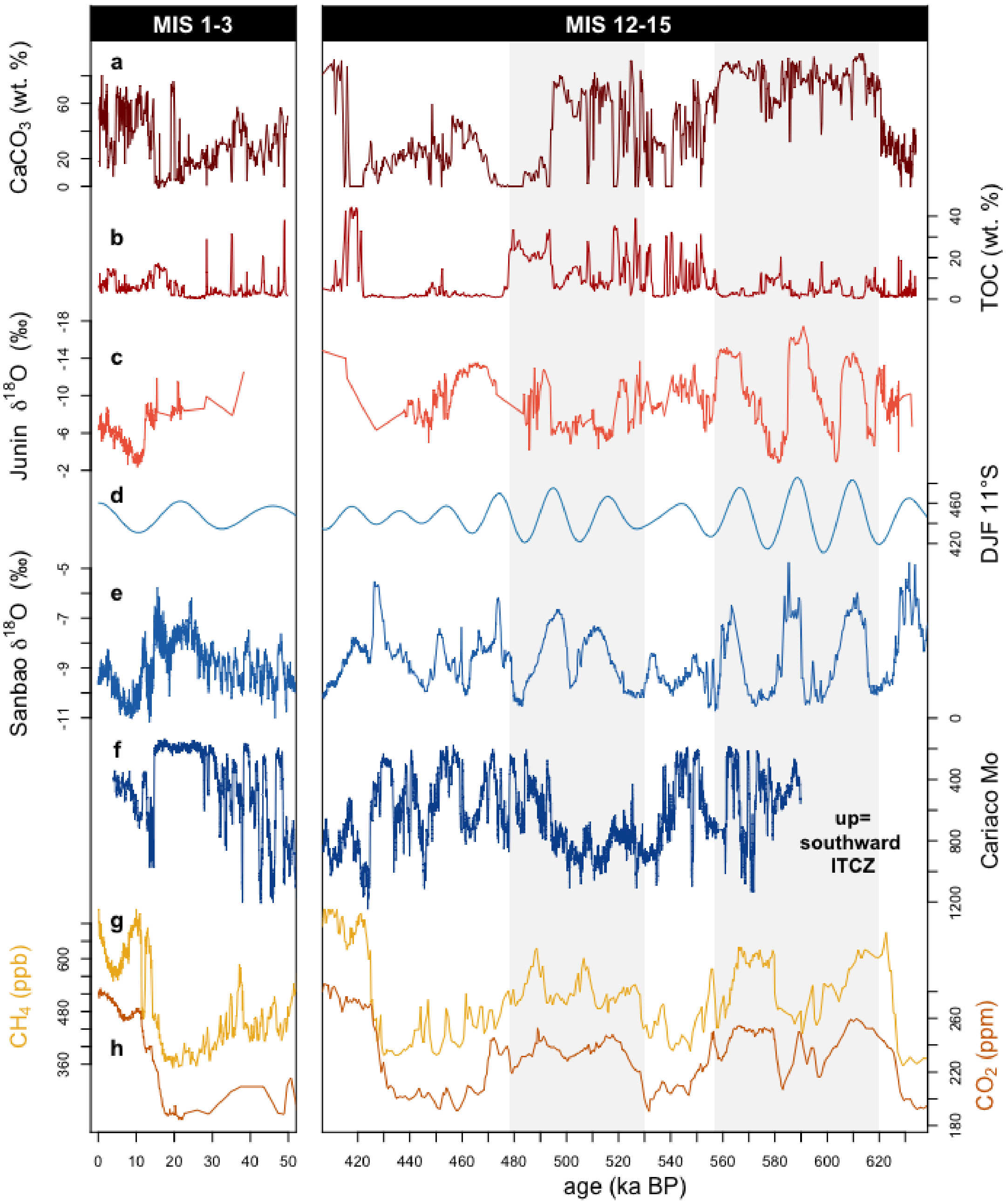

Figure 25. Junín compared to records from the northern tropics. Lake Junín proxies show some similarities with records of monsoon strength from the northern tropics during interglacial periods. a-c are proxies from Lake Junín: a, carbonate content, b, total organic carbon content, c, carbonate $\delta^{18}O$ values. d, Southern Hemisphere summer insolation (Laskar et al., 2004), e, speleothem $\delta^{18}O$ values from Sanbao Cave, China (Cheng et al., 2016), f, XRF counts of molybdenum from Cariaco Basin sediment core (Gibson and Peterson, 2014), g, atmospheric CH_4 concentration (Loulergue et al., 2008) and h, atmospheric CO_2 concentration (Lüthi et al., 2008). The scale for the Sanbao $\delta^{18}O$ record is reversed relative to that of Junín, reflecting the antiphased nature of the Asian and South American monsoon systems. MIS 13 and 15 are indicated by grey shaded bars.

4.4.2 The influence of evaporation on carbonate isotopes and lake hydrology

The isotopic records from Lake Junín provide evidence for the persistent influence of evaporation and lake water residence time across interglacials. This effect is best demonstrated in studies of the modern hydrologic system and in the Holocene carbonate record, which can be related to the patterns observed during MIS 13 and 15. Stream waters in the Junín basin today have $\delta^{18}O$ values between -13 and -15‰ (VSMOW) whereas the lake water $\delta^{18}O$ varies between -7 and -10‰ (Flusche et al. 2005), reflecting the impact of evaporation on the lake's large surface area. During the Holocene, Junín carbonate $\delta^{18}O$ values are similarly 4-6‰ (VPDB) more positive relative to nearby, isotopically-open lake and cave systems (Bird et al. 2011; Kanner et al. 2013), with the largest offset during the early Holocene signifying enhanced aridity and evaporation. Also observed during the Holocene is a relatively strong covariance (r=0.90) between carbonate $\delta^{18}O$ and $\delta^{13}C$ values, an effect that is often seen in closed-basin lakes and primarily attributed to P-E balance/evaporation, or to relatively long residence time in lakes that are not closed (Talbot 1990; Li and Ku 1997; Horton et al 2016).

During MIS 15, the covariance between $\delta^{18}O$ and $\delta^{13}C$ (r=0.93) (Figure 21) is stronger than the Holocene, even across the intervals of greatly enhanced monsoon strength during MIS 15. It has been suggested that stability of covariant trends across long periods of time and across large climatic shifts points to considerable stability of basin hydrology despite changing P-E conditions (Talbot 1990), which may explain why no major unconformities are apparent in the sedimentary sequence even during the relatively drier intervals of MIS 15.

The overall covariant trend during MIS 13 is considerably weaker (r=0.43). While poor covariance between lake water carbon and oxygen isotopes is often interpreted to reflect a hydrologically open system (Talbot 1990; Li and Ku 1997; Leng and Marshall 2004), such conditions are unlikely to characterize Lake Junín during MIS 13. Closer inspection reveals that most of the scatter arises from a subset of samples that have exceptionally negative $\delta^{13}C$ values (< 0‰), low $CaCO_3$ content, and that coincide with organic-rich intervals at the onset and end of MIS 13. Such organic-rich facies suggest expansion of peatlands and shallow lake level fluctuations, which would facilitate the oxidation of organic matter and lead to more negative inorganic $\delta^{13}C$ values due to the localized availability of ^{12}C. Furthermore, two linear groupings are apparent in the cross plot, one with $\delta^{13}C$ values < 7‰ and one with $\delta^{13}C$ values > 7‰ (Figure 21). The $\delta^{18}O$ values of these samples overlap isotopically with typical late Holocene values of -5 to -8‰ implying that P-E balance during mid-MIS 13 was similar to the Holocene, a time of continual evaporative influence. In contrast, the TOC content during early and late MIS 13 (20-40%) is significantly higher than the Holocene or MIS 15 (both with TOC <20%), suggesting prevalent low stands and the driest conditions of any interglacial discussed here. Contributions of ^{18}O-depleted glacial meltwater to the lake may explain the more negative $\delta^{18}O$ values (<-8‰) that are otherwise difficult to reconcile with these apparently dry periods.

Further evidence for the influence of evaporation at Junín is demonstrated by the abrupt positive shifts in $\delta^{18}O$ and $\delta^{13}C$ values with each precession cycle during MIS 15, whereas the shifts to negative values are gradual. The positive transitions are more abrupt than would be expected from insolation forcing alone and suggest that decreases in monsoon strength were associated with additional evaporative enrichment of the lake water. While this portion of the age model is tuned to insolation, this phenomenon is likely independent of the chronology because the isotopic transition occurs within the span of centimeters, and across an interval in which $CaCO_3$ content remains high and stable, arguing against any major changes in sedimentation rate or sedimentary environment. Speleothem records of SASM strength, which are not expected to involve a significant evaporative component, do not demonstrate similarly abrupt shifts towards positive $\delta^{18}O$ values when approaching precessional minima (Hai Cheng et al. 2013; Cruz et al. 2005; Burns et al. 2019); those records are limited to the last 250 ka however. Speleothems from central China (Wang et al. 2001; Cheng et al. 2009), however, do show abrupt transitions between insolation extremes, in disagreement with model results that suggest the response to precessional forcing in that region should be smooth (Battisti et al. 2014). These abrupt changes were suggested to result from local processes such as threshold changes in vegetation or soil properties that affect evaporation and/or the flow of water, causing abrupt changes in fractionation (Battisti et al. 2014). The absence of abrupt transitions in the speleothem records from South America that track precession suggests the evaporative effect we observe is related to the longer residence time of Junín lake water rather than being a feature of the SASM response to forcing.

Without records from nearby open systems during these intervals we cannot know the magnitude of isotopic enrichment of the lake water relative to local meteoric water. Yet the evidence for C and O isotope covariance observed for the Holocene, MIS 13 and MIS 15, as well as the abrupt positive shifts in $\delta^{18}O$ values associated with the precessional variation during MIS 15, suggests that evaporation and/or prolonged residence time has likely characterized interglacials at Lake Junín throughout much of its existence.

4.4.3 Negative offset of $\delta^{18}O$ values relative to insolation forcing during MIS 15

During the late Holocene summer insolation maximum (~460 w m^{-2}), typical $\delta^{18}O$ values at Junín were -6 to -8‰, whereas when similar insolation levels occurred during MIS 15 about midway through each precession cycle, Junín $\delta^{18}O$ values reached about -12‰ (Figure 23). Thus, while the amplitude of $\delta^{18}O$ changes during MIS 15 is roughly proportional to the amplitude of insolation forcing, the absolute $\delta^{18}O$ values exhibit an apparent negative offset of 4-6‰ compared to the Holocene. This negative offset suggests a non-linear or disproportional response of $\delta^{18}O$ values to insolation forcing at Lake Junín and may reflect a number of processes including an invigorated SASM, reduced evaporation, and/or additional controls on the isotopic composition of Andean precipitation. It cannot be explained by expected changes in the $\delta^{18}O$ of seawater which was more positive throughout MIS 15 (Sepulcre et al. 2011; Elderfield et al. 2012), assuming the tropical Atlantic was the primary moisture source during both intervals. Furthermore, as insolation peaked during each MIS 15 precession cycle, Junín $\delta^{18}O$ decreased to -12 to -17‰, values that characterize isotopically open systems that record precipitation $\delta^{18}O$ in this region of the tropical Andes (Bird et al. 2011).

Cooler temperatures during MIS 15 may have suppressed surface evaporation, shifting the oxygen isotope composition of the lake water to more negative values that resemble that of meteoric precipitation today. Cores from the Bogotá Basin (4°N) in the Colombian Andes provide the only contemporaneous terrestrial temperature record for tropical South America, inferred from arboreal pollen percentage (AP%), and suggest MIS 15 was a relatively cool interglacial in the tropical highlands (Torres et al. 2013). Such conditions may have reduced evaporation to some extent, yet the previously discussed evidence for C-O isotope covariation suggests that prolonged residence time and/or evaporation remained an influence on the isotopic evolution of the lake water during MIS 15.

Another possible explanation for the more negative isotopic values during MIS 15 is a difference in moisture recycling upstream that affected average annual precipitation $\delta^{18}O$. The Amazon Basin is known to contribute large amounts of recycled water via evapotranspiration to air masses transported by the easterly trade winds (Salati et al. 1979; Martinelli et al. 1996; Staal et al. 2018, Ampuero et al 2020), with estimates for the contribution to local Amazon rainfall ranging from 32-80% (Salati et al. 1979; Martinelli et al. 1996; Staal et al. 2018). Plant transpiration is the largest component of this moisture flux and is a non-fractionating process when tropical humidity is high (Gat et al. 1994; Koster et al. 1993; Gat 1996). Today, the isotopic gradient associated with moisture transport and rainout across the Amazon Basin is approximately -1‰ per 1000 km (Vuille et al. 2003), and this gradient is attenuated by plant transpiration (Salati et al. 1979). If rainforest coverage in the Amazon was less dense during MIS 15, water vapor advected/supplied to the Andes would undergo less transpiration leading to a smaller contribution of recycled ^{18}O-enriched moisture. This mechanism has been invoked to explain the greater isotopic offset between eastern and western Amazon speleothems during the last glacial period relative to the Holocene (Wang et al. 2017).

Only one available record can be used to infer forest conditions in Amazonia during MIS 15. Terrigenous sediments from the Ceara Rise in the western equatorial Atlantic record variability in Amazon Basin lowland conditions during the past 1 Ma (Harris and Mix 1999). Iron oxides in Amazon suspended sediment originate from chemical weathering of lowland soils, and the relative proportion of iron oxides (G/G+H) serves as a proxy for lowland precipitation and vegetation because goethite (G) is favored over hematite (H) with increasing precipitation and/or increasing soil organic carbon content (Harris and Mix 1999). Higher values during interglacials relative to glacials implies wetter conditions and rainforest expansion, especially at the onset of interglacials. Average values during MIS 15, however, are lower and more variable compared to subsequent interglacials, suggesting the Amazon was somewhat drier and/or less vegetated, although the relatively low-resolution record ends at 4.4 ka making it difficult to extend this comparison to the Holocene. Lower temperatures may have contributed to suppressed rainforest expansion during MIS 15, thus modifying the isotopic gradient across the Amazon Basin and driving the $\delta^{18}O$ of Andean precipitation to the more negative values reflected in the Junín record.

4.4.4 Atypical MIS 13

MIS 13 was a particularly cool interglacial according to many records. Antarctic ice cores suggest that surface air temperatures were approximately 4°C lower than the Holocene (Jouzel et al. 2007), consistent with very low CO_2 and CH_4 concentrations for an interglacial (Loulergue et al. 2008; Lüthi et al. 2008). More positive marine benthic $\delta^{18}O$ values suggest greater global ice volume compared to other interglacials of the past 800 ka (Lisiecki and Raymo 2005; Elderfield et al. 2012), and several mid- to high-latitude marine records from both hemispheres also indicate cold SSTs (Voelker et al. 2010; Becquey and Gersonde 2003; McClymont et al. 2005; King and Howard 2000). The Junín record seems consistent with a globally cooler interglacial, with elevated Ti counts suggesting possible glacier presence in the watershed, and the high TOC content and laminations pointing to lower and fluctuating lake level especially during early and late MIS 13. Yet tropical hydroclimate during this interglacial appears rather complicated with many records showing contradictory findings.

MIS 13 has been recognized for its unusual expression in several monsoon records, beginning with an equatorial Indian ocean record of surface water salinity showing a wet event centered at 525 ka that was considered anomalous because it does not align with precession (Bassinot et al. 1994). This event was later correlated to an unusually thick sapropel layer in the Mediterranean Sea dated to 528-525 ka indicative of a strong African monsoon (Rossignol-Strick et al. 1998). Because this precipitation anomaly spanned two ocean basins and occurred during relatively low summer insolation, it was suggested that MIS 13 was characterized by an atypical monsoon (Rossignol-Strick et al. 1998). Subsequent studies have also suggested unusual Asian monsoon strength during MIS 13. Loess records from northern China (~35°N) indicate an extremely strong summer monsoon based on the development of a widespread soil complex/paleosol showing high levels of chemical weathering and soil redness, indicative of warm and humid conditions (Guo et al. 2000; Yin and Guo 2008; Guo et al. 2009; Hao et al. 2015). However, the strong monsoon events captured in the Mediterranean and Indian Ocean records are only a few millennia in duration, whereas the enhanced Asian monsoon spans the entire interglacial (~50 kyr), implying different forcing mechanisms.

Based on limited pollen evidence for a reduced Greenland ice sheet during MIS 13 (de Vernal and Hillaire-Marcel 2008), it was hypothesized that larger Antarctic ice volume may primarily be responsible for the high benthic $\delta^{18}O$ signature during MIS 13 (Yin and Guo 2008; Guo et al. 2009). This configuration could result in stronger asymmetry of hemispheric climates and a northward ITCZ shift, reinforcing summer monsoon circulation in Asia and throughout the Northern Hemisphere tropics. Such a scenario has implications for the interpretation of the Junín record because Chinese and South American speleothems are strongly anticorrelated, at least on millennial and precessional timescales, likely reflecting changes in ITCZ position (Wang et al. 2004; Cheng et al. 2013). If the prevailing climate pattern during MIS 13 affected long-term mean ITCZ position, the southern tropics might exhibit a coherent response of weaker summer monsoons. The other two long records available from South America do not fit this pattern, however. The Ceara Rise sediment record of Amazon lowlands moisture suggests wetter interglacial conditions during MIS 13 that were of longer duration but average magnitude relative to subsequent interglacials (Harris and Mix 1999). The Bogota basin, in the northern tropical Andes, suggests lower lake levels during interglacials including MIS 13, although there is a temporary return to higher lake level during mid-MIS 13 (Torres et al. 2013). Together, these records highlight an inconsistent moisture pattern for tropical South America, with only the Junín stratigraphy supporting a weaker SASM.

Alternative interpretations of tropical climate during MIS 13 have arisen in more recent studies. Salinity and SST data from the Indian Ocean and Arabian Sea suggest that summer monsoon strength in the region cannot be considered atypical in terms of timing or magnitude during MIS 13 (Caley et al. 2011; Alonso-Garcia et al. 2019; Ziegler et al. 2010), and a Borneo stalagmite (4°N) suggests hydroclimate in the West Pacific Warm Pool during MIS 13 was similar to subsequent interglacials and not unusual (Meckler et al. 2012). Given these findings from other northern tropical sites, it appears that unusually strong MIS 13 monsoons are primarily a feature of the Chinese Loess Plateau/Asian monsoon.

The greatest variability in the Chinese loess and paleosol records occurs on glacial/interglacial scales, suggesting primary forcing in common with high latitude climate/temperature. Other Asian monsoon records show a different pattern of long-term variability. The $\delta^{18}O$ record from nearby Sanbao cave (31°N) that spans the past 640 ka broadly tracks July insolation at 65°N, and from this relationship it has been asserted that Asian summer monsoon intensity is controlled by northern high latitude insolation forcing (Wang et al. 2008; Cheng et al. 2009; Cheng et al. 2016). A recent analysis of the Sanbao record instead suggests that the $\delta^{18}O$ signal is responding to low latitude summer insolation (e.g., July 30°N), which exhibits a nearly identical phasing and overall pattern of variation that primarily reflects precession (Beck et al. 2018). This study also presents a record of cosmogenic ^{10}Be flux preserved in the loess, a proxy for East Asian Summer Monsoon rainfall intensity, which along with Sanbao $\delta^{18}O$ exhibits strong forcing at precessional periods; the ^{10}Be rainfall record is also highly correlated with ice volume proxies (Beck et al. 2018), supporting both high and low latitude drivers of monsoon rainfall. Notably, during MIS 13 the speleothem is not unusual, with $\delta^{18}O$ variability roughly proportional to the strength of insolation forcing throughout the record. Similarly, the ^{10}Be rainfall record does not indicate a stronger summer monsoon relative to subsequent interglacials. While it is possible that unusual Northern Hemisphere warmth amplified the Asian monsoon and caused increased convection and precipitation, given the subtropical location and the strong continentality of the Asian landmass, it's unclear why this increase in rainfall wouldn't also be reflected in the ^{10}Be record and speleothem. Alternatively, the temperature-sensitive proxies measured in the loess deposits may be responding to warmer summer conditions, but not necessarily wetter –

soil redness largely reflects soil temperature, and the chemical weathering index depends on both temperature and summer moisture (Guo et al. 1998; 2000; Yang and Ding 2003; Vidic et al. 2000). As it stands, the available records from tropical regions including South America show a range of climatic conditions during MIS 13 but the dominant forcing mechanisms appear to vary by region and proxy, and further exploration of tropical hydroclimate during this time interval would benefit from the application of more unambiguous proxies for monsoon strength and rainfall.

4.5 Discussion – glacial periods

4.5.1 Differences in tropical Andean glaciation

MIS 14 stands out in marine and ice core records as being one of the weakest glacial periods of the last 800 ka (Lang and Wolff 2011). Sea level reconstructions suggest only a moderate increase in global ice volume and a rather unpronounced onset and termination compared to other glacial/interglacial transitions (Elderfield et al. 2012; Shakun et al. 2015). Temperatures during the first half of MIS 14 were similar to those of mid-MIS 15, perhaps explaining why glacial inputs initially remained moderate to low at Junín, based on Ti counts. Once temperatures dropped further, shortly after ~550 ka according to both the Antarctic ice core record (Lüthi et al. 2008; Jouzel et al. 2007) and the Bogotá Basin temperature record (Torres et al. 2013), deposition of a homogenous glacial silt unit with high levels of Ti and mineral matter suggests glaciers expanded appreciably at Junín. Local glacial maximum conditions persisted from ~545 to 530 ka, and a ^{10}Be age of 546.5 ± 28.7 ka corroborates the approximate timing of this glacial advance (Smith et al. 2005). Notably, even though MIS 14 was the briefest and smallest glaciation of the past 700 ka, it still stands out as a distinct glacial period in the Junín record. This is not the case in several other records showing such mild conditions that the interval from MIS 15 to MIS 13 instead resembles a single prolonged interglacial, including sites from the West Antarctic continental margin (Hillenbrand et al. 2009), central equatorial Indian Ocean (Alonso-Garcia et al. 2019), Siberia (Prokopenko et al. 2002), and the Chinese Loess Plateau region (Hao et al. 2015).

MIS 12, in contrast, is one of the largest Pleistocene glaciations (Lisiecki and Raymo 2005; Elderfield et al. 2012), perhaps in part because it followed such a mild interglacial period. The variations in Ti at Junín indicate discontinuous glacier growth implying an initial rapid increase followed by more moderate and variable levels of glaciation (Figure 24). This contrasts somewhat with the more stable growth of high latitude ice sheets inferred from steady increases in benthic $\delta^{18}O$ throughout MIS 12 (Figure 26). Peak cold conditions associated with the late-MIS 12 glacial maximum were more severe than any time during MIS 14 or the LGM, and Ti inputs to Junín increased accordingly from 440-420 ka, indicating MIS 12 was a major period of glacial expansion in the tropical Andes. Cosmogenic exposure ages of 445 ±22, 427 ±22 and 420 ±22 ka (Smith et al. 2005) also support significant glacial advance in the Junín watershed during late MIS 12.

Greater paleoglacier mass balance at Junín, based on inputs of Ti and residual mineral matter, generally coincide with intervals of higher lake level (e.g., low-TOC intervals without visible peat layers), a result that is expected given the moisture-sensitive nature of glaciers in this region of the Andes (Sagredo et al. 2014; Kaser 2001). Furthermore, tropical Andean glaciers are known to act as moisture buffers that constrain the degree to which lakes and landscapes dry out during arid intervals (Mark and Seltzer 2003; Kaser et al. 2003), which may contribute to the perception of wet glacial periods derived from some Andean proxy records (Fritz et al. 2007). Nonetheless, the record of clastic inputs and peat layers from Junín from MIS 3, 12, and 14 demonstrates that extended intervals of both wetter and drier conditions can occur within any given glacial period.

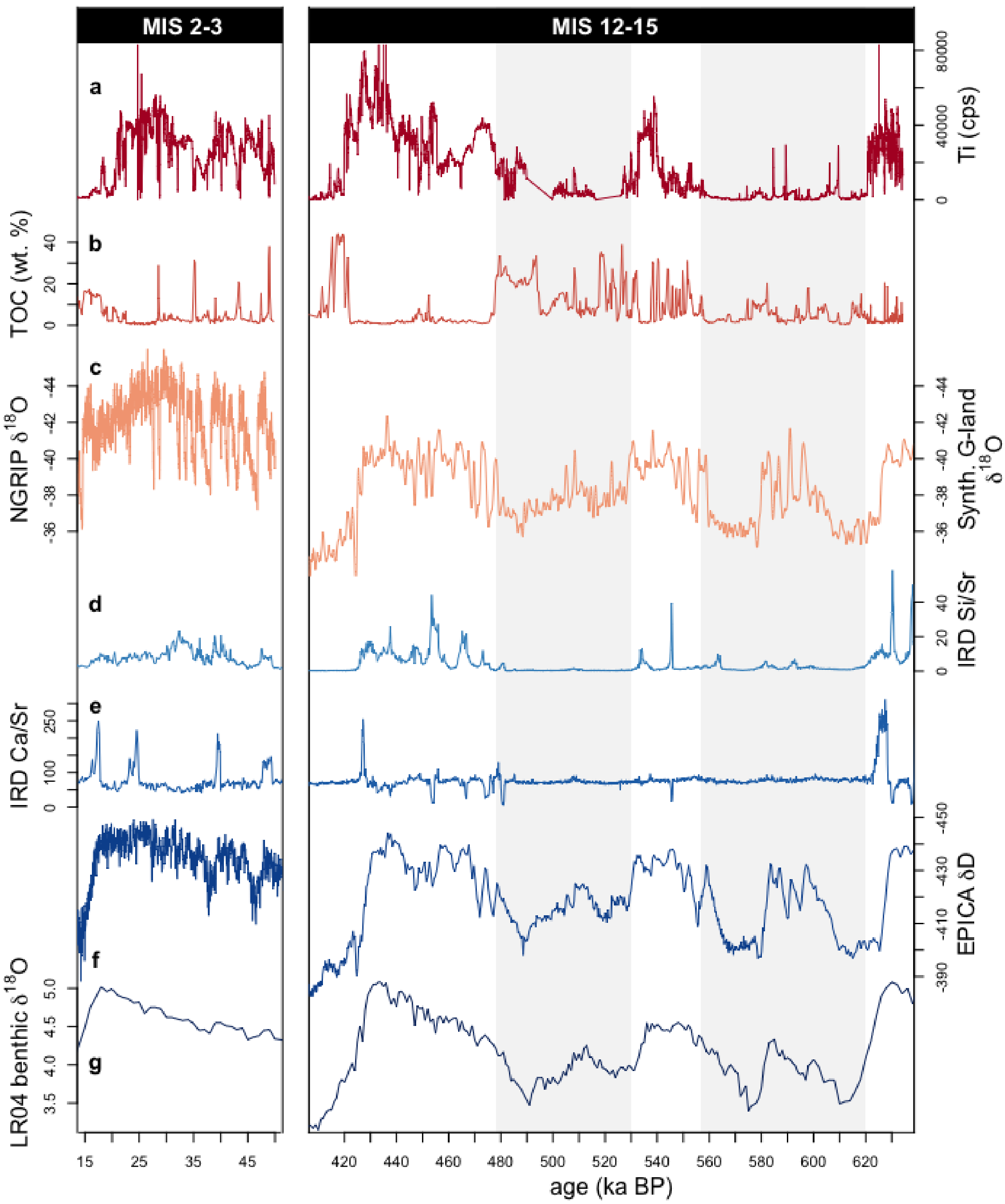

Figure 26. Comparison of Junín and records of high latitude glaciation. a, Junín Ti counts, b, Junín TOC content, c, NGRIP ice core $\delta^{18}O$ values for MIS 2-3 (left panel, Svensson et al., 2008) and synthetic Greenland $\delta^{18}O$ values (right panel, Barker et al., 2011), d, IRD based on Si/Sr values (Hodell et al. 2008), e, IRD based on Ca/Sr values (Hodell et al., 2008), f, Antarctic ice core δD values (Jouzel et al., 2007), g, benthic $\delta^{18}O$ values (Lisiecki & Raymo, 2005). MIS 13 and 15 are indicated by grey shaded bars.

4.5.2 Millennial scale variability during glacial periods

The late Pleistocene glacial periods feature various forms of millennial scale variability that are best documented during the last glacial. Temperature in the North Atlantic region and associated changes in thermohaline circulation during DO cycles and Heinrich events were major influences on SASM strength throughout MIS 3, resulting in millennial scale fluctuations in moisture that were antiphased between hemispheres. These moisture variations are apparent in records of speleothem $\delta^{18}O$ (Cheng et al. 2013; Cruz et al. 2007, 200; Kanner et al. 2012), lake level (Fritz et al. 2010; Placzek et al. 2006; Baker et al. 2001; Woods et al. 2020), Andean glacier mass balance (Martin et al. 2018; Woods et al. 2020), and Amazon River discharge (Zhang et al. 2017).

The pattern of alternating peat/glacial silt during MIS 14 (Figure 22) is reminiscent of Junín's response to DO cycles during the last 50 ka (Woods et al. 2020), which correspond within age model error to the NGRIP $\delta^{18}O$ record (Andersen et al. 2006; Svensson et al. 2008). The Greenland ice cores only extend to ~120 ka, however, (Rasmussen et al. 2014; NEEM community members 2013) so DO cycles have not been directly identified in previous glacial periods. The synthetic Greenland record does show millennial scale variability during MIS 14 (Barker et al. 2011) that broadly resembles the Junín Ti record (Figure 26), although the Greenland record is lower resolution and does not capture as many interstadial events as are shown by the Junín peat layers.

Other forms of high frequency variability have been documented in previous glacials, such as Heinrich events; these events lead to a strengthened SASM via a slowdown of the AMOC and a southward ITCZ displacement, similar to the response observed during DO stadials but possibly arising from different underlying causes. The first occurrence of Hudson Strait Heinrich events in the North Atlantic was recorded during MIS 16, indicated by large amounts of IRD sourced from the Laurentide ice sheet (Hodell et al. 2008; Naafs et al. 2011). Heinrich-like layers were not detected during MIS 14 however (Figure 26), and it has been hypothesized that the Laurentide ice sheet did not achieve sufficient thickness during this shorter duration glacial period to destabilize and generate ice surges (Hodell et al. 2008; Naafs et al. 2013). As such, the cause of millennial scale variations in the Junín record during MIS 14 remain unclear.

MIS 12, on the other hand, is characterized by large and frequent Hudson Strait IRD pulses (Hodell et al. 2008; Naafs et al. 2011), suggesting the Laurentide ice sheet grew sufficiently large to destabilize in the Hudson Strait region and trigger ice rafting. Beginning with MIS 12, glacial periods also demonstrate abrupt, high frequency cold events on the Iberian margin (Rodrigues et al. 2011; Martrat et al. 2007). This suggests that meltwater pulses to the northeast Atlantic associated with Heinrich events reached the Iberian margin and contributed to lower SST, implying a southward deflection of the subpolar front (Rodrigues et al. 2017). (Toucanne et al. 2009) also show extensive melting of European ice sheets and freshwater discharge events beginning in MIS 12. Given this evidence for climatic instability in the North Atlantic that presumably could have disrupted AMOC strength during MIS 12, it is interesting that Junín generally lacks peat layers during this time, suggesting more stable lake level. There is some variation in Ti levels and residual mineral content that could be related to millennial scale changes in precipitation, but not enough to cause prolonged lake lowstands, possibly owing to larger glacier mass balance that buffered intervals of reduced rainfall.

4.5.3 Abrupt glacial terminations in the tropical Andes

The terminations of MIS 14 and 12 at Junín are marked by rapid loss of the clastic signal and particularly thick peat deposition (e.g., ~20-40 cm) (Figure 22), indicating low lake levels and prolonged periods of aridity. This is similar to the LGM termination at Junín, wherein early deglaciation relative to the northern hemisphere was attributed to two closely spaced peat layers representing a ~1300 year interval of aridity (Woods et al. 2020). This pattern of dry conditions accompanying glacial retreat suggests that deglaciation in this region of the tropical Andes may be more sensitive to rapid scale changes in monsoon strength affecting P-E balance than it is to global temperature and greenhouse gas concentrations. The droughts associated with the most recent deglaciation at Junín do not have counterparts in the NGRIP record even though they were sedimentologically equivalent to Junín's response to DO events, suggesting that substantial reductions in SASM precipitation occurred even in the absence of high latitude North Atlantic forcing.

A pattern of millennial scale periods of weakened monsoon strength associated with glacial terminations has also been observed in the northern tropics. A stalagmite from the tropical west Pacific (4°N) shows large increases in $\delta^{18}O$ during terminations III-V, similar to the response observed during Heinrich event 1. These events were interpreted as intervals of profound drought, possibly related to a southward ITCZ shift associated with millennial scale cooling in the Northern Hemisphere, as occurred during the most recent glacial termination (Meckler et al. 2012). Millennia-long intervals of reduced Asian monsoon rainfall, termed weak monsoon intervals, have been observed in Chinese speleothems for each of the last seven terminations (Cheng et al. 2009; Cheng et al. 2016) and coincide with Heinrich events triggered by deglacial ice sheet instability. The age model for this portion of the Junín record does not permit assessment of leads/lags in the timing of tropical deglaciation, but the weak monsoon events associated with glacial terminations in the northern tropics cannot also be responsible for the deglacial drying at Junín. However, if rapidly transmitted teleconnections linked to the Atlantic sector and/or ITCZ shifts are involved, the dry events in the southern tropics would likely occur in close temporal proximity to those in the northern tropics.

4.6 Conclusions

The record presented here from Lake Junín during MIS 12-15 reveals that past glacial and interglacial periods are markedly different from each other in terms of monsoon strength, P-E balance, and glaciation. MIS 15 shows large changes in $\delta^{18}O$ values that track precession, and the stratigraphy indicates corresponding changes in lake level, indicating greatly enhanced monsoon intensity. MIS 13 is a unique interglacial in that the $\delta^{18}O$ values lack a clear precession signal and are inconsistent with stratigraphic evidence for lower lake level, suggesting possible decoupling of monsoon strength from local P-E balance. Additionally, proxies sensitive to clastic sediment imply some glacial ice in the watershed during MIS 13 likely related to globally cooler temperatures. Despite the large climatic differences among interglacials, covariation between carbon and oxygen isotopes suggests prolonged residence time and stability of basin hydrology over long periods of time. MIS 14 shows a series of peat layers indicating millennial scale variations in lake level and glacial inputs that resemble the pattern during the last glacial period in association with DO events. Elevated clastic inputs during late-MIS 14 suggest considerable expansion of ice volume despite relatively mild temperatures globally. Ice presence was even larger during MIS 12 consistent with pronounced global cooling, and the absence of peat layers suggests that larger ice volume may have contributed to higher and more stable lake level.

5.0 Summary and future directions

This dissertation presents a paleoclimate perspective on monsoon strength and glaciation in the tropical Andes on multiple timescales, showing considerable diversity of P-E balance among individual glacial and interglacial climate states and highlighting the sensitivity of this region to a variety of climate forcings. Chapter 2 focuses on the more recent paleoclimate history using a series of cores from the depocenter to the shallow lake margins to assess the timing and patterns of sedimentation across the Junín basin during the last deglaciation and Holocene. Targeted radiocarbon dating of stratigraphic transitions and unconformities revealed a complex sequence of changes in paleoglacier mass balance and lake level. Deglaciation of the Junín watershed was complete by ~18 ka, earlier than many mid- to high-latitude regions and likely due to locally drier conditions. A delayed onset of wet conditions during Heinrich Stadial 1 is observed, a surprising result given the timing of climatic changes in the North Atlantic region but in agreement with some Altiplano records. The improved age model suggests that the abrupt positive isotope excursion observed in many Andean records occurred earlier than previously thought, and possibly during the Younger Dryas. Finally, isotopic evidence for reduced SASM strength and enhanced evaporation during the early and middle Holocene is supported by several unconformities indicating lake level drops of up to 8 meters. The findings demonstrate that some millennial scale hydroclimate changes fit within a Northern Hemisphere forcing framework, whereas in other cases the timing is inconsistent and suggests alternative mechanisms driving changes in Andean P-E balance.

Chapter 3 extends our knowledge of the recent lake history back further into the last glacial period, an interval characterized by a series of abrupt millennial scale temperature fluctuations in the Northern Hemisphere that affected tropical circulation. Speleothem records have shown that warm episodes in the Greenland ice cores are linked to a weakening of the SASM, but less is known about the response of Andean glaciers and precipitation during these abrupt events. Reduced clastic inputs to Lake Junín indicating rapid glacial retreat occurred during nearly every DO event, and these episodes were accompanied by the formation of peat layers suggesting lower lake level. This evidence for aridity demonstrates the magnitude of the hydroclimatic disruptions in the tropical Andes that could previously only be inferred from isotopic records, and the results highlight the sensitivity of Andean P-E balance to Northern Hemisphere forcing.

Chapter 4 explores a period of deep geologic time at unprecedented resolution. It looks at two complete glacial-interglacial cycles from 420-620 ka, an interval that is not captured in any existing records from the southern tropical Andes, thus providing new insights into long-term variability in monsoon strength and paleoglacier activity. The high amplitude precessional-scale variations in $\delta^{18}O$ values during MIS 15 suggest greatly enhanced SASM intensity, and the carbonate stratigraphy indicates corresponding high and lowstands. MIS 13 is unique in that no precession signal is apparent, and instead, thick peat accumulation suggests frequent aridity, possibly related to a northward ITCZ position. The stratigraphy during MIS 14 closely resembles that of the last glacial period, suggesting DO-like climatic instability although there is currently no evidence for corresponding changes in ITCZ position or AMOC strength. Significantly larger ice volume during MIS 12 likely contributed to higher and more stable lake level. This chapter highlights the diverse climatic expression of individual glacial and interglacial periods at Lake Junín in terms of stratigraphy and proxy signatures, and shows that any given interval can display a spectrum of changes in P-E balance.

This work opens up a variety of avenues for future research using the Junín record. Detailed exploration of the remaining glacial and interglacial periods (e.g., MIS 4-11) will generate a more robust understanding of the long-term controls on monsoon strength and glacier activity in the region. The MIS 13 record in particular demonstrates that the role of insolation forcing in this system requires further investigation. That Junín contains both authigenic carbonate and sufficient organic content for the measurement of molecular biomarkers such as leaf waxes offers a rare opportunity to assess whether the isotopic signatures of alternative proxy systems record similar climatic signals and would refine our understanding of these tools. The application of additional temperature-sensitive proxies such as GDGTs would also help to clarify the relative influence of temperature and precipitation on changes in paleoglacier mass balance. Finally, a more refined understanding of P-E balance in the region requires additional isotopic records – pairing open-system speleothems with the closed-basin Junín record during previous interglacial periods would be a powerful way to separate the role of regional monsoon strength from local evaporative influences. To this end, new oxygen-17 techniques also offer a promising approach for quantifying the effects of changes in the isotopic composition of input water versus evaporation of the lake water. Ultimately such approaches will enable us to better characterize the sensitivity of the Junín system to a wider variety of climatic forcings, an important step in understanding how the tropical Andes may respond to future climate changes.

Bibliography

Abbott, Mark B, Geoffrey O Seltzer, Kerry R Kelts, and John Southon. 1997. "Holocene Paleohydrology of the Tropical Andes from Lake Records." *Quaternary Research* 47: 70–80.

Abbott, Mark B, Brent B Wolfe, Alexander P Wolfe, Geoffrey O Seltzer, Ramon Aravena, Brian G Mark, Pratigya J Polissar, Donald T Rodbell, Harry D Rowe, and Mathias Vuille. 2003. "Holocene Paleohydrology and Glacial History of the Central Andes Using Multiproxy Lake Sediment Studies." *Palaeogeography, Palaeoclimatology, Palaeoecology* 194 (1–3): 123–38. https://doi.org/10.1016/S0031-0182(03)00274-8.

Alley, Richard B. 2000. "The Younger Dryas Cold Interval as Viewed from Central Greenland." *Quaternary Science Reviews* 19 (1–5): 213–26. https://doi.org/10.1016/S0277-3791(99)00062-1.

Alonso-Garcia, M., T. Rodrigues, F. Abrantes, M. Padilha, C.A. Alvarez-Zarikian, T. Kunkelova, J.D. Wright, and C. Betzler. 2019. "Sea-Surface Temperature, Productivity and Hydrological Changes in the Northern Indian Ocean (Maldives) during the Interval ~575-175 Ka (MIS 14 to 7)." *Palaeogeography, Palaeoclimatology, Palaeoecology* 536 (December): 109376. https://doi.org/10.1016/j.palaeo.2019.109376.

Andersen, Katrine K., Anders Svensson, Sigfus J. Johnsen, Sune O. Rasmussen, Matthias Bigler, Regine Röthlisberger, Urs Ruth, Marie-Louise Siggaard-Andersen, Jørgen Peder Steffensen, and Dorthe Dahl-Jensen. 2006. "The Greenland Ice Core Chronology 2005, 15–42ka. Part 1: Constructing the Time Scale." *Quaternary Science Reviews* 25 (23–24): 3246–57. https://doi.org/10.1016/j.quascirev.2006.08.002.

Andriessen, P.A.M., K.F. Helmens, H. Hooghiemstra, P.A. Riezebos, and T. Van der Hammen. 1993. "Absolute Chronology of the Pliocene-Quaternary Sediment Sequence of the Bogota Area, Colombia." *Quaternary Science Reviews* 12: 483–501.

Apaéstegui, James, Francisco William Cruz, Mathias Vuille, Jens Fohlmeister, Jhan Carlo Espinoza, Abdelfettah Sifeddine, Nicolas Strikis, et al. 2018. "Precipitation Changes over the Eastern Bolivian Andes Inferred from Speleothem (Δ18O) Records for the Last 1400 Years." *Earth and Planetary Science Letters* 494 (July): 124–34. https://doi.org/10.1016/j.epsl.2018.04.048.

Arbuszewski, Jennifer A., Peter B. deMenocal, Caroline Cléroux, Louisa Bradtmiller, and Alan Mix. 2013. "Meridional Shifts of the Atlantic Intertropical Convergence Zone since the Last Glacial Maximum." *Nature Geoscience* 6 (11): 959–62. https://doi.org/10.1038/ngeo1961.

Arz, Helge W., Jürgen Pätzold, and Gerold Wefer. 1998. "Correlated Millennial-Scale Changes in Surface Hydrography and Terrigenous Sediment Yield Inferred from Last-Glacial Marine Deposits off Northeastern Brazil." *Quaternary Research* 50 (02): 157–66. https://doi.org/10.1006/qres.1998.1992.

Baker, P. A., G. O. Seltzer, S. C. Fritz, R B Dunbar, M. J. Grove, P M Tapia, S. L. Cross, H D Rowe, and J. P. Broda. 2001. "The History of South American Tropical Precipitation for the Past 25,000 Years." *Science* 291 (5504): 640–43. https://doi.org/10.1126/science.291.5504.640.

Baker, Paul A., Catherine A. Rigsby, Geoffrey O. Seltzer, Sherilyn C. Fritz, Tim K. Lowenstein, Niklas P. Bacher, and Carlos Veliz. 2001. "Tropical Climate Changes at Millennial and Orbital Timescales on the Bolivian Altiplano." *Nature* 409 (6821): 698–701. https://doi.org/10.1038/35055524.

Bakke, Jostein, Øyvind Lie, Einar Heegaard, Trond Dokken, Gerald H. Haug, Hilary H. Birks, Peter Dulski, and Trygve Nilsen. 2009. "Rapid Oceanic and Atmospheric Changes during the Younger Dryas Cold Period." *Nature Geoscience* 2 (3): 202–5. https://doi.org/10.1038/ngeo439.

Bard, E., F. Rostek, J.L. Turon, and S. Gendreau. 2000. "Hydrological Impact of Heinrich Events in the Subtropical Northeast Atlantic." *Science* 289 (5483): 1321–24. https://doi.org/10.1126/science.289.5483.1321.

Barker, S., G. Knorr, R. L. Edwards, F. Parrenin, A. E. Putnam, L. C. Skinner, E. Wolff, and M. Ziegler. 2011. "800,000 Years of Abrupt Climate Variability." *Science* 334 (6054): 347–51. https://doi.org/10.1126/science.1203580.

Barker, Stephen, Paula Diz, Maryline J. Vautravers, Jennifer Pike, Gregor Knorr, Ian R. Hall, and Wallace S. Broecker. 2009. "Interhemispheric Atlantic Seesaw Response during the Last Deglaciation." *Nature* 457 (7233): 1097–1102. https://doi.org/10.1038/nature07770.

Bassinot, Frank C., Laurent D. Labeyrie, Edith Vincent, Xavier Quidelleur, Nicholas J. Shackleton, and Yves Lancelot. 1994. "The Astronomical Theory of Climate and the Age of the Brunhes-Matuyama Magnetic Reversal." *Earth and Planetary Science Letters* 126 (1–3): 91–108. https://doi.org/10.1016/0012-821X(94)90244-5.

Battisti, D. S., Qinghua Ding, and G. H. Roe. 2014. "Coherent Pan-Asian Climatic and Isotopic Response to Orbital Forcing of Tropical Insolation." *Journal of Geophysical Research: Atmospheres* 119 (21): 11,997-12,020. https://doi.org/10.1002/2014JD021960.

Beck, J. Warren, Weijian Zhou, Cheng Li, Zhenkun Wu, Lara White, Feng Xian, Xianghui Kong, and Zhisheng An. 2018. "A 550,000-Year Record of East Asian Monsoon Rainfall from 10Be in Loess." *Science* 360 (6391): 877–81. https://doi.org/10.1126/science.aam5825.

Becquey, Sabine, and Rainer Gersonde. 2003. "A 0.55-Ma Paleotemperature Record from the Subantarctic Zone: Implications for Antarctic Circumpolar Current Development: PALEOTEMPERATURE RECORD." *Paleoceanography* 18 (1): n/a-n/a. https://doi.org/10.1029/2000PA000576.

Biasutti, Michela, Aiko Voigt, William R. Boos, Pascale Braconnot, Julia C. Hargreaves, Sandy P. Harrison, Sarah M. Kang, et al. 2018. "Global Energetics and Local Physics as Drivers of Past, Present and Future Monsoons." *Nature Geoscience* 11 (6): 392–400. https://doi.org/10.1038/s41561-018-0137-1.

Bird, B. W., M. B. Abbott, M. Vuille, D. T. Rodbell, N. D. Stansell, and M. F. Rosenmeier. 2011. "A 2,300-Year-Long Annually Resolved Record of the South American Summer Monsoon from the Peruvian Andes." *Proceedings of the National Academy of Sciences* 108 (21): 8583–88. https://doi.org/10.1073/pnas.1003719108.

Bird, Broxton W., Mark B. Abbott, Donald T. Rodbell, and Mathias Vuille. 2011. "Holocene Tropical South American Hydroclimate Revealed from a Decadally Resolved Lake Sediment Δ18O Record." *Earth and Planetary Science Letters* 310 (3–4): 192–202. https://doi.org/10.1016/j.epsl.2011.08.040.

Bischoff, Tobias, Tapio Schneider, and Anna Nele Meckler. 2017. "A Conceptual Model for the Response of Tropical Rainfall to Orbital Variations." *Journal of Climate* 30 (20): 8375–91. https://doi.org/10.1175/JCLI-D-16-0691.1.

Blaauw, Maarten. 2012. "Out of Tune: The Dangers of Aligning Proxy Archives." *Quaternary Science Reviews* 36 (March): 38–49. https://doi.org/10.1016/j.quascirev.2010.11.012.

Blaauw, Maarten, and J. Andrés Christen. 2011. "Flexible Paleoclimate Age-Depth Models Using an Autoregressive Gamma Process." *Bayesian Analysis* 6 (3): 457–74. https://doi.org/10.1214/11-BA618.

Blard, P.-H., J. Lavé, K.A. Farley, M. Fornari, N. Jiménez, and V. Ramirez. 2009. "Late Local Glacial Maximum in the Central Altiplano Triggered by Cold and Locally-Wet Conditions during the Paleolake Tauca Episode (17–15ka, Heinrich 1)." *Quaternary Science Reviews* 28 (27–28): 3414–27. https://doi.org/10.1016/j.quascirev.2009.09.025.

Blard, P.-H., F. Sylvestre, A.K. Tripati, C. Claude, C. Causse, A. Coudrain, T. Condom, et al. 2011. "Lake Highstands on the Altiplano (Tropical Andes) Contemporaneous with Heinrich 1 and the Younger Dryas: New Insights from 14C, U–Th Dating and Δ18O of Carbonates." *Quaternary Science Reviews* 30 (27–28): 3973–89. https://doi.org/10.1016/j.quascirev.2011.11.001.

Blunier, T., J. Chappellaz, J. Schwander, A. Dällenbach, B. Stauffer, T. F. Stocker, D. Raynaud, et al. 1998. "Asynchrony of Antarctic and Greenland Climate Change during the Last Glacial Period." *Nature* 394 (6695): 739–43. https://doi.org/10.1038/29447.

Boos, William R., and Robert L. Korty. 2016. "Regional Energy Budget Control of the Intertropical Convergence Zone and Application to Mid-Holocene Rainfall." *Nature Geoscience* 9 (12): 892–97. https://doi.org/10.1038/ngeo2833.

Bosmans, J. H. C., F. J. Hilgen, E. Tuenter, and L. J. Lourens. 2015. "Obliquity Forcing of Low-Latitude Climate." *Climate of the Past* 11 (10): 1335–46. https://doi.org/10.5194/cp-11-1335-2015.

Breukelen, M.R. van, H.B. Vonhof, J.C. Hellstrom, W.C.G. Wester, and D. Kroon. 2008. "Fossil Dripwater in Stalagmites Reveals Holocene Temperature and Rainfall Variation in Amazonia." *Earth and Planetary Science Letters* 275 (1–2): 54–60. https://doi.org/10.1016/j.epsl.2008.07.060.

Broecker, W. S., D. M. Peteet, and D. Rind. 1985. “Does the Ocean–Atmosphere System Have More than One Stable Mode of Operation?” *Nature* 315 (6014): 21–26.

Broecker, W. S., and A. E. Putnam. 2013. “Hydrologic Impacts of Past Shifts of Earth’s Thermal Equator Offer Insight into Those to Be Produced by Fossil Fuel CO2.” *Proceedings of the National Academy of Sciences* 110 (42): 16710–15. https://doi.org/10.1073/pnas.1301855110.

Broecker, Wallace S. 1998. “Paleocean Circulation during the Last Deglaciation: A Bipolar Seesaw?” *Paleoceanography* 13 (2): 119–21. https://doi.org/10.1029/97PA03707.

Bromley, Gordon R.M., Joerg M. Schaefer, Brenda L. Hall, Kurt M. Rademaker, Aaron E. Putnam, Claire E. Todd, Matthew Hegland, Gisela Winckler, Margaret S. Jackson, and Peter D. Strand. 2016. “A Cosmogenic 10Be Chronology for the Local Last Glacial Maximum and Termination in the Cordillera Oriental, Southern Peruvian Andes: Implications for the Tropical Role in Global Climate.” *Quaternary Science Reviews* 148 (September): 54–67. https://doi.org/10.1016/j.quascirev.2016.07.010.

Buizert, C., V. Gkinis, J. P. Severinghaus, F. He, B. S. Lecavalier, P. Kindler, M. Leuenberger, et al. 2014. “Greenland Temperature Response to Climate Forcing during the Last Deglaciation.” *Science* 345 (6201): 1177–80. https://doi.org/10.1126/science.1254961.

Burns, Stephen J., Lisa Kanner Welsh, Nick Scroxton, Hai Cheng, and R. Lawrence Edwards. 2019. “Millennial and Orbital Scale Variability of the South American Monsoon during the Penultimate Glacial Period.” *Scientific Reports* 9 (1): 1234. https://doi.org/10.1038/s41598-018-37854-3.

Bush, Mark B., Barbara C. S. Hansen, Donald T. Rodbell, Geoffrey O. Seltzer, Kenneth R. Young, Blanca León, Mark B. Abbott, Miles R. Silman, and William D. Gosling. 2005. “A 17 000-Year History of Andean Climate and Vegetation Change from Laguna de Chochos, Peru.” *Journal of Quaternary Science* 20 (7–8): 703–14. https://doi.org/10.1002/jqs.983.

Bustamante, M.G., F.W. Cruz, M. Vuille, J. Apaéstegui, N. Strikis, G. Panizo, F.V. Novello, et al. 2016. “Holocene Changes in Monsoon Precipitation in the Andes of NE Peru Based on Δ18O Speleothem Records.” *Quaternary Science Reviews* 146 (August): 274–87. https://doi.org/10.1016/j.quascirev.2016.05.023.

Byrne, Michael P., Angeline G. Pendergrass, Anita D. Rapp, and Kyle R. Wodzicki. 2018. “Response of the Intertropical Convergence Zone to Climate Change: Location, Width, and Strength.” *Current Climate Change Reports* 4 (4): 355–70. https://doi.org/10.1007/s40641-018-0110-5.

Caley, Thibaut, Bruno Malaizé, Marie Revel, Emmanuelle Ducassou, Karine Wainer, Mohamed Ibrahim, Dina Shoeaib, Sébastien Migeon, and Vincent Marieu. 2011. “Orbital Timing of the Indian, East Asian and African Boreal Monsoons and the Concept of a ‘Global Monsoon.’” *Quaternary Science Reviews* 30 (25–26): 3705–15. https://doi.org/10.1016/j.quascirev.2011.09.015.

Carrivick, Jonathan L., and Fiona S. Tweed. 2013. “Proglacial Lakes: Character, Behaviour and Geological Importance.” *Quaternary Science Reviews* 78 (October): 34–52. https://doi.org/10.1016/j.quascirev.2013.07.028.

Chen, Christine Y., David McGee, Arielle Woods, Liseth Pérez, Robert G. Hatfield, R. Lawrence Edwards, Hai Cheng, et al. 2020. "U-Th Dating of Lake Sediments: Lessons from the 700 Ka Sediment Record of Lake Junín, Peru." *Quaternary Science Reviews* 244 (September): 106422. https://doi.org/10.1016/j.quascirev.2020.106422.

Cheng, H., R. L. Edwards, W. S. Broecker, G. H. Denton, X. Kong, Y. Wang, R. Zhang, and X. Wang. 2009. "Ice Age Terminations." *Science* 326 (5950): 248–52. https://doi.org/10.1126/science.1177840.

Cheng, Hai, R. Lawrence Edwards, Ashish Sinha, Christoph Spötl, Liang Yi, Shitao Chen, Megan Kelly, et al. 2016. "The Asian Monsoon over the Past 640,000 Years and Ice Age Terminations." *Nature* 534 (7609): 640–46. https://doi.org/10.1038/nature18591.

Cheng, Hai, Ashish Sinha, Francisco W. Cruz, Xianfeng Wang, R. Lawrence Edwards, Fernando M. d'Horta, Camila C. Ribas, Mathias Vuille, Lowell D. Stott, and Augusto S. Auler. 2013. "Climate Change Patterns in Amazonia and Biodiversity." *Nature Communications* 4 (1): 1411. https://doi.org/10.1038/ncomms2415.

Chiang, John C. H., Michela Biasutti, and David S. Battisti. 2003. "Sensitivity of the Atlantic Intertropical Convergence Zone to Last Glacial Maximum Boundary Conditions: LGM ATLANTIC ITCZ." *Paleoceanography* 18 (4): n/a-n/a. https://doi.org/10.1029/2003PA000916.

Chiang, John C.H., and Andrew R. Friedman. 2012. "Extratropical Cooling, Interhemispheric Thermal Gradients, and Tropical Climate Change." *Annual Review of Earth and Planetary Sciences* 40 (1): 383–412. https://doi.org/10.1146/annurev-earth-042711-105545.

Church, Michael, and June Ryder. 1972. "Paraglacial Sedimentation: A Consideration of Fluvial Processes Conditioned by Glaciation." *Geological Society of America Bulletin* 83 (10): 3059–72.

Clark, P. U., A. S. Dyke, J. D. Shakun, A. E. Carlson, J. Clark, B. Wohlfarth, J. X. Mitrovica, S. W. Hostetler, and A. M. McCabe. 2009. "The Last Glacial Maximum." *Science* 325 (5941): 710–14. https://doi.org/10.1126/science.1172873.

Clark, Peter U., Nicklas G. Pisias, Thomas F. Stocker, and Andrew J. Weaver. 2002. "The Role of the Thermohaline Circulation in Abrupt Climate Change." *Nature* 415 (6874): 863–69. https://doi.org/10.1038/415863a.

Clement, A. C., A. Hall, and A. J. Broccoli. 2004. "The Importance of Precessional Signals in the Tropical Climate." *Climate Dynamics* 22 (4): 327–41. https://doi.org/10.1007/s00382-003-0375-8.

Cobbing, E.J., W.S. Pitcher, J.J. Wilson, J.W. Baldock, W.P. Taylor, W. McCourt, and N.J. Snelling. 1981. "The Geology of the Western Cordillera of Northern Peru." *Great Britain Institute of Geological Sciences, Natural Environmental Research Council* 5.

Cruz, Francisco W., Stephen J. Burns, Michael Jercinovic, Ivo Karmann, Warren D. Sharp, and Mathias Vuille. 2007. "Evidence of Rainfall Variations in Southern Brazil from Trace Element

Ratios (Mg/Ca and Sr/Ca) in a Late Pleistocene Stalagmite." *Geochimica et Cosmochimica Acta* 71 (9): 2250–63. https://doi.org/10.1016/j.gca.2007.02.005.

Cruz, Francisco W., Stephen J. Burns, Ivo Karmann, Warren D. Sharp, Mathias Vuille, Andrea O. Cardoso, José A. Ferrari, Pedro L. Silva Dias, and Oduvaldo Viana. 2005. "Insolation-Driven Changes in Atmospheric Circulation over the Past 116,000 Years in Subtropical Brazil." *Nature* 434 (7029): 63–66. https://doi.org/10.1038/nature03365.

Cruz, Francisco W., Mathias Vuille, Stephen J. Burns, Xianfeng Wang, Hai Cheng, Martin Werner, R. Lawrence Edwards, Ivo Karmann, Augusto S. Auler, and Hanh Nguyen. 2009. "Orbitally Driven East–West Antiphasing of South American Precipitation." *Nature Geoscience* 2 (3): 210–14. https://doi.org/10.1038/ngeo444.

Dansgaard, W. 1964. "Stable Isotopes in Precipitation." *Tellus* 16 (4): 436–68. https://doi.org/10.1111/j.2153-3490.1964.tb00181.x.

Deininger, Michael, Brittany Marie Ward, Valdir F. Novello, and Francisco W. Cruz. 2019. "Late Quaternary Variations in the South American Monsoon System as Inferred by Speleothems—New Perspectives Using the SISAL Database." *Quaternary* 2 (1): 6. https://doi.org/10.3390/quat2010006.

deMenocal, P. B., J. D. Ortiz, T.P. Guilderson, J Adkins, M Sarnthein, L Baker, and M Yarusinsky. 2000. "Abrupt Onset and Termination of the African Humid Period:: Rapid Climate Responses to Gradual Insolation Forcing." *Quaternary Science Reviews* 19 (1–5): 347–61.

Deplazes, Gaudenz, Andreas Lückge, Larry C. Peterson, Axel Timmermann, Yvonne Hamann, Konrad A. Hughen, Ursula Röhl, et al. 2013. "Links between Tropical Rainfall and North Atlantic Climate during the Last Glacial Period." *Nature Geoscience* 6 (3): 213–17. https://doi.org/10.1038/ngeo1712.

Donohoe, Aaron, John Marshall, David Ferreira, and David Mcgee. 2013. "The Relationship between ITCZ Location and Cross-Equatorial Atmospheric Heat Transport: From the Seasonal Cycle to the Last Glacial Maximum." *Journal of Climate* 26 (11): 3597–3618. https://doi.org/10.1175/JCLI-D-12-00467.1.

Earle, Lisa R., Barry G. Warner, and Ramon Aravena. 2003. "Rapid Development of an Unusual Peat-Accumulating Ecosystem in the Chilean Altiplano." *Quaternary Research* 59 (1): 2–11. https://doi.org/10.1016/S0033-5894(02)00011-X.

Elderfield, H., P. Ferretti, M. Greaves, S. Crowhurst, I. N. McCave, D. Hodell, and A. M. Piotrowski. 2012. "Evolution of Ocean Temperature and Ice Volume Through the Mid-Pleistocene Climate Transition." *Science* 337 (6095): 704–9. https://doi.org/10.1126/science.1221294.

Escobar, Jaime, David A. Hodell, Mark Brenner, Jason H. Curtis, Adrian Gilli, Andreas D. Mueller, Flavio S. Anselmetti, et al. 2012. "A ~43-Ka Record of Paleoenvironmental Change in the Central American Lowlands Inferred from Stable Isotopes of Lacustrine Ostracods." *Quaternary Science Reviews* 37 (March): 92–104. https://doi.org/10.1016/j.quascirev.2012.01.020.

Escobar, Jaime, Yuliana Serna, Natalia Hoyos, Maria I. Velez, and Alex Correa-Metrio. 2020. "Why We Need More Paleolimnology Studies in the Tropics." *Journal of Paleolimnology* 64 (1): 47–53. https://doi.org/10.1007/s10933-020-00120-6.

Fiorella, Richard P., Christopher J. Poulsen, Ramiro S. Pillco Zolá, Jason B. Barnes, Clay R. Tabor, and Todd A. Ehlers. 2015. "Spatiotemporal Variability of Modern Precipitation δ^{18}O in the Central Andes and Implications for Paleoclimate and Paleoaltimetry Estimates: MODERN CENTRAL ANDES PRECIPITATION δ^{18}O." *Journal of Geophysical Research: Atmospheres* 120 (10): 4630–56. https://doi.org/10.1002/2014JD022893.

Flusche, Mark A., Geoffrey Seltzer, Donald Rodbell, Donald Siegel, and Scott Samson. 2005. "Constraining Water Sources and Hydrologic Processes from the Isotopic Analysis of Water and Dissolved Strontium, Lake Junin, Peru." *Journal of Hydrology* 312 (1–4): 1–13. https://doi.org/10.1016/j.jhydrol.2005.02.021.

Fonkén, M S Maldonado. 2014. "An Introduction to the Bofedales of the Peruvian High Andes." *Mires and Peat* 15 (5).

Fritz, S.C., P.A. Baker, E. Ekdahl, G.O. Seltzer, and L.R. Stevens. 2010. "Millennial-Scale Climate Variability during the Last Glacial Period in the Tropical Andes." *Quaternary Science Reviews* 29 (7–8): 1017–24. https://doi.org/10.1016/j.quascirev.2010.01.001.

Fritz, Sherilyn C., Paul A. Baker, Tim K. Lowenstein, Geoffrey O. Seltzer, Catherine A. Rigsby, Gary S. Dwyer, Pedro M. Tapia, Kimberly K. Arnold, Teh-Lung Ku, and Shangde Luo. 2004. "Hydrologic Variation during the Last 170,000 Years in the Southern Hemisphere Tropics of South America." *Quaternary Research* 61 (01): 95–104. https://doi.org/10.1016/j.yqres.2003.08.007.

Fritz, Sherilyn C., Paul A. Baker, Geoffrey O. Seltzer, Ashley Ballantyne, Pedro Tapia, Hai Cheng, and R. Lawrence Edwards. 2007. "Quaternary Glaciation and Hydrologic Variation in the South American Tropics as Reconstructed from the Lake Titicaca Drilling Project." *Quaternary Research* 68 (03): 410–20. https://doi.org/10.1016/j.yqres.2007.07.008.

Garreaud, R. D. 2009. "The Andes Climate and Weather." *Advances in Geosciences* 22 (October): 3–11. https://doi.org/10.5194/adgeo-22-3-2009.

Garreaud, Rene D, and Patricio Aceituno. 2001. "Interannual Rainfall Variability over the South American Altiplano." *Journal of Climate* 14: 11.

Garreaud, René D., Mathias Vuille, Rosa Compagnucci, and José Marengo. 2009. "Present-Day South American Climate." *Palaeogeography, Palaeoclimatology, Palaeoecology* 281 (3–4): 180–95. https://doi.org/10.1016/j.palaeo.2007.10.032.

Gat, J R. 1996. "Oxygen and Hydrogen Isotopes in the Hydrologic Cycle." *Annual Review of Earth and Planetary Sciences* 24 (1) 225-262.

Gat, Joel R., Carl J. Bowser, and Carol Kendall. 1994. "The Contribution of Evaporation from the Great Lakes to the Continental Atmosphere: Estimate Based on Stable Isotope Data." *Geophysical Research Letters* 21 (7): 557–60. https://doi.org/10.1029/94GL00069.

Gibson, Kelly Ann, and Larry C. Peterson. 2014. "A 0.6 Million Year Record of Millennial-Scale Climate Variability in the Tropics." *Geophysical Research Letters* 41 (3): 969–75. https://doi.org/10.1002/2013GL058846.

Gottschalk, Julia, Luke C. Skinner, Sambuddha Misra, Claire Waelbroeck, Laurie Menviel, and Axel Timmermann. 2015. "Abrupt Changes in the Southern Extent of North Atlantic Deep Water during Dansgaard–Oeschger Events." *Nature Geoscience* 8 (12): 950–54. https://doi.org/10.1038/ngeo2558.

Govin, A., C. M. Chiessi, M. Zabel, A. O. Sawakuchi, D. Heslop, T. Hörner, Y. Zhang, and S. Mulitza. 2014. "Terrigenous Input off Northern South America Driven by Changes in Amazonian Climate and the North Brazil Current Retroflection during the Last 250 Ka." *Climate of the Past* 10 (2): 843–62. https://doi.org/10.5194/cp-10-843-2014.

Gregory, J. M., K. W. Dixon, R. J. Stouffer, A. J. Weaver, E. Driesschaert, M. Eby, T. Fichefet, et al. 2005. "A Model Intercomparison of Changes in the Atlantic Thermohaline Circulation in Response to Increasing Atmospheric CO2 Concentration." *Geophysical Research Letters* 32 (12). https://doi.org/10.1029/2005GL023209.

Groot, M. H. M., R. G. Bogotá, L. J. Lourens, H. Hooghiemstra, M. Vriend, J. C. Berrio, E. Tuenter, et al. 2011. "Ultra-High Resolution Pollen Record from the Northern Andes Reveals Rapid Shifts in Montane Climates within the Last Two Glacial Cycles." *Climate of the Past* 7 (1): 299–316. https://doi.org/10.5194/cp-7-299-2011.

Guo, Z T, A Berger, Q Z Yin, and L Qin. 2009. "Strong Asymmetry of Hemispheric Climates during MIS-13 Inferred from Correlating China Loess and Antarctica Ice Records." *Clim. Past*, 11.

Guo, Zhengtang, Pierre Biscaye, Lanying Wei, Xihui Chen, Shuzhen Peng, and Tungsheng Liu. 2000. "Summer Monsoon Variations over the Last 1.2 Ma from the Weathering of Loess-Soil Sequences in China." *Geophysical Research Letters* 27 (12): 1751–54. https://doi.org/10.1029/1999GL008419.

Guo, Zhengtang, Tungsheng Liu, Nicolas Fedoroff, Lanying Wei, Zhongli Ding, Naiqin Wu, Huoyuan Lu, Wenying Jiang, and Zhisheng An. 1998. "Climate Extremes in Loess of China Coupled with the Strength of Deep-Water Formation in the North Atlantic." *Global and Planetary Change* 18 (3–4): 113–28. https://doi.org/10.1016/S0921-8181(98)00010-1.

Hanselman, Jennifer A., Mark B. Bush, William D. Gosling, Aaron Collins, Christopher Knox, Paul A. Baker, and Sheri C. Fritz. 2011. "A 370,000-Year Record of Vegetation and Fire History around Lake Titicaca (Bolivia/Peru)." *Palaeogeography, Palaeoclimatology, Palaeoecology* 305 (1–4): 201–14. https://doi.org/10.1016/j.palaeo.2011.03.002.

Hansen, B.C.S, H. E. Wright, and J.P. Bradbury. 1984. "Pollen Studies in the Junín Area, Central Peruvian Andes." *Geological Society of America Bulletin* 95: 1454–65.

Hao, Qingzhen, Luo Wang, Frank Oldfield, and Zhengtang Guo. 2015. "Extra-Long Interglacial in Northern Hemisphere during MISs 15-13 Arising from Limited Extent of Arctic Ice Sheets in Glacial MIS 14." *Scientific Reports* 5 (1): 12103. https://doi.org/10.1038/srep12103.

Harris, Sara E., and Alan C. Mix. 1999. "Pleistocene Precipitation Balance in the Amazon Basin Recorded in Deep Sea Sediments." *Quaternary Research* 51 (1): 14–26. https://doi.org/10.1006/qres.1998.2008.

Hartman, Brett D., Bodo Bookhagen, and Oliver A. Chadwick. 2016. "The Effects of Check Dams and Other Erosion Control Structures on the Restoration of Andean Bofedal Ecosystems: Restoration of Andean Bofedal Ecosystems." *Restoration Ecology* 24 (6): 761–72. https://doi.org/10.1111/rec.12402.

Hatfield, R. G., A. Woods, S. B. Lehmann, N. Weidhaas, C. Y. Chen, J. Kück, S. Pierdominici, J. S. Stoner, M. B. Abbott, and D. T. Rodbell. 2020a. "Stratigraphic Correlation and Splice Generation for Sediments Recovered from a Large-Lake Drilling Project: An Example from Lake Junín, Peru." *Journal of Paleolimnology* 63 (1): 83–100. https://doi.org/10.1007/s10933-019-00098-w.

———. 2020b. "Stratigraphic Correlation and Splice Generation for Sediments Recovered from a Large-Lake Drilling Project: An Example from Lake Junín, Peru." *Journal of Paleolimnology* 63 (1): 83–100. https://doi.org/10.1007/s10933-019-00098-w.

Hatfield, Robert G., Joseph S. Stoner, Katharine E. Solada, Ann E. Morey, Arielle Woods, Christine Y. Chen, David McGee, Mark B. Abbott, and Donald T. Rodbell. 2020. "Paleomagnetic Constraint of the Brunhes Age Sedimentary Record From Lake Junín, Peru." *Frontiers in Earth Science* 8 (June): 147. https://doi.org/10.3389/feart.2020.00147.

Haug, G. H., Hughen, K. A., Sigman, D. M., Peterson, L. C., and Röhl, U. 2001. "Southward Migration of the Intertropical Convergence Zone Through the Holocene." *Science* 293 (5533): 1304–8. https://doi.org/10.1126/science.1059725.

Haylock, M. R., T. C. Peterson, L. M. Alves, T. Ambrizzi, Y. M. T. Anunciação, J. Baez, V. R. Barros, et al. 2006. "Trends in Total and Extreme South American Rainfall in 1960–2000 and Links with Sea Surface Temperature." *Journal of Climate* 19 (8): 1490–1512. https://doi.org/10.1175/JCLI3695.1.

Heiri, Oliver, André F Lotter, and Gerry Lemcke. 2001. "Loss on Ignition as a Method for Estimating Organic and Carbonate Content in Sediments: Reproducibility and Comparability of Results." *Journal of Paleolimnology* 25 (1): 101–10.

Held, Isaac M., and Brian J. Soden. 2006. "Robust Responses of the Hydrological Cycle to Global Warming." *Journal of Climate* 19 (21): 5686–99. https://doi.org/10.1175/JCLI3990.1.

Henry, L. G., J. F. McManus, W. B. Curry, N. L. Roberts, A. M. Piotrowski, and L. D. Keigwin. 2016. "North Atlantic Ocean Circulation and Abrupt Climate Change during the Last Glaciation." *Science* 353 (6298): 470–74. https://doi.org/10.1126/science.aaf5529.

Heyman, Jakob, Patrick J. Applegate, Robin Blomdin, Natacha Gribenski, Jonathan M. Harbor, and Arjen P. Stroeven. 2016. "Boulder Height – Exposure Age Relationships from a Global Glacial 10Be Compilation." *Quaternary Geochronology* 34 (August): 1–11. https://doi.org/10.1016/j.quageo.2016.03.002.

Hillenbrand, C.-D., G. Kuhn, and T. Frederichs. 2009. "Record of a Mid-Pleistocene Depositional Anomaly in West Antarctic Continental Margin Sediments: An Indicator for Ice-Sheet Collapse?" *Quaternary Science Reviews* 28 (13–14): 1147–59. https://doi.org/10.1016/j.quascirev.2008.12.010.

Hillyer, Rachel, Bryan G. Valencia, Mark B. Bush, Miles R. Silman, and Miriam Steinitz-Kannan. 2009. "A 24,700-Yr Paleolimnological History from the Peruvian Andes." *Quaternary Research* 71 (1): 71–82. https://doi.org/10.1016/j.yqres.2008.06.006.

Hodell, David A., James E. T. Channell, Jason H. Curtis, Oscar E. Romero, and Ursula Röhl. 2008. "Onset of 'Hudson Strait' Heinrich Events in the Eastern North Atlantic at the End of the Middle Pleistocene Transition (~640 Ka)?: PLEISTOCENE HEINRICH EVENTS." *Paleoceanography* 23 (4): n/a-n/a. https://doi.org/10.1029/2008PA001591.

Hooghiemstra, H., J.L. Melice, A. Berger, and N.J. Shackleton. 1993. "Frequency Spectra and Paleoclimatic Variability of the High-Resolution 30–1450 Ka Funza I Pollen Record (Eastern Cordillera, Colombia)." *Quaternary Science Reviews* 12 (2): 141–56. https://doi.org/10.1016/0277-3791(93)90013-C.

Horton, Travis W., William F. Defliese, Aradhna K. Tripati, and Christopher Oze. 2016. "Evaporation Induced 18O and 13C Enrichment in Lake Systems: A Global Perspective on Hydrologic Balance Effects." *Quaternary Science Reviews* 131 (January): 365–79. https://doi.org/10.1016/j.quascirev.2015.06.030.

Jomelli, V., V. Favier, M. Vuille, R. Braucher, L. Martin, P.-H. Blard, C. Colose, et al. 2014. "A Major Advance of Tropical Andean Glaciers during the Antarctic Cold Reversal." *Nature* 513 (7517): 224–28. https://doi.org/10.1038/nature13546.

Jouzel, J., V. Masson-Delmotte, O. Cattani, G. Dreyfus, S. Falourd, G. Hoffmann, B. Minster, et al. 2007. "Orbital and Millennial Antarctic Climate Variability over the Past 800,000 Years." *Science, New Series* 317 (5839): 793–96.

Kanner, L. C., S. J. Burns, H. Cheng, and R. L. Edwards. 2012. "High-Latitude Forcing of the South American Summer Monsoon During the Last Glacial." *Science* 335 (6068): 570–73. https://doi.org/10.1126/science.1213397.

Kanner, Lisa C., Stephen J. Burns, Hai Cheng, R. Lawrence Edwards, and Mathias Vuille. 2013. "High-Resolution Variability of the South American Summer Monsoon over the Last Seven Millennia: Insights from a Speleothem Record from the Central Peruvian Andes." *Quaternary Science Reviews* 75 (September): 1–10. https://doi.org/10.1016/j.quascirev.2013.05.008.

Kaser, Georg. 2001. "Glacier-Climate Interaction at Low Latitudes." *Journal of Glaciology* 47 (157): 195–204. https://doi.org/10.3189/172756501781832296.

Kaser, Georg, Irmgard Juen, Christian Georges, Jesús Gómez, and William Tamayo. 2003. "The Impact of Glaciers on the Runoff and the Reconstruction of Mass Balance History from Hydrological Data in the Tropical Cordillera Blanca, Perú." *Journal of Hydrology* 282 (1–4): 130–44. https://doi.org/10.1016/S0022-1694(03)00259-2.

Kelly, M. A., T. V. Lowell, P. J. Applegate, C. A. Smith, F. M. Phillips, and A. M. Hudson. 2012. "Late Glacial Fluctuations of Quelccaya Ice Cap, Southeastern Peru." *Geology* 40 (11): 991–94. https://doi.org/10.1130/G33430.1.

Kelly, Meredith A., Thomas V. Lowell, Patrick J. Applegate, Fred M. Phillips, Joerg M. Schaefer, Colby A. Smith, Hanul Kim, Katherine C. Leonard, and Adam M. Hudson. 2015. "A Locally Calibrated, Late Glacial 10 Be Production Rate from a Low-Latitude, High-Altitude Site in the Peruvian Andes." *Quaternary Geochronology* 26 (February): 70–85. https://doi.org/10.1016/j.quageo.2013.10.007.

King, A.L., and W.R. Howard. 2000. "Middle Pleistocene Sea-Surface Temperature Change in the Southwest Pacific Ocean on Orbital and Suborbital Time Scales." *Geology* 28 (7): 659–62.

Konecky, B. L., D. C. Noone, and K. M. Cobb. 2019. "The Influence of Competing Hydroclimate Processes on Stable Isotope Ratios in Tropical Rainfall." *Geophysical Research Letters*, February, 2018GL080188. https://doi.org/10.1029/2018GL080188.

Koster, Randal D., D. Perry de Valpine, and Jean Jouzel. 1993. "Continental Water Recycling and $H_2^{18}O$ Concentrations." *Geophysical Research Letters* 20 (20): 2215–18. https://doi.org/10.1029/93GL01781.

Kutzbach, J. E. 1981. "Monsoon Climate of the Early Holocene: Climate Experiment with the Earth's Orbital Parameters for 9000 Years Ago." *Science* 214 (4516): 59–61. https://doi.org/10.1126/science.214.4516.59.

Kutzbach, J. E., and P. J. Guetter. 1986. "The Influence of Changing Orbital Parameters and Surface Boundary Conditions on Climate Simulations for the Past 18 000 Years." *Journal of Atmospheric Sciences* 43 (16): 1726–59.

Lang, N., and E. W. Wolff. 2011. "Interglacial and Glacial Variability from the Last 800 Ka in Marine, Ice and Terrestrial Archives." *Climate of the Past* 7 (2): 361–80. https://doi.org/10.5194/cp-7-361-2011.

Laskar, J., P. Robutel, F. Joutel, M. Gastineau, A. C. M. Correia, and B. Levrard. 2004. "A Long-Term Numerical Solution for the Insolation Quantities of the Earth." *Astronomy & Astrophysics* 428 (1): 261–85. https://doi.org/10.1051/0004-6361:20041335.

Lee, June-Yi, and Bin Wang. 2014. "Future Change of Global Monsoon in the CMIP5." *Climate Dynamics* 42 (1–2): 101–19. https://doi.org/10.1007/s00382-012-1564-0.

Lee, Jung-Eun, and Inez Fung. 2008. "'Amount Effect' of Water Isotopes and Quantitative Analysis of Post-Condensation Processes." *Hydrological Processes* 22 (1): 1–8. https://doi.org/10.1002/hyp.6637.

Lee, Jung-Eun, Kathleen Johnson, and Inez Fung. 2009. "Precipitation over South America during the Last Glacial Maximum: An Analysis of the 'Amount Effect' with a Water Isotope-Enabled General Circulation Model." *Geophysical Research Letters* 36 (19): L19701. https://doi.org/10.1029/2009GL039265.

Leng, Melanie J, and Jim D Marshall. 2004. "Palaeoclimate Interpretation of Stable Isotope Data from Lake Sediment Archives." *Quaternary Science Reviews* 23 (7–8): 811–31. https://doi.org/10.1016/j.quascirev.2003.06.012.

Li, HC, and TL Ku. 1997. "Δ13C–Δ18C Covariance as a Paleohydrological Indicator for Closed-Basin Lakes." *Palaeogeography, Palaeoclimatology, Palaeoecology* 133: 69–80.

Lin, Jia-Lin. 2007. "The Double-ITCZ Problem in IPCC AR4 Coupled GCMs: Ocean–Atmosphere Feedback Analysis." *Journal of Climate* 20 (18): 4497–4525. https://doi.org/10.1175/JCLI4272.1.

Lisiecki, Lorraine E., and Maureen E. Raymo. 2005. "A Pliocene-Pleistocene Stack of 57 Globally Distributed Benthic Δ18O Records." *Paleoceanography* 20 (1). https://doi.org/10.1029/2004PA001071.

Liu, Xiaojuan, and David S. Battisti. 2015. "The Influence of Orbital Forcing of Tropical Insolation on the Climate and Isotopic Composition of Precipitation in South America." *Journal of Climate* 28 (12): 4841–62. https://doi.org/10.1175/JCLI-D-14-00639.1.

Loulergue, Laetitia, Adrian Schilt, Renato Spahni, Valérie Masson-Delmotte, Thomas Blunier, Bénédicte Lemieux, Jean-Marc Barnola, Dominique Raynaud, Thomas F. Stocker, and Jérôme Chappellaz. 2008. "Orbital and Millennial-Scale Features of Atmospheric CH4 over the Past 800,000 Years." *Nature* 453 (7193): 383–86. https://doi.org/10.1038/nature06950.

Lüthi, Dieter, Martine Le Floch, Bernhard Bereiter, Thomas Blunier, Jean-Marc Barnola, Urs Siegenthaler, Dominique Raynaud, et al. 2008. "High-Resolution Carbon Dioxide Concentration Record 650,000–800,000 Years before Present." *Nature* 453 (7193): 379–82. https://doi.org/10.1038/nature06949.

Lynch-Stieglitz, Jean. 2017. "The Atlantic Meridional Overturning Circulation and Abrupt Climate Change." *Annual Review of Marine Science* 9 (1): 83–104. https://doi.org/10.1146/annurev-marine-010816-060415.

Marcott, Shaun A., Thomas K. Bauska, Christo Buizert, Eric J. Steig, Julia L. Rosen, Kurt M. Cuffey, T. J. Fudge, et al. 2014. "Centennial-Scale Changes in the Global Carbon Cycle during the Last Deglaciation." *Nature* 514 (7524): 616–19. https://doi.org/10.1038/nature13799.

Marengo, J. A. 2004. "Interdecadal Variability and Trends of Rainfall across the Amazon Basin." *Theoretical and Applied Climatology* 78 (1–3). https://doi.org/10.1007/s00704-004-0045-8.

Marengo, J. A., B. Liebmann, A. M. Grimm, V. Misra, P. L. Silva Dias, I. F. A. Cavalcanti, L. M. V. Carvalho, et al. 2012. "Recent Developments on the South American Monsoon System: RECENT DEVELOPMENTS ON THE SOUTH AMERICAN MONSOON SYSTEM." *International Journal of Climatology* 32 (1): 1–21. https://doi.org/10.1002/joc.2254.

Mark, B., N. Stansell, and G. Zeballos. 2017. "The Last Deglaciation of Peru and Bolivia." *Cuadernos de Investigación Geográfica* 43 (2): 591. https://doi.org/10.18172/cig.3265.

Mark, Bryan G., and Geoffrey O. Seltzer. 2003. "Tropical Glacier Meltwater Contribution to Stream Discharge: A Case Study in the Cordillera Blanca, Peru." *Journal of Glaciology* 49 (165): 271–81. https://doi.org/10.3189/172756503781830746.

Martin, Alan J., J.Jay McNee, and Thomas F. Pedersen. 2001. "The Reactivity of Sediments Impacted by Metal-Mining in Lago Junin, Peru." *Journal of Geochemical Exploration* 74 (1–3): 175–87. https://doi.org/10.1016/S0375-6742(01)00183-2.

Martin, L.C.P., P.-H. Blard, J. Lavé, R. Braucher, M. Lupker, T. Condom, J. Charreau, V. Mariotti, ASTER Team, and E. Davy. 2015. "In Situ Cosmogenic 10Be Production Rate in the High Tropical Andes." *Quaternary Geochronology* 30 (October): 54–68. https://doi.org/10.1016/j.quageo.2015.06.012.

Martin, L.C.P., P.-H. Blard, J. Lavé, V. Jomelli, J. Charreau, T. Condom, M. Lupker, et al. 2020. "Antarctic-like Temperature Variations in the Tropical Andes Recorded by Glaciers and Lakes during the Last Deglaciation." *Quaternary Science Reviews* 247 (November): 106542. https://doi.org/10.1016/j.quascirev.2020.106542.

Martin, L.C.P, P.-H. Blard, Jérôme Lavé, Thomas Condom, Mélody Prémaillon, Vincent Jomelli, Daniel Brunstein, et al. 2018. "Lake Tauca Highstand (Heinrich Stadial 1a) Driven by a Southward Shift of the Bolivian High." *Science Advances* 4 (8): eaar2514. https://doi.org/10.1126/sciadv.aar2514.

Martinelli, Luiz Antonio, Reynaldo Luiz Victoria, Leonel Silveira Lobo Sternberg, Aristides Ribeiro, and Marcelo Zacharias Moreira. 1996. "Using Stable Isotopes to Determine Sources of Evaporated Water to the Atmosphere in the Amazon Basin." *Journal of Hydrology* 183 (3–4): 191–204. https://doi.org/10.1016/0022-1694(95)02974-5.

Martrat, B., J. O. Grimalt, N. J. Shackleton, L. de Abreu, M. A. Hutterli, and T. F. Stocker. 2007. "Four Climate Cycles of Recurring Deep and Surface Water Destabilizations on the Iberian Margin." *Science* 317 (5837): 502–7. https://doi.org/10.1126/science.1139994.

Maslin, Mark A, and Stephen J Burns. 2000. "Reconstruction of the Amazon Basin Effective Moisture Availability over the Past 14,000 Years" 290: 3.

McClymont, Erin L., Antoni Rosell-Melé, Jacques Giraudeau, Catherine Pierre, and Jerry M. Lloyd. 2005. "Alkenone and Coccolith Records of the Mid-Pleistocene in the South-East Atlantic: Implications for the U37K' Index and South African Climate." *Quaternary Science Reviews* 24 (14–15): 1559–72. https://doi.org/10.1016/j.quascirev.2004.06.024.

McGee, David. 2020. "Glacial–Interglacial Precipitation Changes." *Annual Review of Marine Science* 12 (1): 525–57. https://doi.org/10.1146/annurev-marine-010419-010859.

McGee, David, Aaron Donohoe, John Marshall, and David Ferreira. 2014. "Changes in ITCZ Location and Cross-Equatorial Heat Transport at the Last Glacial Maximum, Heinrich Stadial 1, and the Mid-Holocene." *Earth and Planetary Science Letters* 390 (March): 69–79. https://doi.org/10.1016/j.epsl.2013.12.043.

McGee, David, Eduardo Moreno-Chamarro, Brian Green, John Marshall, Eric Galbraith, and Louisa Bradtmiller. 2018. "Hemispherically Asymmetric Trade Wind Changes as Signatures of Past ITCZ Shifts." *Quaternary Science Reviews* 180 (January): 214–28. https://doi.org/10.1016/j.quascirev.2017.11.020.

McManus, J. F., R. Francois, J.-M. Gherardi, L. D. Keigwin, and S. Brown-Leger. 2004. "Collapse and Rapid Resumption of Atlantic Meridional Circulation Linked to Deglacial Climate Changes." *Nature* 428 (6985): 834–37. https://doi.org/10.1038/nature02494.

Meckler, A. N., M. O. Clarkson, K. M. Cobb, H. Sodemann, and J. F. Adkins. 2012. "Interglacial Hydroclimate in the Tropical West Pacific Through the Late Pleistocene." *Science* 336 (6086): 1301–4. https://doi.org/10.1126/science.1218340.

Meyers, P.A., and J.L. Teranes. 2001. *Sediment Organic Matter. In: Tracking Environmental Changes Using Lake Sediments, Physical and Chemical Techniques*. Edited by W.M. Last and J.P. Smol. Vol. II. Dordrecht.

Mohtadi, Mahyar, Matthias Prange, and Stephan Steinke. 2016. "Palaeoclimatic Insights into Forcing and Response of Monsoon Rainfall." *Nature* 533 (7602): 191–99. https://doi.org/10.1038/nature17450.

Mosblech, Nicole A. S., Mark B. Bush, William D. Gosling, David Hodell, Louise Thomas, Peter van Calsteren, Alexander Correa-Metrio, Bryan G. Valencia, Jason Curtis, and Robert van Woesik. 2012. "North Atlantic Forcing of Amazonian Precipitation during the Last Ice Age." *Nature Geoscience* 5 (11): 817–20. https://doi.org/10.1038/ngeo1588.

Naafs, B. David A., Jens Hefter, Patrizia Ferretti, Ruediger Stein, and Gerald H. Haug. 2011. "Sea Surface Temperatures Did Not Control the First Occurrence of Hudson Strait Heinrich Events during MIS 16." *Paleoceanography* 26 (4): 2011PA002135. https://doi.org/10.1029/2011PA002135.

Naafs, B.D.A., J. Hefter, and R. Stein. 2013. "Millennial-Scale Ice Rafting Events and Hudson Strait Heinrich(-like) Events during the Late Pliocene and Pleistocene: A Review." *Quaternary Science Reviews* 80 (November): 1–28. https://doi.org/10.1016/j.quascirev.2013.08.014.

Neelin, J. D., M. Munnich, H. Su, J. E. Meyerson, and C. E. Holloway. 2006. "Tropical Drying Trends in Global Warming Models and Observations." *Proceedings of the National Academy of Sciences* 103 (16): 6110–15. https://doi.org/10.1073/pnas.0601798103.

NEEM community members. 2013. "Eemian Interglacial Reconstructed from a Greenland Folded Ice Core." *Nature* 493 (7433): 489–94. https://doi.org/10.1038/nature11789.

Novello, Valdir F., Francisco W. Cruz, Mathias Vuille, Nicolás M. Stríkis, R. Lawrence Edwards, Hai Cheng, Suellyn Emerick, et al. 2017. "A High-Resolution History of the South American Monsoon from Last Glacial Maximum to the Holocene." *Scientific Reports* 7 (1): 44267. https://doi.org/10.1038/srep44267.

Olsson, IU. 1986. "Radiometric Dating." *Handbook of Holocene Palaeoecology and Palaeohydrology*.

Paegle, Julia N, and Kingtse C Mo. 2002. "Linkages between Summer Rainfall Variability over South America and Sea Surface Temperature Anomalies." *Journal of Climate* 15: 19.

Past Interglacials Working Group of PAGES. 2016. "Interglacials of the Last 800,000 Years: Interglacials of the Last 800,000 Years." *Reviews of Geophysics* 54 (1): 162–219. https://doi.org/10.1002/2015RG000482.

Pedro, J. B., T. D. van Ommen, S. O. Rasmussen, V. I. Morgan, J. Chappellaz, A. D. Moy, V. Masson-Delmotte, and M. Delmotte. 2011. "The Last Deglaciation: Timing the Bipolar Seesaw." *Climate of the Past* 7 (2): 671–83. https://doi.org/10.5194/cp-7-671-2011.

Pedro, Joel B., Helen C. Bostock, Cecilia M. Bitz, Feng He, Marcus J. Vandergoes, Eric J. Steig, Brian M. Chase, et al. 2016. "The Spatial Extent and Dynamics of the Antarctic Cold Reversal." *Nature Geoscience* 9 (1): 51–55. https://doi.org/10.1038/ngeo2580.

Peterson, L. C., G. H. Haug, K. A. Hughen, and U. Röhl. 2000. "Rapid Changes in the Hydrologic Cycle of the Tropical Atlantic During the Last Glacial." *Science* 290 (s): 1947–51. https://doi.org/10.1126/science.290.5498.1947.

Peterson, Larry C., and Gerald H. Haug. 2006. "Variability in the Mean Latitude of the Atlantic Intertropical Convergence Zone as Recorded by Riverine Input of Sediments to the Cariaco Basin (Venezuela)." *Palaeogeography, Palaeoclimatology, Palaeoecology* 234 (1): 97–113. https://doi.org/10.1016/j.palaeo.2005.10.021.

Placzek, C., J. Quade, and P. J. Patchett. 2006. "Geochronology and Stratigraphy of Late Pleistocene Lake Cycles on the Southern Bolivian Altiplano: Implications for Causes of Tropical Climate Change." *Geological Society of America Bulletin* 118 (5–6): 515–32. https://doi.org/10.1130/B25770.1.

Placzek, C., J. Quade, and P.J. Patchett. 2013. "A 130ka Reconstruction of Rainfall on the Bolivian Altiplano." *Earth and Planetary Science Letters* 363 (February): 97–108. https://doi.org/10.1016/j.epsl.2012.12.017.

Portilho-Ramos, R. C., C. M. Chiessi, Y. Zhang, S. Mulitza, M. Kucera, M. Siccha, M. Prange, and A. Paul. 2017. "Coupling of Equatorial Atlantic Surface Stratification to Glacial Shifts in the Tropical Rainbelt." *Scientific Reports* 7 (1): 1561. https://doi.org/10.1038/s41598-017-01629-z.

Prokopenko, Alexander A., Douglas F. Williams, Mikhail I. Kuzmin, Eugene B. Karabanov, Galina K. Khursevich, and John A. Peck. 2002. "Muted Climate Variations in Continental Siberia during the Mid-Pleistocene Epoch." *Nature* 418 (6893): 65–68. https://doi.org/10.1038/nature00886.

Rahmstorf, Stefan. 2002. "Ocean Circulation and Climate during the Past 120,000 Years." *Nature* 419 (6903): 207–14. https://doi.org/10.1038/nature01090.

Rasmussen, Sune O., Matthias Bigler, Simon P. Blockley, Thomas Blunier, Susanne L. Buchardt, Henrik B. Clausen, Ivana Cvijanovic, et al. 2014. "A Stratigraphic Framework for Abrupt Climatic Changes during the Last Glacial Period Based on Three Synchronized Greenland Ice-

Core Records: Refining and Extending the INTIMATE Event Stratigraphy." *Quaternary Science Reviews* 106 (December): 14–28. https://doi.org/10.1016/j.quascirev.2014.09.007.

Reimer, Paula J, Edouard Bard, Alex Bayliss, J Warren Beck, Paul G Blackwell, Christopher Bronk Ramsey, Caitlin E Buck, et al. 2013. "IntCal13 and Marine13 Radiocarbon Age Calibration Curves 0–50,000 Years Cal BP." *Radiocarbon* 55 (4): 1869–87. https://doi.org/10.2458/azu_js_rc.55.16947.

Renssen, Hans, Hugues Goosse, Didier M. Roche, and Heikki Seppä. 2018. "The Global Hydroclimate Response during the Younger Dryas Event." *Quaternary Science Reviews* 193 (August): 84–97. https://doi.org/10.1016/j.quascirev.2018.05.033.

Rodbell, Donald T., Erin M. Delman, Mark B. Abbott, Mark T. Besonen, and Pedro M. Tapia. 2014. "The Heavy Metal Contamination of Lake Junín National Reserve, Peru: An Unintended Consequence of the Juxtaposition of Hydroelectricity and Mining." *GSA Today*, August, 4–10. https://doi.org/10.1130/GSATG200A.1.

Rodbell, Donald T., and Geoffrey O. Seltzer. 2000. "Rapid Ice Margin Fluctuations during the Younger Dryas in the Tropical Andes." *Quaternary Research* 54 (3): 328–38. https://doi.org/10.1006/qres.2000.2177.

Rodbell, Donald T., Geoffrey O. Seltzer, Bryan G. Mark, Jacqueline A. Smith, and Mark B. Abbott. 2008. "Clastic Sediment Flux to Tropical Andean Lakes: Records of Glaciation and Soil Erosion." *Quaternary Science Reviews* 27 (15–16): 1612–26. https://doi.org/10.1016/j.quascirev.2008.06.004.

Rodbell, Donald T., Jacqueline A. Smith, and Bryan G. Mark. 2009. "Glaciation in the Andes during the Lateglacial and Holocene." *Quaternary Science Reviews* 28 (21–22): 2165–2212. https://doi.org/10.1016/j.quascirev.2009.03.012.

Rodrigues, T., M. Alonso-García, D.A. Hodell, M. Rufino, F. Naughton, J.O. Grimalt, A.H.L. Voelker, and F. Abrantes. 2017. "A 1-Ma Record of Sea Surface Temperature and Extreme Cooling Events in the North Atlantic: A Perspective from the Iberian Margin." *Quaternary Science Reviews* 172 (September): 118–30. https://doi.org/10.1016/j.quascirev.2017.07.004.

Rodrigues, T., A. H. L. Voelker, J. O. Grimalt, F. Abrantes, and F. Naughton. 2011. "Iberian Margin Sea Surface Temperature during MIS 15 to 9 (580–300 Ka): Glacial Suborbital Variability versus Interglacial Stability." *Paleoceanography* 26 (1): PA1204. https://doi.org/10.1029/2010PA001927.

Rossignol-Strick, M., M. Paterne, F. C. Bassinot, K.-C. Emeis, and G. J. De Lange. 1998. "An Unusual Mid-Pleistocene Monsoon Period over Africa and Asia." *Nature* 392 (6673): 269–72. https://doi.org/10.1038/32631.

Rowe, Harold D, Robert B Dunbar, David A Mucciarone, Geoffrey O Seltzer, Paul A Baker, and Sherilyn Fritz. 2002. "Insolation, Moisture Balance and Climate Change on the South American Altiplano Since the Last Glacial Maximum." *Climatic Change* 52: 175–99.

Rowe, Harold D, Thomas P Guilderson, Robert B Dunbar, John R Southon, Geoffrey O Seltzer, David A Mucciarone, Sherilyn C Fritz, and Paul A Baker. 2003. "Late Quaternary Lake-Level Changes Constrained by Radiocarbon and Stable Isotope Studies on Sediment Cores from Lake Titicaca, South America." *Global and Planetary Change* 38 (3–4): 273–90. https://doi.org/10.1016/S0921-8181(03)00031-6.

Sagredo, Esteban A., Summer Rupper, and Thomas V. Lowell. 2014. "Sensitivities of the Equilibrium Line Altitude to Temperature and Precipitation Changes along the Andes." *Quaternary Research* 81 (2): 355–66. https://doi.org/10.1016/j.yqres.2014.01.008.

Salati, Eneas, Attilio Dall'Olio, Eiichi Matsui, and Joel R. Gat. 1979. "Recycling of Water in the Amazon Basin: An Isotopic Study." *Water Resources Research* 15 (5): 1250–58. https://doi.org/10.1029/WR015i005p01250.

Salvador, F, J Monerris, and L Rochefort. 2014. "Peatlands of the Peruvian Puna Ecoregion: Types, Characteristics and Disturbance." *Mires and Peat* 15 (03): 1–17.

Samuels-Crow, Kimberly E., Joseph Galewsky, Douglas R. Hardy, Zachary D. Sharp, John Worden, and Carsten Braun. 2014. "Upwind Convective Influences on the Isotopic Composition of Atmospheric Water Vapor over the Tropical Andes: CONVECTION AND ΔD IN THE TROPICAL ANDES." *Journal of Geophysical Research: Atmospheres* 119 (12): 7051–63. https://doi.org/10.1002/2014JD021487.

Schittek, Karsten, Markus Forbriger, Frank Schäbitz, and Bernhard Eitel. 2012. "Cushion Peatlands - Fragile Water Resources in the High Andes of Southern Peru." *Landscape and Sustainable Development* 4: 63–84.

Schneider, Tapio, Tobias Bischoff, and Gerald H. Haug. 2014. "Migrations and Dynamics of the Intertropical Convergence Zone." *Nature* 513 (7516): 45–53. https://doi.org/10.1038/nature13636.

Seltzer, G. O., Rodbell, D. T., Baker, P. A., Fritz, S. C., Tapia, P. M., Rowe, H. D., and Dunbar, R. B. 2002. "Early Warming of Tropical South America at the Last Glacial-Interglacial Transition." *Science* 296 (5573): 1685–86. https://doi.org/10.1126/science.1070136.

Seltzer, Geoffrey O, Paul Baker, Scott Cross, Robert Dunbar, and Sherilyn Fritz. 1998. "High-Resolution Seismic Reflection Profiles from Lake Titicaca, Peru-Bolivia: Evidence for Holocene Aridity in the Tropical Andes." *Geology* 26 (2): 167–70.

Seltzer, Geoffrey, Donald Rodbell, and Stephen Burns. 2000. "Isotopic Evidence for Late Quaternary Climatic Change in Tropical South America." *Geology* 28 (1): 35–38.

Sepulcre, S., L. Vidal, K. Tachikawa, F. Rostek, and E. Bard. 2011. "Sea-Surface Salinity Variations in the Northern Caribbean Sea across the Mid-Pleistocene Transition." *Climate of the Past* 7 (1): 75–90. https://doi.org/10.5194/cp-7-75-2011.

Shakun, Jeremy D., and Anders E. Carlson. 2010. "A Global Perspective on Last Glacial Maximum to Holocene Climate Change." *Quaternary Science Reviews* 29 (15–16): 1801–16. https://doi.org/10.1016/j.quascirev.2010.03.016.

Shakun, Jeremy D., Peter U. Clark, Feng He, Nathaniel A. Lifton, Zhengyu Liu, and Bette L. Otto-Bliesner. 2015. "Regional and Global Forcing of Glacier Retreat during the Last Deglaciation." *Nature Communications* 6 (1): 8059. https://doi.org/10.1038/ncomms9059.

Shakun, Jeremy D., Peter U. Clark, Shaun A. Marcott, Edward J. Brook, Nathaniel A. Lifton, Marc Caffee, and William R. Shakun. 2015. "Cosmogenic Dating of Late Pleistocene Glaciation, Southern Tropical Andes, Peru." *Journal of Quaternary Science* 30 (8): 841–47. https://doi.org/10.1002/jqs.2822.

Singarayer, Joy S., Paul J. Valdes, and William H. G. Roberts. 2017. "Ocean Dominated Expansion and Contraction of the Late Quaternary Tropical Rainbelt." *Scientific Reports* 7 (1): 9382. https://doi.org/10.1038/s41598-017-09816-8.

Smith, Jacqueline A., Robert C. Finkel, Daniel L. Farber, Donald T. Rodbell, and Geoffrey O. Seltzer. 2005. "Moraine Preservation and Boulder Erosion in the Tropical Andes: Interpreting Old Surface Exposure Ages in Glaciated Valleys." *Journal of Quaternary Science* 20 (7–8): 735–58. https://doi.org/10.1002/jqs.981.

Smith, Jacqueline A., Bryan G. Mark, and Donald T. Rodbell. 2008. "The Timing and Magnitude of Mountain Glaciation in the Tropical Andes." *Journal of Quaternary Science* 23 (6–7): 609–34. https://doi.org/10.1002/jqs.1224.

Smith, Jacqueline A., and Donald T. Rodbell. 2010. "Cross-Cutting Moraines Reveal Evidence for North Atlantic Influence on Glaciers in the Tropical Andes." *Journal of Quaternary Science* 25 (3): 243–48. https://doi.org/10.1002/jqs.1393.

Smith, Jacqueline A., Geoffrey O. Seltzer, Daniel L. Farber, Donald T. Rodbell, and Robert C. Finkel. 2005. "Early Local Last Glacial Maximum in the Tropical Andes." *Science* 308 (5722): 678–81. https://doi.org/10.1126/science.1107075.

Smith, Jacqueline A., Geoffrey O. Seltzer, Donald T. Rodbell, and Andrew G. Klein. 2005. "Regional Synthesis of Last Glacial Maximum Snowlines in the Tropical Andes, South America." *Quaternary International*, Snowlines at the Last Glacial Maximum and tropical cooling, 138–139 (September): 145–67. https://doi.org/10.1016/j.quaint.2005.02.011.

Squeo, Francisco A, Barry G Warner, Ramón Aravena, and Diana Espinoza. 2006. "Bofedales: High Altitude Peatlands of the Central Andes." *Revista Chilena de Historia Natural* 79 (2). https://doi.org/10.4067/S0716-078X2006000200010.

Staal, Arie, Obbe A. Tuinenburg, Joyce H. C. Bosmans, Milena Holmgren, Egbert H. van Nes, Marten Scheffer, Delphine Clara Zemp, and Stefan C. Dekker. 2018. "Forest-Rainfall Cascades Buffer against Drought across the Amazon." *Nature Climate Change* 8 (6): 539–43. https://doi.org/10.1038/s41558-018-0177-y.

Stansell, Nathan D., Mark B. Abbott, Pratigya J. Polissar, Alexander P. Wolfe, Maximiliano Bezada, and Valentí Rull. 2005. "Late Quaternary Deglacial History of the Mérida Andes, Venezuela." *Journal of Quaternary Science* 20 (7–8): 801–12. https://doi.org/10.1002/jqs.973.

Stansell, Nathan D., Joseph M. Licciardi, Donald T. Rodbell, and Bryan G. Mark. 2017. "Tropical Ocean-Atmospheric Forcing of Late Glacial and Holocene Glacier Fluctuations in the Cordillera Blanca, Peru: CORDILLERA BLANCA GLACIER FLUCTUATIONS." *Geophysical Research Letters* 44 (9): 4176–85. https://doi.org/10.1002/2016GL072408.

Stríkis, Nicolás M., Cristiano M. Chiessi, Francisco W. Cruz, Mathias Vuille, Hai Cheng, Eline A. de Souza Barreto, Gesine Mollenhauer, et al. 2015. "Timing and Structure of Mega-SACZ Events during Heinrich Stadial 1: MEGA-SACZ DURING HEINRICH STADIAL 1." *Geophysical Research Letters* 42 (13): 5477-5484A. https://doi.org/10.1002/2015GL064048.

Stríkis, Nicolás M., Francisco W. Cruz, Eline A. S. Barreto, Filipa Naughton, Mathias Vuille, Hai Cheng, Antje H. L. Voelker, et al. 2018. "South American Monsoon Response to Iceberg Discharge in the North Atlantic." *Proceedings of the National Academy of Sciences* 115 (15): 3788–93. https://doi.org/10.1073/pnas.1717784115.

Stuiver, M, and HA Polach. 1977. "Discussion Reporting of 14C Data." *Radiocarbon* 19 (3): 355–63.

Sturm, Christophe, Françoise Vimeux, and Gerhard Krinner. 2007. "Intraseasonal Variability in South America Recorded in Stable Water Isotopes." *Journal of Geophysical Research* 112 (D20): D20118. https://doi.org/10.1029/2006JD008298.

Svensson, A, K K Andersen, M Bigler, H B Clausen, D Dahl-Jensen, S M Davies, S J Johnsen, et al. 2008. "A 60 000 Year Greenland Stratigraphic Ice Core Chronology." *Clim. Past* 4 (1): 47–57.

Sylvestre, Florence, Michel Servant, Simone Servant-Vildary, Christiane Causse, Marc Fournier, and Jean-Pierre Ybert. 1999. "Lake-Level Chronology on the Southern Bolivian Altiplano (18°–23°S) During Late-Glacial Time and the Early Holocene." *Quaternary Research* 51 (1): 54–66. https://doi.org/10.1006/qres.1998.2017.

Talbot, M.R. 1990. "A Review of the Palaeohydrological Interpretation of Carbon and Oxygen Isotopic Ratios in Primary Lacustrine Carbonates." *Chemical Geology: Isotope Geoscience Section* 80 (4): 261–79. https://doi.org/10.1016/0168-9622(90)90009-2.

Thompson, L. G., E. Mosley-Thompson, H. Brecher, M. Davis, B. Leon, D. Les, P.-N. Lin, T. Mashiotta, and K. Mountain. 2006. "Abrupt Tropical Climate Change: Past and Present." *Proceedings of the National Academy of Sciences* 103 (28): 10536–43. https://doi.org/10.1073/pnas.0603900103.

Thompson, L. G., E. Mosley-Thompson, M. E. Davis, P. -N. Lin, K. A. Henderson, J. Cole-Dai, J. F. Bolzan, and K. -b. Liu. 1995. "Late Glacial Stage and Holocene Tropical Ice Core Records from Huascaran, Peru." *Science* 269 (5220): 46–50. https://doi.org/10.1126/science.269.5220.46.

Toggweiler, J. R. 2009. "Climate Change: Shifting Westerlies." *Science* 323 (5920): 1434–35. https://doi.org/10.1126/science.1169823.

Torres, Vladimir, Henry Hooghiemstra, Lucas Lourens, and P. Chronis Tzedakis. 2013. "Astronomical Tuning of Long Pollen Records Reveals the Dynamic History of Montane

Biomes and Lake Levels in the Tropical High Andes during the Quaternary." *Quaternary Science Reviews* 63 (March): 59–72. https://doi.org/10.1016/j.quascirev.2012.11.004.

Toucanne, S., S. Zaragosi, J.F. Bourillet, P.L. Gibbard, F. Eynaud, J. Giraudeau, J.L. Turon, et al. 2009. "A 1.2Ma Record of Glaciation and Fluvial Discharge from the West European Atlantic Margin." *Quaternary Science Reviews* 28 (25–26): 2974–81. https://doi.org/10.1016/j.quascirev.2009.08.003.

Urrego, Dunia H., Mark B. Bush, and Miles R. Silman. 2010. "A Long History of Cloud and Forest Migration from Lake Consuelo, Peru." *Quaternary Research* 73 (2): 364–73. https://doi.org/10.1016/j.yqres.2009.10.005.

Vera, C., W. Higgins, J. Amador, T. Ambrizzi, R. Garreaud, D. Gochis, D. Gutzler, et al. 2006. "Toward a Unified View of the American Monsoon Systems." *Journal of Climate* 19 (20): 4977–5000. https://doi.org/10.1175/JCLI3896.1.

Vernal, A. de, and C. Hillaire-Marcel. 2008. "Natural Variability of Greenland Climate, Vegetation, and Ice Volume During the Past Million Years." *Science* 320 (5883): 1622–25. https://doi.org/10.1126/science.1153929.

Verpoorter, Charles, Tiit Kutser, David A. Seekell, and Lars J. Tranvik. 2014. "A Global Inventory of Lakes Based on High-Resolution Satellite Imagery." *Geophysical Research Letters* 41 (18): 6396–6402. https://doi.org/10.1002/2014GL060641.

Vidic, N. J., J. D. TenPas, K. L. Verosub, and M. J. Singer. 2000. "Separation of Pedogenic and Lithogenic Components of Magnetic Susceptibility in the Chinese Loess/Palaeosol Sequence as Determined by the CBD Procedure and a Mixing Analysis." *Geophysical Journal International* 142 (2): 551–62. https://doi.org/10.1046/j.1365-246x.2000.00178.x.

Vimeux, F, R Gallaire, S Bony, G Hoffmann, and J Chiang. 2005. "What Are the Climate Controls on ΔD in Precipitation in the Zongo Valley (Bolivia)? Implications for the Illimani Ice Core Interpretation." *Earth and Planetary Science Letters* 240 (2): 205–20. https://doi.org/10.1016/j.epsl.2005.09.031.

Voelker, A. H. L., T. Rodrigues, K. Billups, D. Oppo, J. McManus, R. Stein, J. Hefter, and J. O. Grimalt. 2010. "Variations in Mid-Latitude North Atlantic Surface Water Properties during the Mid-Brunhes (MIS 9–14) and Their Implications for the Thermohaline Circulation." *Climate of the Past* 6 (4): 531–52. https://doi.org/10.5194/cp-6-531-2010.

Vuille, M., R.S. Bradley, M. Werner, R. Healy, and F. Keimig. 2003. "Modeling Δ18O in Precipitation over the Tropical Americas: 1. Interannual Variability and Climatic Controls." *Journal of Geophysical Research* 108 (D6): 4174. https://doi.org/10.1029/2001JD002038.

Vuille, M., S. J. Burns, B. L. Taylor, F. W. Cruz, B. W. Bird, M. B. Abbott, L. C. Kanner, H. Cheng, and V. F. Novello. 2012. "A Review of the South American Monsoon History as Recorded in Stable Isotopic Proxies over the Past Two Millennia." *Climate of the Past* 8 (4): 1309–21. https://doi.org/10.5194/cp-8-1309-2012.

Vuille, M., and M. Werner. 2005. "Stable Isotopes in Precipitation Recording South American Summer Monsoon and ENSO Variability: Observations and Model Results." *Climate Dynamics* 25 (4): 401–13. https://doi.org/10.1007/s00382-005-0049-9.

Vuille, Mathias, Raymond S. Bradley, Martin Werner, and Frank Keimig. 2003. "20th Century Climate Change in the Tropical Andes: Observations and Model Results." Edited by Henry F. Diaz. *Climatic Change*, Advances in Global Change Research, 15: 75–99. https://doi.org/10.1007/978-94-015-1252-7_5.

Waelbroeck, C., L. Labeyrie, E. Michel, J.C. Duplessy, J.F. McManus, K. Lambeck, E. Balbon, and M. Labracherie. 2002. "Sea-Level and Deep Water Temperature Changes Derived from Benthic Foraminifera Isotopic Records." *Quaternary Science Reviews* 21 (1–3): 295–305. https://doi.org/10.1016/S0277-3791(01)00101-9.

WAIS Divide Project Members, Christo Buizert, Betty Adrian, Jinho Ahn, Mary Albert, Richard B. Alley, Daniel Baggenstos, et al. 2015. "Precise Interpolar Phasing of Abrupt Climate Change during the Last Ice Age." *Nature* 520 (7549): 661–65. https://doi.org/10.1038/nature14401.

WAIS Divide Project Members, T. J. Fudge, Eric J. Steig, Bradley R. Markle, Spruce W. Schoenemann, Qinghua Ding, Kendrick C. Taylor, et al. 2013. "Onset of Deglacial Warming in West Antarctica Driven by Local Orbital Forcing." *Nature* 500 (7463): 440–44. https://doi.org/10.1038/nature12376.

Wang, Xianfeng, Augusto S. Auler, R. Lawrence Edwards, Hai Cheng, Patricia S. Cristalli, Peter L. Smart, David A. Richards, and Chuan-Chou Shen. 2004. "Wet Periods in Northeastern Brazil over the Past 210 Kyr Linked to Distant Climate Anomalies." *Nature* 432 (7018): 740–43. https://doi.org/10.1038/nature03067.

Wang, Xianfeng, R. Lawrence Edwards, Augusto S. Auler, Hai Cheng, Xinggong Kong, Yongjin Wang, Francisco W. Cruz, Jeffrey A. Dorale, and Hong-Wei Chiang. 2017. "Hydroclimate Changes across the Amazon Lowlands over the Past 45,000 Years." *Nature* 541 (7636): 204–7. https://doi.org/10.1038/nature20787.

Wang, Y., H. Cheng, R.L. Edwards, X. Kong, X. Shao, S. Chen, J. Wu, X. Jiang, X. Wang, and Z. An. 2008. "Millennial- and Orbital-Scale Changes in the East Asian Monsoon over the Past 224,000 Years." *Nature* 451 (7182): 1090–93.

Wang, Y. J., H. Cheng, R L Edwards, Z. An, J. Wu, Chuan-Chou Shen, and Jeffrey A. Dorale. 2001. "A High-Resolution Absolute-Dated Late Pleistocene Monsoon Record from Hulu Cave, China." *Science* 294 (5550): 2345–48. https://doi.org/10.1126/science.1064618.

Ward, Brittany Marie, Corinne I. Wong, Valdir F. Novello, David McGee, Roberto V. Santos, Lucas C.R. Silva, Francisco W. Cruz, Xianfeng Wang, R. Lawrence Edwards, and Hai Cheng. 2019a. "Reconstruction of Holocene Coupling between the South American Monsoon System and Local Moisture Variability from Speleothem Δ18O and 87Sr/86Sr Records." *Quaternary Science Reviews* 210 (April): 51–63. https://doi.org/10.1016/j.quascirev.2019.02.019.

———. 2019b. "Reconstruction of Holocene Coupling between the South American Monsoon System and Local Moisture Variability from Speleothem Δ18O and 87Sr/86Sr Records." *Quaternary Science Reviews* 210 (April): 51–63. https://doi.org/10.1016/j.quascirev.2019.02.019.

Weidhaas, Nicholas. 2017. "A 25,000-Year Lake Level History of Lake Junín, Peru from Stratigraphic and Oxygen Isotope Studies." *Masters Thesis, University of Pittsburgh*, 61.

Weninger, Bernhard, and Olaf Jöris. 2008. "A 14C Age Calibration Curve for the Last 60 Ka: The Greenland-Hulu U/Th Timescale and Its Impact on Understanding the Middle to Upper Paleolithic Transition in Western Eurasia." *Journal of Human Evolution* 55 (5): 772–81. https://doi.org/10.1016/j.jhevol.2008.08.017.

Woods, Arielle, Donald T. Rodbell, Mark B. Abbott, Robert G. Hatfield, Christine Y. Chen, Sophie B. Lehmann, David McGee, et al. 2020. "Andean Drought and Glacial Retreat Tied to Greenland Warming during the Last Glacial Period." *Nature Communications* 11 (1): 5135. https://doi.org/10.1038/s41467-020-19000-8.

Wortham, Barbara E., Corinne I. Wong, Lucas C.R. Silva, David McGee, Isabel P. Montañez, E. Troy Rasbury, Kari M. Cooper, Warren D. Sharp, Justin J.G. Glessner, and Roberto V. Santos. 2017. "Assessing Response of Local Moisture Conditions in Central Brazil to Variability in Regional Monsoon Intensity Using Speleothem 87Sr/86Sr Values." *Earth and Planetary Science Letters* 463 (April): 310–22. https://doi.org/10.1016/j.epsl.2017.01.034.

Wright, H. E. 1983. "Late-Pleistocene Glaciation and Climate around the Junín Plain, Central Peruvian Highlands." *Geografiska Annaler. Series A, Physical Geography* 65 (1/2): 35. https://doi.org/10.2307/520719.

Yang, S.L., and Z.L. Ding. 2003. "Color Reflectance of the Chinese Loess and Its Implications for Climate Gradient Changes during the Last Two Glacial-Interglacial Cycles." *Geophysical Research Letters* 30 (20).

Yin, Q Z, and Z T Guo. 2008. "Strong Summer Monsoon during the Cool MIS-13." *Clim. Past*, 7.

Zech, Roland, Jacqueline Smith, and Michael R. Kaplan. 2009. "Chronologies of the Last Glacial Maximum and Its Termination in the Andes (∼10–55°S) Based on Surface Exposure Dating." Edited by Francoise Vimeux, Florence Sylvestre, and Myriam Khodri. *Past Climate Variability in South America and Surrounding Regions* 14: 61–87. https://doi.org/10.1007/978-90-481-2672-9_3.

Zhang, Yancheng, Cristiano M. Chiessi, Stefan Mulitza, André O. Sawakuchi, Christoph Häggi, Matthias Zabel, Rodrigo C. Portilho-Ramos, Enno Schefuß, Stefano Crivellari, and Gerold Wefer. 2017. "Different Precipitation Patterns across Tropical South America during Heinrich and Dansgaard-Oeschger Stadials." *Quaternary Science Reviews* 177 (December): 1–9. https://doi.org/10.1016/j.quascirev.2017.10.012.

Zhou, Jiayu, and K.M. Lau. 1998. "Does a Monsoon Climate Exist over South America?" *JOURNAL OF CLIMATE* 11: 21.

Zhou, Jiayu, and K.-M. Lau. 2001. "Principal Modes of Interannual and Decadal Variability of Summer Rainfall over South America." *International Journal of Climatology* 21 (13): 1623–44. https://doi.org/10.1002/joc.700.

Ziegler, M., L. J. Lourens, E. Tuenter, and G.-J. Reichart. 2010. "High Arabian Sea Productivity Conditions during MIS 13 – Odd Monsoon Event or Intensified Overturning Circulation at the End of the Mid-Pleistocene Transition?" *Climate of the Past* 6 (1): 63–76. https://doi.org/10.5194/cp-6-63-2010.